Universidad Autónoma de Madrid
Escuela politécnica superior

Proyecto fin de carrera

RECONOCIMIENTO BIOMÉTRICO BASADO EN IMÁGENES SIMULADAS EN LA BANDA DE ONDAS MILIMÉTRICAS

Ingeniería de Telecomunicación

Miriam Moreno Moreno
Junio 2012

RECONOCIMIENTO BIOMÉTRICO BASADO EN IMÁGENES SIMULADAS EN LA BANDA DE ONDAS MILIMÉTRICAS

AUTOR: Miriam Moreno Moreno
TUTOR: Julián Fiérrez Aguilar

Área de Tratamiento de Voz y Señales
Dpto. de Tecnología Electrónica y de las Comunicaciones
Escuela Politécnica Superior
Universidad Autónoma de Madrid
Junio 2012

Abstract

In this M.Sc. Thesis, a biometric recognition system based on images simulated at the millimeter wave band of the electromagnetic spectrum is implemented and tested. In particular, body geometry information obtained from the silhouette of the body is used to determine the user's identity.

In order to achieve this goal, firstly, some existing human body imaging technologies working beyond the visible spectrum are revised. Specifically the X-ray, infrared, millimeter and submillimeter wave imaging technologies are considered. The benefits and drawbacks of each technology as well as their biometric applications are also studied.

Secondly, the generation of a new database is carried out. This database, called BIOGIGA, is composed of simulated images of people at 94GHz (within the millimeter wave band). The generation of this database was motivated by the lack of public databases of images of people at the mentioned spectral band. This lack is due to the recent development of imaging systems at that band and to the privacy concerns these images present.

After that, the implementation of a biometric system based on the images of BIOGIGA is performed, including a feature selection module that considerably improves the error rates of the system. The main novelty of the proposed system with respect to another approaches already published, is that it is based on different geometric measures extracted from the silhouette of the body, such as the height, the wingspan, the waist width, the chest width, etc. This highly reduces the computational cost of the system.

In the experimental section, by performing several experiments, the performance of the system under different conditions is evaluated. The effects of different conditions on the performance of the system are analyzed.

Lastly, once the system is tested, the conclusions drawn throughout the work are presented together with the future work proposals.

Key words

Millimeter wave images, 94 GHz, image simulation, synthetic database, biometrics, biometric recognition, biometric system, image processing, body geometry, distance-based features, feature extraction, feature selection, SFFS algorithm, identification, verification.

Resumen

En este proyecto se implementa y evalúa un sistema de reconocimiento biométrico basado en imágenes simuladas en la banda de ondas milimétricas. En concreto, para determinar la identidad del usuario, se ha usado información de la geometría del cuerpo humano, obtenida de la silueta del cuerpo.

Para lograr este objetivo, en primer lugar, se han revisado las diferentes tecnologías de captura de imagen fuera del espectro visible. Concretamente se estudian las tecnologías de rayos-X, infrarrojo, ondas milimétricas y submilimétricas. Asimismo se estudian las ventajas e inconvenientes de cada una así como sus aplicaciones en biometría.

En segundo lugar, se llevó a cabo la generación de una base de datos. Esta base de datos, llamada BIOGIGA, está compuesta de imágenes simuladas de personas a 94 GHz (frecuencia dentro de la banda de las ondas milimétricas). La generación de esta base de datos se vio motivada por la carencia de bases de datos públicas de imágenes en esta banda espectral. Esta carencia es debida al reciente desarrollo de los sistemas de captura de imagen en esa banda y a los problemas de privacidad que presentan dichas imágenes.

Después, se realiza la implementación de un sistema biométrico basado en las imágenes de BIOGIGA, incluyendo una etapa de selección de características que mejora considerablemente el rendimiento del sistema. La gran novedad del sistema propuesto con respecto a otros ya publicados, es que está basado en diferentes medidas geométricas extraídas de la silueta del cuerpo, como la estatura, la envergadura, la anchura de la cintura, del pecho, etc. Este enfoque reduce considerablemente el coste computacional del sistema.

En la sección experimental del proyecto, mediante la realización de varios experimentos, se evalúa el rendimiento del sistema bajo diferentes condiciones. Se analiza la influencia de dichas condiciones sobre el rendimiento del sistema.

Finalmente, una vez que el sistema se ha evaluado, se presentan las conclusiones extraídas a lo largo del trabajo junto con las propuestas de trabajo futuro.

Palabras Clave

Imágenes en la banda de ondas milimétricas, 94 GHz, simulación de imágenes, base de datos sintética, biometría, reconocimiento biométrico, sistema biométrico, procesamiento de imágenes, geometría del cuerpo humano, características basadas en distancias, extracción de características, selección de características, algoritmo SFFS, identificación, verificación.

Agradecimientos

"Los cambios son siempre buenos, nos ayudan a evaluar y buscar prioridades, nos ayudan a reencontrarnos con lo que realmente deseamos para nuestra vida y para ello necesitamos el valor para aceptar que terminó una etapa de nuestra vida para dar comienzo a otra". Sin la oportunidad que me brindó Javier Ortega no habría dado paso a esta etapa, que ahora acaba, de trabajo, aprendizaje y crecimiento tanto profesional como personal que he experimentado en el Biometric Recognition Group - ATVS, muchas gracias **Javier**.

Por supuesto mil gracias a **Julián**, no sólo por ser mi tutor del proyecto, sino también mi consejero, compañero de viaje y en ocasiones confidente, *maquinota tú*! Me has enseñado multitud de cosas en el terreno de investigación, pero más incluso en el personal. Ha sido un placer tenerte como tutor. La temporada de pádel no acaba aquí, eh?

No podía faltar a continuación mi querido **Rubén**, mi *RunVera*, quien me bautizó como *La Moren*. Siempre has estado ahí para todas mis consultas sin negarte a atenderme en ningún momento. Además has tenido la paciencia de aguantarme en nuestro viaje a *Balti**moren*** + Washington + NYC y eso ya es un logro. *Cangreg palits*, *La gente está muy loca*, *Absolutely!*, *You are very welcome*, ***Moren*** que no te enteras!, *What the tiem?*, *Oh my God!*, *pringued!*, *Te mola?* son tus famosas frases que no olvidaré. Además eres *sevillano-salsero* ☺. Pero he de decirte que te libraste de aparecer en *Desagradacimientos* por los pelos ;).

Peter ToMe, has sido una de las personas que más me han ayudado en el laboratorio, sobre todo cuando me peleaba con LaTeX(si ahora lo entiendo un poco más es gracias a ti). Sufrimos juntos en el *verano BioID* y disfrutamos, al menos yo, con nuestras charlas replanteándonos nuestras vidas. Me has gastado el apodo de ***Moren*** de tanto decirlo junto con tu versión sofisticada, ***Super Moren Station***. Y encima eres *fujitsu-salsero*! OMG! Pero por favor, no me pongas más ***caritas rojas*** ☹.

Gracias al resto de ***ATVSianos***, en especial a: Dani (*¿por qué vais vestidos?*), Galbally (*mujer de bellas piernas*), Javi *Manga* (*Javi, no somos unos alcohólicos!*), Iñaki *Perri* (compañero de pádel y *NYC host*), Javi *Pájaro* (el más cuerdo del lab, no *estantería*!), Marta (con sus pócimas y Hello Kitty dominará el mundo, no dejes que *Peter* y *RunVera* te hinchen a pelotazos ni *frutazos*!), Ruifang (OMG! You know you are my hero, you canNOT dissapear now ;), Ram (I want you to speak Spanish. See you in all the ATVS-parties! :P), Mary Gates (crack!, lo que ha ganado USA, la ciencia y la gastronomía contigo!), Almudena (te echamos de menos everyday, me parece *muy fuerte* que ya casi no te veamos, gracias por ser así, y por tus pegatinas!), Rudolf (Bubu, I am not Marta! I am Miriam *Morena Morena*). Gracias a JB por tu ayuda con algunos temas del PFC y mucha suerte en USA! Y cómo no, gracias a mis queridísimas Sara y Sandra que me han ayudado, escuchado y aconsejado tanto, gracias por estar ahí, en los buenos y en los malos momentos, no sé que haría sin vosotras. Y gracias a todos los proyectandos que han pasado por el ATVS y a los que se encuentran *proyectando*, mucho ánimo! Darwin, Fer (no pierdas esa sonrisa) y Silvia (envidio tu pelo, echaré de menos los momentos chicas en el lab a última hora ;). Aunque no ATVSiano, gracias a Richard por haber sido un *LaTeXassistant* y por ser fotógrafo más que *amateur* (hay que planear la siguiente sesión con ***Barbie Moren***).

Creo que siempre me quedaré corta dando las gracias a mis **padres**, Ana y Pedro, pilares fundamentales en mi vida, que siempre han estado ahí, apoyándome incondicionalmente, con la único deseo de verme feliz. Por supuesto, debo dar las gracias a esa persona que tanto me dio y tanto hizo por mí sin esperar nada a cambio, gracias Álex. Gracias a mis abuelos y tíos. Gracias también a Tomasa (y a sus comiditas), y a Ana y Miguel. Mención especial a *tíoDavid*, y sobre todo a Marisa, gracias por nuestras charlas y por tu compresión, tú me entiendes casi mejor que nadie. A mis tías paternas por estar pendientes de mí y por los dulces que han preparado para celebrar el fin de este proyecto.

Gracias a mis ***viej@s amig@s***: Susana, Almudena, María y Raquel, sé que siempre puedo contar con vosotras a pesar de que nos puedan separar miles de kilómetros o de que nuestras vidas hayan cambiado. Cuidado con las despedidas de soltera! David, espero que nunca te conviertas en *ex-amigo*, ya verás que en la próxima partida tendremos las mejores cartas, gracias por tus conversaciones. Amelia, cómo me alegro de haberme apuntado al British Council! Así puede conocerte. Gracias por mantener esta amistad tan bonita. Ana, qué sabia eres, gracias por tus consejos, entendimiento y ánimos. Nos vemos por Madrid o por Segovia :).

Gracias a mis ***telec@s*** o ***cuasi-telec@s***: Sandra F. Huertas (de las mejores personas que conozco, muak!), *Xe* (siempre mirando al futuro), Pablo (top model de mi proyecto), Álvaro (me enseñaste a trabajar en equipo), Eva (tú sí que vales!), Pilar (nos vemos! pero fuera de la uni! Eh?), Arturo (*keep in touch!*), Tamara, Antonio, Javi (gran monologuista :), Noe, María Davó, Sandra Díaz, Patri (nos queda tanto por vivir ;), Ana (*Cocktail Girls Party* again!), D. de Castro (conquistando U.K.), Moni (suerte en Amsterdam y no dejes el Body Combat!), Héctor (No hay huevos!), Kiri, Miguel, Diego, Davor (:P), Jose...

Gracias a mis ***físic@s/químic@s***: Merche (a otra cosa mariposa ;), Fran (qué gran amigo eres!), Lorena (ejemplo a seguir), Rodrigo (la paciencia personificada), Isadora (somos *física y química*, *pepis*!), Nicoleta (suerte en Portugal!)...

Gracias a mis ***salser@s***: Jorge (a.k.a. *Ken*), Elisa (*Ángeles de Robin* o *princesa Peach*), Katsu (*Ryu*), Isa (me encanta hablar contigo!), Bea (el salero y carácter personificado), Aarón (*mujer!*), Marti (la gracia hecha mujer), Pablo (*super Mario*), Pablo (*pádel professional*), Fany (*Ángeles de Robin*), Robin (UAM, Handyman, Diversia, Sacedón...), Fadi (cómo me marea bailar contigo :P), Miguel (gran avance bailando), Fabri (bachatero), Fer (ritmo en las venas), salseros cursos anteriores...

Por supuesto gracias a todos ***mis modelos***, que colaboraron donando sus medidas corporales a la ciencia ☺: Ana, Pedro, Álex, *Mery Mery*, Ruifang, Jorge, Pablo, Antonio, Bader, Tamara, *Julius*, Sandra F. Huertas, Álvaro, *Xe*, Laura, Javi Pérez, Arturo, Cristina, Iciar, Julio, Marisa, David, Shaomei, María Davó, Patri, Paco, Rudolf, Jose, Bruno, Richard, Eva, Sara Antequera, Belma, Santi, Marta, Jaime, Sara García-Nina, Fátima, Sandra Uceda, María Lucena, *Chino*, Alejandro Huerta, Julia, Isa, Julián, Rubén, Sandra Díaz y María Puertas.

Y gracias a todo aquél que habiendo leído todo esto, no haya encontrado su nombre, simplemente se me *pasó*. Ya sólo por haber leído esta *parrafada* se merece mi agradecimiento.

MUCHAS GRACIAS A TODOS

Shoot for your dreams.
Work hard, follow your heart,
and piece by piece,
it may just someday come together.

Ve tras tus sueños.
Trabaja duro, sigue a tu corazón,
y poco a poco,
todo podría acabar en su lugar.

Erica Fuchs
Carnegie Mellon University, USA

El trabajo de investigación que ha dado lugar a este Proyecto Fin de Carrera fue desarrollado en el *Área de Tratamiento de Voz y Señales*, Departamento de Tecnología Electrónica y de las Comunicaciones, Escuela Politécnica Superior, Universidad Autónoma de Madrid.

A mis padres.

A Álex.

Contents

List of Figures

List of Tables

Abbreviations

- **AI**: Active Indoors (referring to imaging system).
  Active imaging system working indoors. See AMMW or ASMW.
- **AMMW**: Active Millimeter Wave (Imaging System).
  Imaging system that emits millimeter wave radiation to the scene and then collects the reflected radiation to form the image.
- **AO**: Active Outdoors (referring to imaging system).
  Active imaging system working outdoors. See AMMW or ASMW.
- **ASMW**: Active Subillimeter Wave (Imaging System).
  Imaging system that emits submillimeter wave radiation to the scene and then collects the reflected radiation to form the image.
- ***cr***: With Clothing (from the Spanish expression "con ropa").
  Abbreviation used to describe the clothing condition of a user in the images used in the experiments.
- **CMC**: Cumulative Match Curve.
  Curve that graphically shows the identification performance of a biometric system. It plots the rank-n recognition rate (See R-n) versus n (being n the number of the candidates considered at the beginning of the list).
- **DET**: Detection Error Tradeoff Curve.
  Curve widely used to show graphically the verification performance of a biometric system. It plots the FRR versus the FAR for all the different threshold values with logarithmic axes.
- **EER**: Equal Error Rate.
  Error rate at which both error rates (FRR and FAR) coincide, for a certain threshold value.
- **FAR**: False Acceptance Rate.
  Probability that an impostor is accepted by a biometric system as a genuine user.
- **FRR**: False Rejection Rate.
  Probability that a genuine user is rejected by a biometric system.
- **IR**: Infrared.
  Electromagnetic radiation with wavelength in the range of 0.7-100 μm ($4.3{\cdot}10^{14}$-$3{\cdot}10^{12}$ Hz).
- **LWIR**: Long Wave Infrared.
  Infrared radiation with wavelength in the range of 8-14 μm.
- **MMW**: Millimeter Waves.
  Electromagnetic radiation that, together with the submillimeter waves, fills the gap between the infrared and microwave bands in the electromagnetic spectrum. Millimeter waves lie in the band of 1-10 mm (300-30 GHz). Clothing is highly transparent to the MMW radiation.

- **MWIR**: Medium Wave Infrared.
  Infrared radiation with wavelength in the range of 3-5 μm.

- **NIR**: Near Infrared.
  Infrared radiation with wavelength in the range of 0.7-1 μm.

- **PCA**: Principal Component Analysis.
  Mathematical procedure that uses an orthogonal transformation to convert a set of observations of possibly correlated variables into a set of values of linearly uncorrelated variables called principal components.

- **PI**: Passive Indoors (referring to imaging system).
  Passive imaging system working indoors. See PMMW or PSMW.

- **PDF**: Probability Density Function.
  Function that describes the relative likelihood for a random variable to take on a given value.

- **PMMW**: Passive Millimeter Wave (Imaging System).
  Imaging system that collects natural millimeter wave radiation that has been emitted and reflected from the scene, to form the image.

- **PO**: Passive Outdoors (referring to imaging system).
  Passive imaging system working outdoors. See PMMW or PSMW.

- **PSMW**: Passive Submillimeter Wave (Imaging System).
  Imaging system that collects natural submillimeter wave radiation that has been emitted and reflected from the scene, to form the image.

- ***R-1***: Rank-1 Recognition Rate.
  Number of users correctly identified by a biometric system with the first candidate of the list given by the system over the total number of users.

- ***R-5***: Rank-5 Recognition Rate.
  Number of users correctly identified by a biometric system with any of the 5 first candidates of the list given by the system over the total number of users.

- ***R-n***: Rank-n Recognition Rate.
  Number of users correctly identified by a biometric system with any of the n first candidates of the list given by the system over the total number of users.

- **ROC**: Receiving Operating Characteristic.
  Curve employed to plot the performance of a biometric system. It plots the TPR versus the FAR.

- **SFFS**: Sequential Floating Forward Selection.
  Feature Selection algorithm. It is a suboptimal searching technique, an iterative process in which, in each iteration, a new set of features (whose choice is based on the results of previous subsets) is used to compute a certain criterion. This is done until the criterion does not improve.

- **SMW**: Submillimeter Waves.
  Electromagnetic radiation that, together with the millimeter wave radiation, fills the gap between the infrared and microwave bands in the electromagnetic spectrum. Submillimeter waves lie in the range of 0.1-1 mm (0.3-3 THz). Clothing is partially transparent to the SMW radiation.

- **SNR**: Signal to Noise Ratio.
  Measure that compares the level of a desired signal to the level of background noise. It is defined as the ratio of signal power to the noise power.

- ***sr***: Without Clothing (from the Spanish expression "sin ropa").
  Abbreviation used to describe the clothing condition of a user in the images used in the experiments.

- **SWIR**: Short Wave Infrared.
  Infrared radiation with wavelength in the range of 1-3 μm.

- **VIS**: Visible Spectrum.
  Portion of the electromagnetic spectrum that is visible to the human eye. Electromagnetic radiation in this range of wavelengths (400-700 nm) is usually called light.

- **TPR**: True Positive Rate or Sensitivity.
  Rate of genuine attemps accepted by the biometric system. It corresponds to 1-FRR.

- **VLWIR**: Very Long Wave Infrared.
  Infrared radiation with wavelength in the range of 14-100 μm.

- **XR**: X-ray.
  Electromagnetic radiation with a wavelength that lies between 0.01-10 nm ($3{\cdot}10^{19}$-$3{\cdot}10^{16}$ Hz).

The following *abbreviations* have been used: Sect. (section) and Fig. (figure).

1 Introduction

1.1 Motivation of the Project

Biometric Recognition is the process that allow to associate an identity with an individual automatically, using one or more physical or behavioral characteristics that are inherent in the individual [1, 2]. There are many features that have been used in biometric identification: fingerprint, signature, handwriting, iris, voice, face, hand, etc. Some of these biometric traits, such as ear, face, hand or gait, are usually acquired with cameras working at frequencies within the visible band of the electromagnetic spectrum. Those images are affected by factors such as lighting conditions and occlusions (caused by clothing, makeup, hair, etc.).

To overcome these limitations, imposed by the use of images acquired in the visible spectrum (VIS), researchers in biometrics and security [3] have proposed the use of images acquired in other spectral ranges, namely X-ray (XR) [4], infrared (IR) [5], millimeter waves (MMW) and submillimeter waves (SMW) [6]. In addition to overcome, to some extent, the limitations of images at VIS, pictures taken beyond the visible spectrum have an extra advantage: they are more robust to attacks against biometric systems than other kind of images and other biometric traits.

The spectral band proposed in this project to capture images of biometric features is the one corresponding to the millimeter waves (frequency between 30 and 300 GHz) [7]. The significance of this type of radiation lies in:

- Its ability to penetrate clothing and other occlusions.
- It is innocuous to health.
- The recent development that the GHz-THz imaging systems are experiencing (specially in the area of security).

Unlike imaging technology in the visible or infrared band, GHz-THz technology is under development [8]. This fact, together with the privacy issues that the body images in this band present, have caused that, to date, there are no public databases with images of people acquired in that frequency range. In fact, so far there is only one published work on biometric recognition

based on GHz images [9]. For all the above, in the current project the generation of a database is proposed as a key task, this database comprises simulated images of people at 94 GHz [10]. Then, we will make use of such images to develop a biometric recognition system.

This project is motivated by the advantages offered by the images acquired in the range of millimeter waves and the kind of scenarios where they are acquired:

- Millimeter waves are completely innocuous. Imaging in this band can be done passively (collecting the radiation naturally emitted by the human body in that band and the one reflected by the environment) or actively (illuminating the body with emitting sources at those frequencies and collecting the reflected radiation). In no case this radiation constitutes a hazard to health.
- The transparency of clothing and other non-polar dielectric materials to this radiation. This is the main advantage for biometric recognition because it prevents unwanted occlusions in the images.
- The non-invasiveness of such imaging systems. The cooperation required by the user for the acquisition of these images is minimal.
- The possibility of recognition at a distance and/or on the move.
- The possibility of integrating the biometric recognition system in security systems such as portals and other weapons detection devices.
- The ease of fusion with other biometric traits like face.

By contrast, images acquired in this band have some drawbacks such as:

- They require extremely expensive acquisition equipments, given their recent development.
- The privacy issues caused by this kind of images (mainly because of transparency of clothing).

1.2 Objectives

The project objectives are summarized in three points:

- Creation of a database of simulated images of real people in the millimeter wave band. The first milestone of the project is the generation of such images as an alternative to purchasing equipment to capture images at GHz and given the absence of free distribution database of such images.
- Development of a biometric recognition system based on the above images. This system will have several modules: image processing, most distinctive feature extraction, feature selection, similarity measures and decision maker.
- Evaluation of the previous system by performing different experiments. The main purpose of the experiments is to quantify the influence of different conditions on the system performance. Conditions of interest include pose and clothing variation between train and test data and the amount of train data.

1.3 Methodology

The work methodology is divided in the following steps:

Literature Survey.

- The first step will be a study of different imaging systems outside the visible range, particularly those used for biometric purposes.
- Here we review the state of the art in biometric systems based on images acquired outside the visible range.
- To complete the survey phase, the basic techniques of digital image processing will be studied through the material of the Telecommunications Engineering course *Advanced Topics in Signal Processing*, by studying the book [11] and performing some of its examples.

Generation of a synthetic database of real people to 94 GHz. This was done in collaboration with the AMS group at the Autonomous University of Barcelona. This stage has several steps:

- Obtaining body measurements of real people.
- Body model generation from these measurements using a specific software for it.
- Export of the above models to another application where images of such models are simulated at the radiation frequency chosen.

Development of a biometric identification proprietary system. This system will use the features extracted from the images generated in the previous stage. The development will include the following steps:

- Preprocessing of the images.
- Feature extraction.
- Similarity measure.
- Decision-making.

Experiments for the optimization of the system. These experiments focus on the selection of features. They are performed to obtain a set of representative and distinctive features of each user to increase the performance of the system.

Evaluation of the system by performing different experiments.

Evaluation of results and drawing conclusions.

Documentation of work performed.

- Description of followed steps.
- Analysis of results, evaluation.
- Possible future work.

1.4 Memory organization

The present document is structured in 6 chapters as follows:

Chapter 1: Introduction. This chapter presents the subject of this project, the main reasons that have encouraged us to develop this work, the objectives to be obtained, the methodology followed and the memory organization.

Chapter 2: State of the art of biometrics beyond the visible spectrum. This chapter reviews some of the existing human body imaging technologies working beyond the visible spectrum: 1) X-ray, 2) infrared and 3) millimeter and submillimeter wave imaging technologies, and their biometric applications.

Chapter 3: Databases of MMW images. In this chapter two databases of images acquired in the millimeter wave band are described: 1) the one acquired and used in [9] and 2) BIOGIGA, which is the database generated within this project and the one used to develop and test the biometric system [12].

Chapter 4: System, Design and Development. The fourth chapter, after a brief introduction to biometric systems, details the different stages of the design and development of the implemented biometric system: from the preprocessing of the input images to the identity decision.

Chapter 5: Experiments and Results. In this chapter, firstly, a summary of the performance evaluation of biometric systems is presented. Then, the experimental protocols and the classifier employed in the experiments are described. Finally, the results obtained in each experiment are presented and analyzed.

Chapter 6: Conclusions and Future Work. Conclusions are finally drawn in this last chapter along with the possible future work.

Finally, the following sections are at the end of the dissertation: the Bibliography and the following appendices: Introducción (compulsory translation into Spanish of the Chapter 1), Conclusiones y trabajo futuro (compulsory translation into Spanish of the Chapter 6), Project budget, the Schedule of Conditions and the published articles.

1.5 Contributions

The contributions of this M.Sc. Thesis can be summarized in the following points:

- Summary of the state of the art of the biometric recognition research works that make use of images acquired out of the visible spectrum.
- Study of the main advantages and drawbacks of the images acquired at each spectral band.
- The innovative use of images acquired at the millimeter wave band as biometric traits.
- Generation of a synthetic database composed of simulated images of people at 94 GHz.
- Development and implementation of a recognition system based on the previous images.
- Evaluation of the results obtained through our system, under different conditions, to draw the appropriate conclusions about its performance and behavior.

During the project development several articles have been generated and accepted in different national and international conferences:

- Miriam Moreno-Moreno, Julian Fierrez, and Javier Ortega-Garcia. Millimeter- and Submillimeter-Wave Imaging Technologies for Biometric Purposes. In *Proceedings of XXIV Simposium Nacional de Union Científica Internacional de Radio*, September 2009 [13].
- Miriam Moreno-Moreno, Julian Fierrez, and Javier Ortega-Garcia. Biometrics Beyond the Visible Spectrum: Imaging Technologies and Applications. In *Proceedings of BioIDMulticomm 2009*, volume 5707 of LNCS, pages 154-161. Springer, September 2009 [14].
- Miriam Moreno-Moreno, Julian Fierrez, Pedro Tome, and Javier Ortega-Garcia. Análisis de Escenarios para Reconocimiento Biométrico a Distancia Adecuados para la Adquisición de Imágenes MMW. In *Proceedings of XXV Simposium Nacional de Union Científica Internacional de Radio*, September 2010 [15].
- Miriam Moreno-Moreno, Julian Fierrez, Pedro Tome, Ruben Vera-Rodriguez, Josep Parron, and Javier Ortega-Garcia. BIOGIGA: Base de datos de imágenes sintéticas de personas a 94 GHz con Fines Biométricos. In *Proceedings of XXVI Simposium Nacional de Union Científica Internacional de Radio*, September 2011 [12].
- Miriam Moreno-Moreno, Julian Fierrez, Ruben Vera-Rodriguez, and Josep Parron. Distance-based Feature Extraction for Biometric Recognition of Millimeter Wave Body Images. In *Proceedings of 45th IEEE International Carnahan Conference on Security Technology*, pages 326-331, October 2011 [16].
- Miriam Moreno-Moreno, Julian Fierrez, Ruben Vera-Rodriguez, and Josep Parron. Simulation of Millimeter Wave Body Images and its Application to Biometric Recognition. In *Proceedings of SPIE Defense, Security and Sensing 2012*, volume 8362. April 2012 [17].

2

State of the Art in Biometrics Beyond the Visible Spectrum

2.1 Introduction

The ability to capture an image of the whole human body or a part of it has attracted much interest in many areas such as Medicine, Biology, Surveillance and Biometrics [18]. Images acquired at visible spectrum (VIS) are widely used, however they present some limitations, specially when they are used in these fields. Specifically, the most important problems of VIS images in biometric recognition are related to:

- The lighting conditions: poor light, reflections, shadows.
- The body occlusions: clothing, makeup, hair, glasses, hats, etc.

By acquiring images at other spectral ranges, such as X-ray (XR), infrared (IR), millimeter (MMW) and submillimeter (SMW) waves (see Fig. 2.1), some of these limitations can be partially or completely removed. As an example, the Fig. 2.2 shows how the use of IR radiation solves the illumination problems, while the MMW are able to penetrate through clothing providing images free of clothing occlusions.

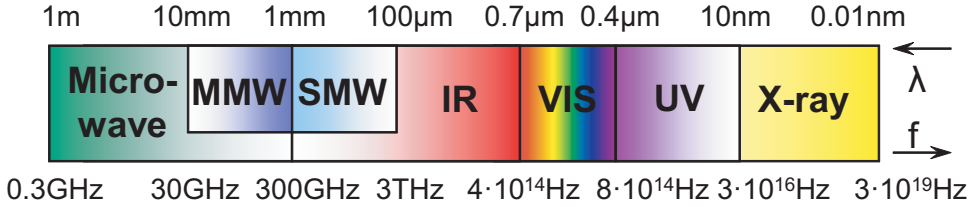

Figure 2.1: Electromagnetic spectrum showing the different spectral bands between the microwaves and the X-rays. IR band is sometimes considered to extend to 1 mm including the SMW region.

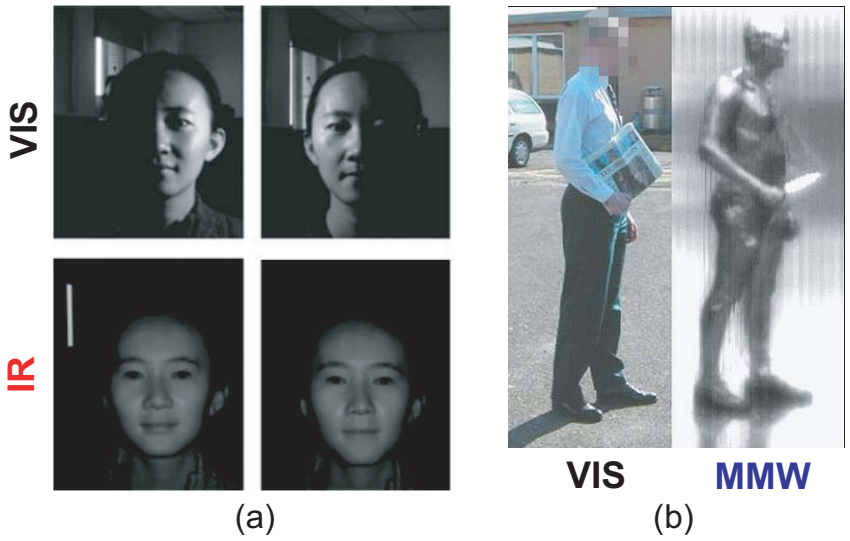

Figure 2.2: (a) Face images acquired at VIS and at IR band. The shadows disappear in the IR image. (b) Body images acquired at VIS and at MMW band. The clothing and the newspaper are transparent to MMW radiation.

2.1.1 Taxonomy

Many imaging technologies beyond the visible spectrum have been used to capture a body part: IR, magnetic resonance, radioisotope, XR, acoustical-, MMW-, SMW-imaging, etc. Not all of them can be used for biometric purposes because of their high level of intrusiveness. The imaging technologies most adequate for biometric applications are: XR, IR, MMW and SMW imaging. A taxonomy of them is shown in Fig. 2.3.

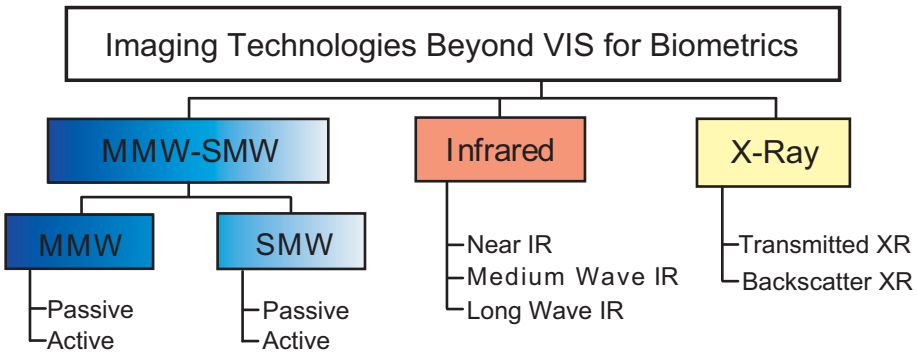

Figure 2.3: A taxonomy of imaging technologies beyond visible spectrum. The figure only shows the technologies adequate for biometrics.

The IR imaging technology is the most used in biometrics beyond the visible spectrum, followed by XR. On the other hand, the images acquired at the MMW/SMW band have been hardly used in biometrics. In fact the work by Alefs *et al.* [9] is, to date, the unique published research work about biometric recognition based on MMW/SMW images.

Although there are much more research on biometrics using IR and XR images than using MMW images, we will provide a brief summary of IR and XR imaging technologies, and we will describe in more detail the MMW/SMW imaging technology. This is due to two main reasons:

- The biometric recognition system developed in this project is based on MMW images.
- The advantages of MMW images in biometrics (see Sect. 1.1).

2.1.2 Fundamentals

Imagery can be classified into two architectures: passive or active. In the former group the image is generated by receiving natural radiation which has been emitted and reflected from the scene, obtaining a map of brightness temperature. On the other hand, in active imaging the radiation is transmitted to the scene and then collected after reflection to form the image, which is a map of reflectivity.

The contrast in the scene in any part of the spectrum is a function of the optical properties of the object being imaged and its background. In particular, the apparent temperature of an object T_0 is defined by:

$$T_0 = T\epsilon + T_s r + T_b t \tag{2.1}$$

where T is the physical temperature of the object, ϵ its emissivity, T_s is the temperature of the background (or of the illuminating source, if present) which is reflected by the object with reflectivity r, T_b is the temperature of the background behind the object and t the object's transmissivity [6]. A picture of this process is shown in Fig. 2.4, while Fig. 2.5 shows an image acquired in each spectral band.

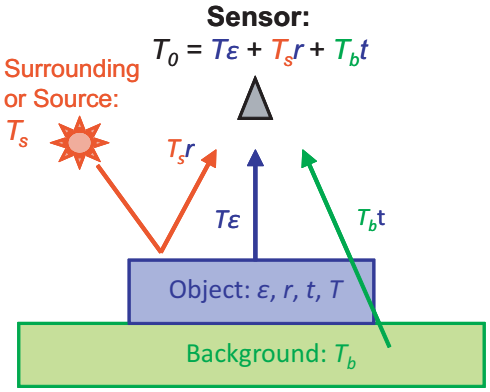

Figure 2.4: Sensor received temperature from an object (apparent temperature of the object).

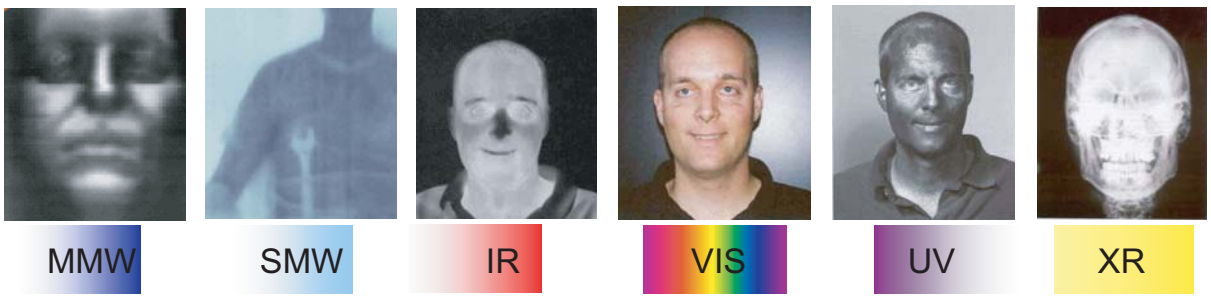

Figure 2.5: Images acquired at different spectral bands.

2.2 X-ray Imaging

X-radiation have a wavelength in the range of 10-0.01 nm ($3{\cdot}10^{16}$-$3{\cdot}10^{19}$ Hz) and enough energy to pass through cloth and human tissues. In addition to cloth penetration, XR imaging provides high image resolution. However, this technology presents some disadvantages: low speed, limitation to very short distances and the health safety concerns it raises because of using ionizing radiation. The natural background X-radiation is too weak to form an image, therefore active imaging is required in both XR imaging modalities: transmission and backscatter X-ray imaging. X-rays are commonly produced by accelerating charged particles.

2.2.1 Transmission X-ray Imaging

Conventional X-ray radiographic systems used for medical purposes produce images relying on this kind of imaging: a uniform X-ray beam incident on the patient interacts with the tissues of the body, producing a variable transmitted X-ray flux dependent on the attenuation along the beam paths. An X-ray-sensitive detector captures the transmitted fraction and converts the X-rays into a visible projection image. Only a few works on biometric identification making use of the conventional X-rays can be found: Shamir *et al.* [19] perform biometric identification using knee X-rays while Chen *et al.* [4] present an automatic method for matching dental radiographs (see Fig. 2.6). These knee or dental X-rays are difficult to forge and present additional advantages: they can be used in forensic identification where the soft tissues are degraded.

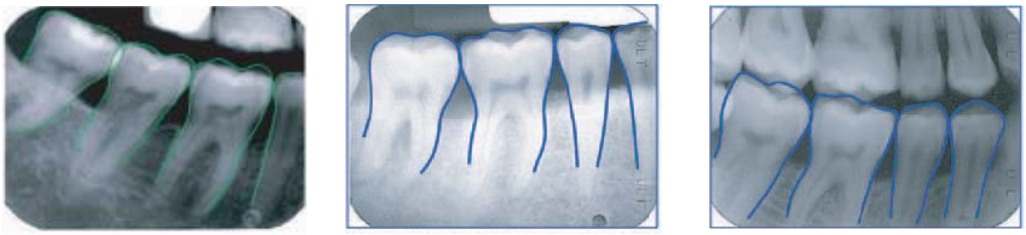

Figure 2.6: Dental radiographs used for human identification, extracted from Chen *et al.* [4].

2.2.2 Backscatter X-ray Imaging

In this technique the XR scattered photons, instead of transmitted photons, are used to construct the image [20]. This technology utilizes high energy X-rays that are more likely to scatter than penetrate materials as compared to lower-energy X-ray used in medical applications. However, this kind of radiation is able to penetrate some materials, such as cloth. A person is scanned by moving a single XR beam over her/his body. The backscattered beam from a known position allows a realistic image to be reconstructed. As only scattered X-rays are used, the registered image is mainly a view of the surface of the scanned person, i.e. her nude form. As the image resolution is high, these images present privacy issues. Some companies (e.g. AS&E) ensure privacy by applying an algorithm to the raw images so that processed images reveal only an outline of the scanned individual. Raw and processed backscatter XR images are shown in Fig. 2.7. According to our knowledge, there are no works on biometrics using backscatter X-ray images. The application of this technique includes medical imaging [21] and passenger screening at airports and homeland security [22]. There are currently different backscatter X-ray imaging systems available on the market to screen people (e.g. AS&E, Rapiscan Systems).

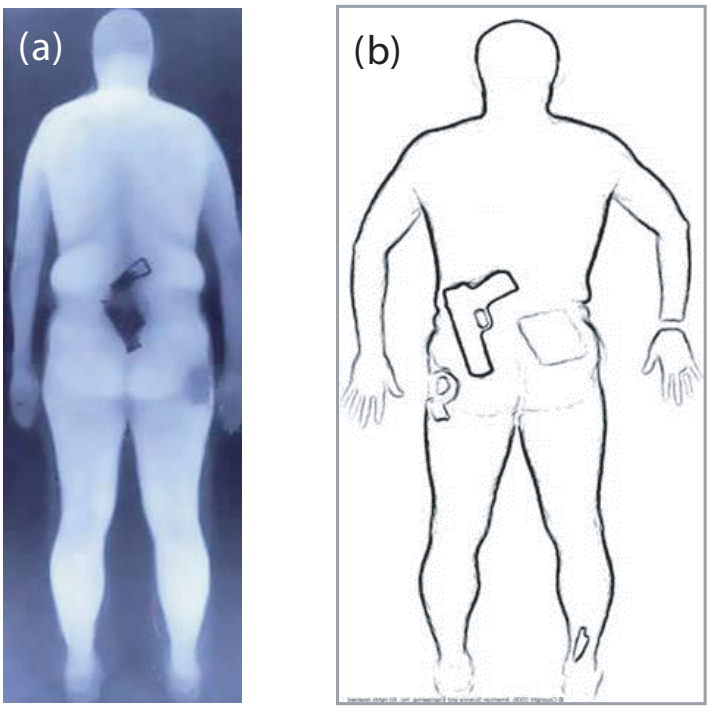

Figure 2.7: (a) A backscatter XR image of a man, it shows the skin surface and objects hidden by clothing (extracted from http://www.elpais.com). (b) A backscatter XR image processed to ensure privacy (extracted from http://www.as-e.com/).

2.3 Infrared Imaging

The infrared band of the electromagnetic spectrum lies between the SMW and VIS regions, with wavelengths in the range of 0.7-100 μm (see Fig. 2.1 and Fig. 2.8). The human body emits IR radiation with a wavelength between 3-14 μm (see Fig. 2.9), hence both active and passive architectures can be used in IR imaging, depending on the considered IR sub-band.

As indicated in Eq. 2.1, the radiation that is actually detected by an IR sensor depends on the surface properties of the object (ϵ, r, t) and on the transmissivity of the medium (atmosphere). According to the properties of the medium and the spectral ranges of the currently available IR detectors, the IR spectrum is divided into five sub-bands, summarized in Fig. 2.8. The limits of these sub-bands are not completely fixed and depend on the specific application. In practice, IR imaging systems usually operate in one of the three following IR sub-bands: the near infrared (NIR), the medium wave infrared (MWIR) or the long wave infrared (LWIR), where the windows of high atmosphere transmissivity are located.

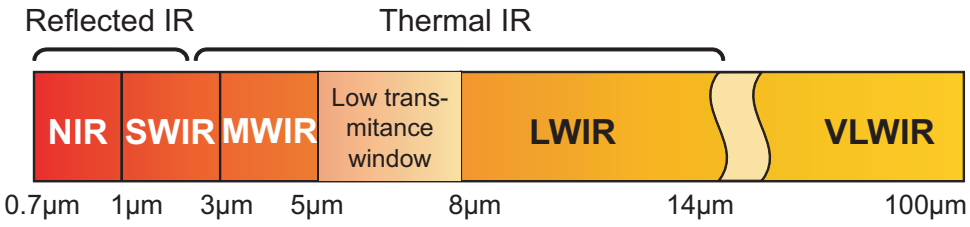

Figure 2.8: Infrared band of the electromagnetic spectrum showing the different IR sub-bands.

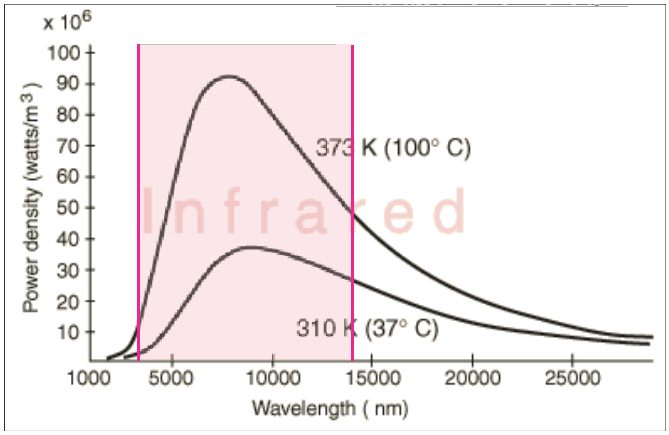

Figure 2.9: Power Spectral Density of a body at 310K (37°C) and a body at 373K (100°C). The 310K-curve corresponds to the case of the human body. It can be seen that it emits radiation mostly between 3000-14000 nm (3-14 μm). It also emits radiation beyond 14 μm.

In Fig. 2.8 the IR band is split in two sub-bands: Reflected IR band (0.7-2.4 μm) and Thermal IR band (beyond 2.4 μm). The Reflected IR band is associated with reflected solar radiation that contains no information about the thermal properties of materials. The Thermal IR band is associated with the thermal radiation emitted by the objects. This division in two bands is also related to the two kind of imaging architectures: active and passive imaging. In the Reflected IR band, external illumination is needed while in the Thermal IR band passive imaging is preferred (natural IR radiation emitted by the person is captured). The three mentioned practical IR sub-bands (i.e. NIR, MWIR and LWIR) present different characteristics. A summary of the properties of these sub-bands is given in Table 2.1 while Fig. 2.10 shows face and hand images acquired at NIR, MWIR and LWIR.

2.3.1 Near Infrared Imaging

As the human body emits IR radiation with a wavelength out of the NIR band (0.7-1 μm) it is necessary to illuminate the body with a NIR source and detect the reflected NIR radiation. The imaging equipment at this band usually is composed by a LED array lamp as NIR source, a NIR camera as detector, and an optical infrared filter to block visible radiation. The images obtained at NIR band are quite similar to the ones acquired at VIS (see Fig. 2.10(a)), however they present several advantages: (i) they are environmental illumination and human body condition invariant, and (ii) they can provide a good quality vein pattern near the skin surface (see Fig. 2.10(d)) [23]. The last one is due to two facts: (i) the incident NIR light can penetrate into the biological tissue approximately 3 mm and (ii) the reduced hemoglobin in venous blood absorbs more of the incident NIR radiation than the surrounding tissues giving darker contrast. Many biometric research works have been developed using the NIR band. Face and hand vein pattern recognition are the most important modalities investigated in this band (see references in Table 2.1).

2.3.2 Medium Wave Infrared Imaging

The human body emits IR radiation in this band (3-5 μm) allowing the passive imaging. Therefore, the images obtained at this frequency range show patterns of radiated heat from the body's surface. As we move further from VIS, the physical mechanisms involved in the imaging process become different. This leads to a different appearance and resolution of the captured images (see Fig. 2.5). A comparison among some images acquired at different IR bands is showed in Fig. 2.10. Very few biometric research works have been developed in this band, probably due

IR Spectral bands	Range (μm)	Archi-tecture	IR camera cost	Image Properties	Applications in Biometrics
Near IR (NIR)	0,7-1	Active	Low, VIS came-ra also sensitive	Good quality, body condition invariant	Face [5] and Hand Vein [23] Recognition
Medium Wave IR (MWIR)	3 - 5	Passive	High	Good quality, sensiti-ve to body conditions	Face [24] and Hand Vein [25] Recognition
Long Wave IR (LWIR)	8 - 14	Passive	Low	Low contrast, sensiti-ve to body conditions	Face [27] and Hand Vein [23] Recognition

Table 2.1: Properties of the most important IR sub-bands.

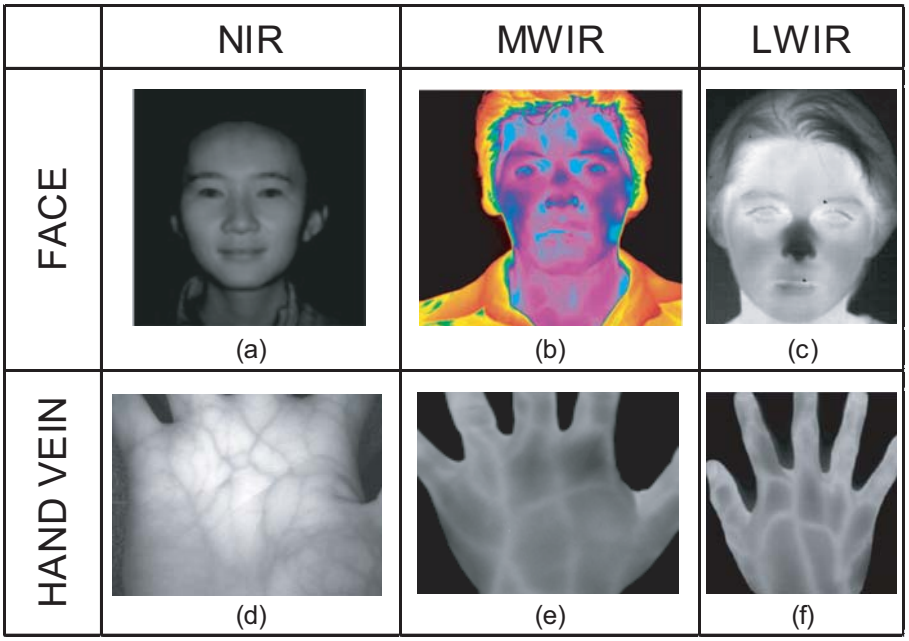

Figure 2.10: Face and hand images acquired at NIR, MWIR and LWIR bands: (a) face at NIR, (b) face at MWIR, (c) face at LWIR, (d) palm at NIR, (e) back of the hand at MWIR and (f) back of the hand at LWIR. The images are extracted respectively from [5], [24], [26], [23], [25] and [23].

to the high cost of MWIR cameras. Buddharaju *et al.* [24] performed face recognition from the thermal imprint of the facial vascular network obtained at the MWIR band. Thermal images of palm dorsa vein acquired in MWIR have been also used to identify individuals [25].

2.3.3 Long Wave Infrared Imaging

Although human body emits IR radiation in both MWIR and LWIR bands, LWIR (8-14 μm) is usually preferred due to: (i) much higher emissions in it, and (ii) the low cost of LWIR cameras. No external illumination is required in this band. Body images acquired at LWIR are quite similar to those acquired in MWIR. Both kinds of images are often called *thermograms*. Fig. 2.10(c, f) shows images acquired at this band. Recognition of faces from images obtained at this band has become an area of growing interest [26, 27]. However the algorithms they used do not differ very much from the algorithms used in the VIS band. Works on vein pattern recognition have been developed at this band as well [23]. In contrast with NIR; LWIR can only capture large veins, not necessary at the skin surface, because large veins carry a higher amount of blood giving a higher temperature. In addition, most of the LWIR images have low levels of contrast and they are sensitive to ambient and body condition.

2.4 Millimeter and Submillimeter Wave Imaging

MMW and SMW radiation fill the gap between the IR and the microwaves (see Fig. 2.1). Specifically, millimeter waves lie in the band of 30-300 GHz (10-1 mm) and the SMW regime lies in the range of 0.3-3 THz (1-0.1 mm).

MMW and SMW radiation can penetrate through many commonly used nonpolar dielectric materials such as paper, plastics, wood, leather, hair and even dry walls with little attenuation [28, 29]. Clothing is highly transparent to the MMW radiation and partially transparent to the SMW radiation [30]. Above 30 GHz, the transmission of the atmosphere varies strongly as a function of frequency due to water vapour and oxygen [6, 31]. There are relatively transparent windows centered at 35, 94, 140 and 220 GHz in the MMW range and less transparent windows in the SMW region located at: 0.34, 0.67, 1.5, 2, 2.1, 2.5, 3.4 and 4.3 THz. Atmosphere attenuation is further increased in poor weather. Liquid water extremely attenuates submillimeter waves while MMW radiation is less attenuated (millions of times) in the presence of clouds, fog, smoke, snow, and sand storms than VIS or IR radiation.

Consequently, natural applications of MMW and SMW imaging include security screening, non-destructive inspection, and medical and biometrics imaging. Low visibility navigation is another application of MMW imaging [7]. The detection of concealed weapons has been the most developed application of MMW/SMW imaging systems so far, in contrast to the biometrics area, where there is only a published research work.

Although most of the radiation emitted by the human body belongs to the MWIR and LWIR bands, it emits radiation in the SMW and MMW regions as well (the tails of the 310K-curve on the right in Fig. 2.9). This allows passive imaging. A key factor in MMW and SMW passive imaging is the sky illumination. This makes images acquired in indoor and outdoor environments to have very different contrast when working with passive systems. Outdoors radiometric temperature contrast can be very large (due to the difference between the temperature of the floor, which is warm $\sim$ 300 K, and the sky, which is cold $\sim$ 100 K), but it is very small indoors. In passive imaging operating indoors, the signal to noise ratio (SNR) of the existing cameras is barely enough for coarse object detection, being usually insufficient for identification (as needed for biometrics). There are two solutions to overcome this problem: (i) cooling the detector or alternatively (ii) using active imaging. Cooling the detector improves the sensitivity but it makes the camera more expensive and difficult to use.

In active imaging, the source that illuminates the scene produces much higher power level than the emitted from the scene, so it can be considered as an object at very high temperature. If the source is incoherent and physically large, active imaging is equivalent to passive imaging with the surroundings at very high temperature, and hence results in much greater contrast within the image. If the source is small, active imaging becomes more complicated. In any case, the power level of the radiation source in active imaging strongly affects the detection resolution. In addition to higher resolution than passive imaging, active imaging provides higher SNR, higher signal levels, and the ability to obtain depth information in the scene.

2.4.1 Millimeter Wave Imaging (MMW)

Passive MMW Imaging (PMMW)

There have been many research groups working on passive MMW imaging (PMMW) since its early developments. Most of them have constructed prototype radiometers that work at a frequency range centered at 35 GHz [32] or at 94 GHz [8, 28, 33, 34]. The images obtained with PMMW imaging systems have low resolution compared to VIS and IR images. This low

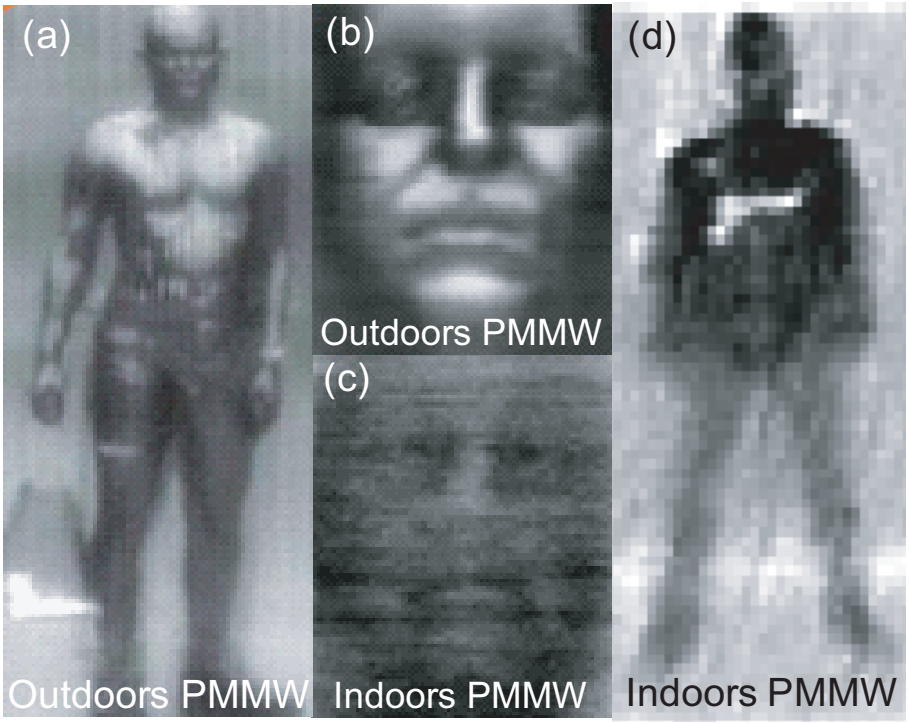

Figure 2.11: Images acquired with PMMW imaging systems. (a) Outdoors PMMW image (94 GHz) of a man carrying a gun in a bag. (b-c) Indoors and outdoors PMMW image of a face. (d) Indoors PMMW image (94 GHz) of a man with a gun concealed under clothing. These figure insets are extracted from: www.vision4thefuture.org (a-c), and www.alfaimaging.com (d). All the people were dressed.

resolution is a consequence of the longer wavelengths used relative to the aperture size of the sensor's collection optics. Further, images acquired indoors will present less contrast than those acquired outdoors, as it is shown in Fig. 2.11. There are multiple commerical PMMW cameras (e.g. Quinetiq, Brijot, Alfa Imaging, Sago Systems, Millivision, and View Systems).

The applications of most of the cited works are the detection of concealed weapons or vision under adverse weather conditions. To date, the unique published biometric application of MMW/SMW is the one by Alefs *et al.* [9]. Specifically, they use a PMMW system (a multi-view stereo radiometric scanner that operates at 94 GHz) schematically shown in Fig. 2.12(a), obtaining the images in Fig. 2.12(b). The details of mentioned work (the characteristics of the database composed by these images, the approaches followed to perform the biometric recognition and the recognition results) will be briefly presented throughout the document.

Active MMW Imaging (AMMW)

Active MMW imaging (AMMW) has gained more and more attention during the last few years for indoor security applications [35, 36, 37, 38]. Sheen *et al.* [35] demonstrated an AMMW imager operating at 27-33 GHz and good quality images were obtained (see Fig. 2.13(a)). Derham *et al.* [36] showed the performance of a prototype AMMW imaging system operating at 60 GHz that uses the frequency-encoding technique. Timms *et al.* [37] developed a 190 GHz active imaging system.

In the active systems, as the image is formed collecting the transmitted and then reflected radiation from the emitting source, the appareance of the images acquired indoors and outdoors is the same (the surrounding temperature does not affect as in the case of PMMW imaging).

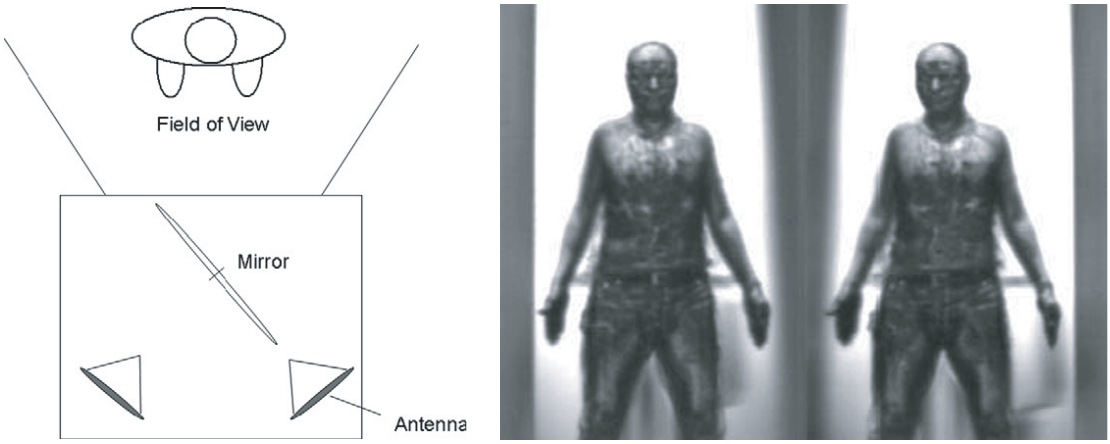

(a) (b)

Figure 2.12: (a) Schematic view of stereo radiometer (top view). The platform is shifted vertically during scanning. (b) Pair of millimetre-wave images acquired at one scan of a person wearing normal clothing. The equivalent surface temperature varies between 225K (light regions) and 300K (dark regions). Images extracted from [9].

Several images obtained with AMMW imaging systems are shown in Fig. 2.13. The higher quality of the images acquired with active systems, when compared with PMMW systems, is clearly noticeable. Again, most of AMMW imaging systems are used as security portals (see Fig. 2.13(d)). Some AMMW imagers are currently available on the market (Agilent and L3-Communications). Agilent's MMW imaging system works at 30 GHz and has a transverse resolution of 1 cm. L-3 Provision MMW body screening portal (Fig. 2.13(d)) has been used since 2007 at some airports (see example images in Fig. 2.13(b and c). However, no biometric application of AMMW imaging has emerged so far.

2.4.2 Submillimeter Wave Imaging (SMW)

The shorter the radiation wavelength is, the better image resolution is available, and hence SMW imaging would provide better resolution than MMW imaging. On the other hand, as the wavelength decreases, the penetration capability decreases. Further, the technology needed in the SMW imaging systems is much less mature than the MMW technology [39].

Passive SMW Imaging (PSMW)

In passive SMW imaging (PSMW) the contrast in the image depends on the operation frequency: at frequencies below 0.5 THz it will be dominated by the reflectivity of the items, while at frequencies of 0.5 THz and above, it will be dominated by the emissivity of the objects and their physical temperature (similar to thermography). This statement agrees with Fig. 2.9: as the frequency increases (wavelength decreases) the power density of a body at a non-null temperature also is bigger.

Some of the more relevant and recent research works on PSMW imaging include [40] and [41]. Luukanen *et al.* [40] developed an imaging system working at 0.1-1 THz. Shen *et al.* [41] performed detection and segmentation of concealed objects in images acquired with the imaging system described in [40]. They obtain good quality images as it can be seen in Fig. 2.14(a). Fig. 2.14(b) shows another PSMW image of a man with a spanner hidden under his T-shirt (acquired at 1.5 THz [42]). These two images show that cloth is less transparent to submilliter

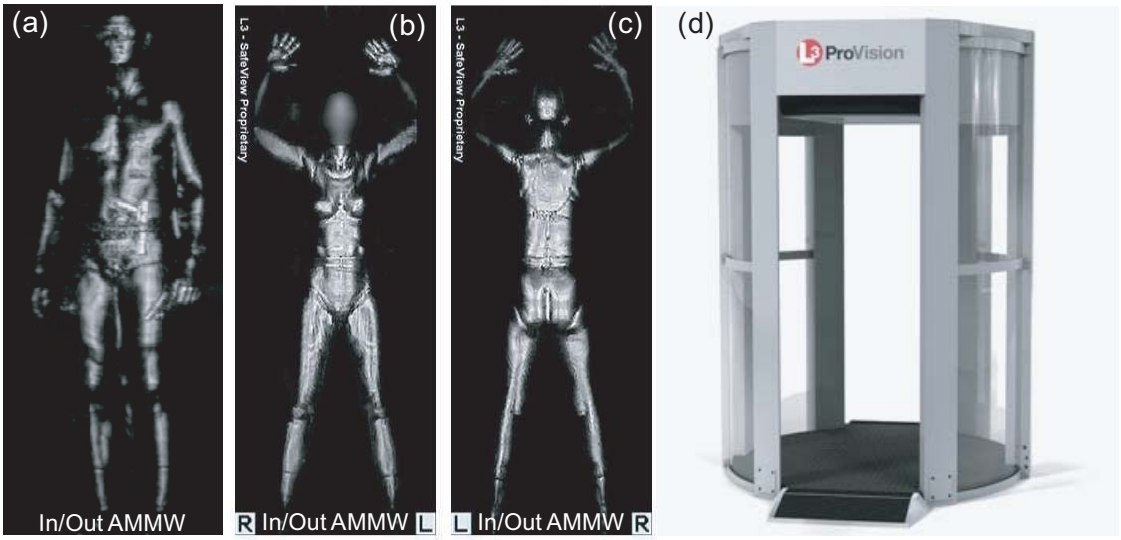

Figure 2.13: Images acquired with AMMW imaging systems (the appearance of the images is the same in both scenes, indoors and outdoors). (a) AMMW image acquired at 27-33 GHz of a dressed man carrying two handguns. (b) and (c) AMMW images of a dressed woman, both acquired by the L3-Communications screening portal, that is shown in (d). These figure insets are extracted from: [35] (a), while (b), (c) and (d) are all extracted from http://www.kelowna.com/2010/04/08/kelowna-airport-using-full-body-scanner/.

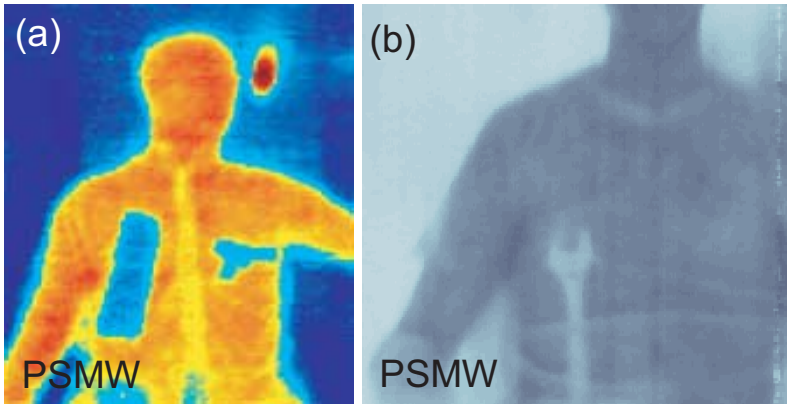

Figure 2.14: Images acquired with PSMW imaging systems. (a) PSMW image (0.1-1 THz) of a man with concealed objects beneath his jacket. (b) PSMW image (1.5 THz) of a man with a spanner under his T-shirt. These figure insets are extracted from: [41] (a) and [42] (b).

waves than to MMW radiation (collar and folds of the weave are visible). A passive system required to penetrate all type of clothing should operate below 0.3-0.5 THz [30, 6].

The higher resolution of SMW images compared to MMW makes SMW more suitable for biometric recognition applications. However the partial clothing opacity to SMW radiation would hinder the performance of biometric systems. To the best of our knowledge, no biometric works have been performed using PSMW imaging.

Regarding commercial PSMW imaging systems, Thruvision currently produces what it seems to be the only commercially available passive THz imaging system.

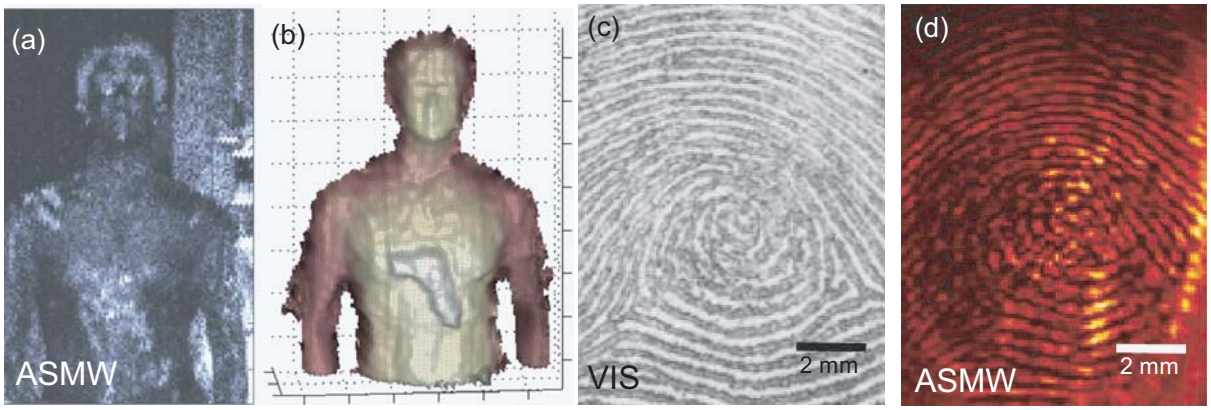

Figure 2.15: Images acquired with ASMW imaging systems. (a) ASMW image of a man hiding a gun beneath his shirt acquired with a 0.6 THz radar. (b) Full 3-D reconstruction of the previous image after smoothing of the back surface. (c) White light (VIS) image of a thumb print. (d) Reflected terahertz 20-frame average image of the same thumb flattened against a polyethylene wedge . These figure insets are extracted from: [43] (a) and (b), [45] (c) and (d).

Radiation	Architecture	Image Properties	Relative Spatial Resolution	Operating Frequencies	Commercial Systems
MMW	Passive	▪ Low resolution compared to VIS and IR ▪ Highly affected by sky illumination	Very Low (indoors) Low-Medium (outdoors)	▪ 35 GHz ▪ 94 GHz	▪ Qinetiq ▪ Brijot ▪ Alfa Imaging ▪ Sago Systems
	Active	▪ Higher quality than Passive MMW images	Medium	▪ 30 GHz ▪ 60 GHz ▪ 190 GHz	▪ Agilent ▪ L-3 Communications
SMW	Passive	▪ Good quality ▪ Partial clothing opacity	Medium-High	▪ 0.1-1 THz ▪ 1.5 THz	▪ Thruvision
	Active	▪ Higher quality than Passive SMW images ▪ Partial clothing opacity	High (at a distance) Very high (near)	▪ 0.6-0.8 THz ▪ 310 GHz ▪ > 1 THz	▪ Picometrix ▪ Teraview

Table 2.2: Properties of MMW and SMW imaging operating with passive or active architecture. The spatial resolution depends on some conditions such as the distance between the target and the detector, the given resolution corresponds to a target-detector distance of some meters.

Active SMW Imaging (ASMW)

Research works on active SMW imaging (ASMW) have only appeared recently [43, 44, 45, 38]. Some of them can image a body part at a distance [43] at 0.6-0.8 THz with a spatial resolution of less than 1 cm, [44, 45] present much better resolution (<2mm) working with relatively close targets at 310 GHz [44], or beyond 1 THz [43]. Finally Sheen *et al.* [38] developed a prototipe system that operates near 350 GHz.

Fig. 2.15 shows images acquired at SMW with the active architecture (see figure caption for more details).

Although images acquired at a distance with ASMW imaging systems present not very high spatial resolution, extracting signals from the noisy scene clutter is possible [43]. Furthermore, images acquired from targets near the system present a reasonable resolution for biometric appli-

cations, as it is shown in Fig. 2.15(d) . This fingerprint acquired at 4.3 THz has enough quality to allow the identification of an individual. On the other hand, the imaging system is quite complicated, and it works only in laboratory environments. Active terahertz imaging systems are available providing high resolution (Picometrix) and additional spectroscopic information (Teraview).

To sum up, the image properties, relative spatial resolution, the operating frequencies as well as examples of commercial systems for each MMW/SMW architecture are summarized in Table 2.2.

3

MMW Images Databases

3.1 Introduction

In order to develop and to test a biometric recognition system, the availability of biometric databases is essential. Furthermore, the biometric databases should be large enough and statistically significant in order to achieve an objective and differentiating comparison among the different algorithms developed in the biometric recognition field.

In the particular case of the proposed research, public databases composed of images acquired out of the VIS band already exist. Most of them contain images acquired at (i) one IR sub-band, (ii) at VIS and one IR sub-band, or (iii) at several VIS and IR sub-bands (multispectral databases). As expected, the hand and the face are the most common traits in these databases. Some of these databases are included in Table 3.1.

Unfortunately the MMW imaging technology is not as mature as the VIS or the IR one. In fact, in comparison with them, it is in its infancy. In addition to this, the privacy concerns the MMW body images present, difficult the acquisition of databases containing body images at that spectral range. As a result, there are only two databases of MMW body images:

- TNO Database. This database is the one created and used by Alefs *et al.* in [9] (the only biometric recognition research based on MMW images published so far).
- BIOGIGA Database. This is the database generated within this project with the purpose of designing, developing and testing the biometric system presented throughout the document.

In the following, the generation of these databases, the characteristics of their images as well as the contents of each database will be described. As the BIOGIGA database is the one used in this project, it will be described in more detail.

Database	Biometric Trait	Spectral Bands
CASIA HFB Database	Face	VIS, NIR, 3D
CASIA NIR Database	Face	NIR
Terravic Facial IR Database	Face	LWIR
Oulu-CASIA NIR&VIS	Face(Facial Expressions)	VIS, NIR
IRIS Thermal/Visible Face Database	Face	VIS, Thermal IR
PolyU Multispectral Palmprint Database	Palmprint	R, G, B and NIR illumination
PolyU NIR Face Database	Face	NIR
USTC-NVIE Database	Face (Facial Expressions)	VIS, IR

Table 3.1: Main databases of hand or face images acquired at VIS and/or IR bands.

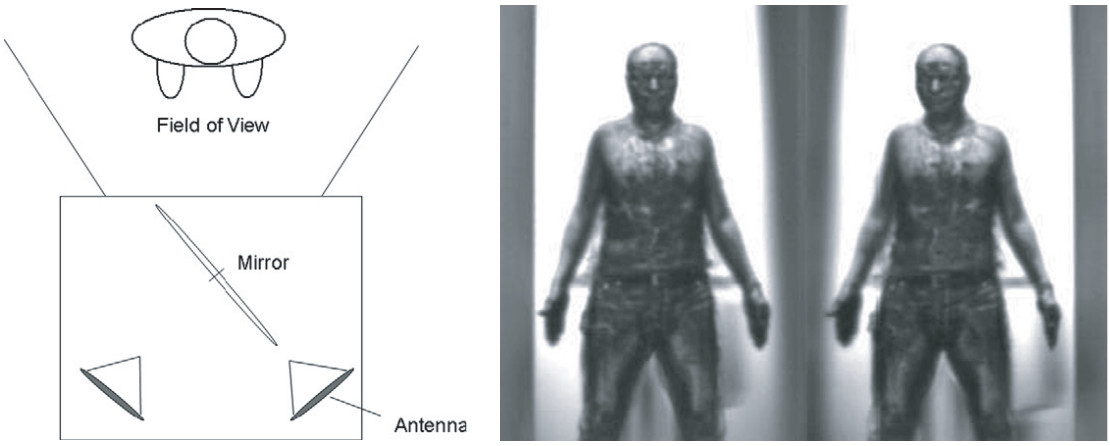

(a) (b)

Figure 3.1: Reproduced from Fig. 2.12. TNO database: (a) Schematic view of the used stereo radiometer (top view). The platform is shifted vertically during scanning. (b) Pair of millimetre-wave images acquired at one scan of a person wearing normal clothing. The equivalent surface temperature varies between 225 K (light regions) and 300 K (dark regions). Images extracted from [9].

3.2 TNO Database

In [9] Alefs *et al.* analyzed the appearance of the upper body and thorax in MMW images to perform human identification. Although the database they created does not have a specific name, we will refer to it as TNO Database (just because that research was carried out in the TNO Defence, Security and Safety Center, located at The Hague, Netherlands).

This database comprises images of 50 people acquired by a passive system at 94 GHz (that frequency corresponds to an average wavelength of about 3.2 mm - MMW range), therefore they are PMMW images.

3.2.1 Image Acquisition and characteristics

The MMW body images were acquired outdoors using a multi-view (stereo) radiometric scanner, which is shown in Fig. 3.1(a). One scan, that takes about 15 s to complete, provides a set of two images from slightly different points of view giving a pair of images like the ones in Fig. 3.1(b).

Those images show a male person of average size and with normal clothing. The radiation pattern is inverted: the bright regions indicate a surface with low radiation and dark regions indicate surface with high radiation. At surfaces with upward directed normals, the amount of

reflected radiation is smaller than the amount reflected from surfaces with downward directed normals. This is due to the fact that the sky has a low temperature compared to the floor. Therefore surfaces with upward directed normals are presented with a bright value. Metallic objects typically appear bright. The background consists of a metal surface that is positioned tilted toward the sky providing a strong contrast to the foreground. Cavities and surfaces with downward directed normal vectors typically provide MMW hot spots, i.e. small dark regions, e.g. eyes and chin. On the contrary, the nose and forehead provide the opposite contrast (they appear white in the MMW image).

3.2.2 Description of the database

The dataset is composed of MMW images from 50 people, all of them are male. Each man was asked to stand in front of the scanner with the head and the arms positioned at a fixed rack and two recordings were made. Each recording contains two images (see Fig. 3.1(b)), each recording with a different pose:

- The first one with the head and the body recorded in frontal view.
- The second one with the head turned leftward.

This was done to increase viewpoint dependent variations. The second recording provides images with side view of the head and some small changes in the appearance of the frontal torso.

A second set of images was recorded with the same people, poses and viewpoints, but now wearing different facial clutter configurations, so that a large part of the face was occluded using an artificial beard or balaclava. The Fig. 3.2 shows the effect of this clutter in VIS and MMW images. Images Fig. 3.2(a) and (b) display VIS images while (c) and (d) display the corresponding MMW images, which are only slightly influenced by the use of the clutter, being the head pose the main influence on the appearance on MMW images.

To summarize, in the TNO database, four images pairs were acquired per person: two different poses with each two different facial clutter configurations. This gives a total of $50 \times 4 \times 2 = 400$ images for this database.

(a) Person with artificial beard.

(b) Person with balaclava.

(c) Mm-wave image of beard.

(d) Mm-wave image of balaclava.

Figure 3.2: TNO database: Facial images acquired at VIS, (a) and (b), and at 94 GHz, (c) and (d), for one person with different face occlusions. Images extracted from [9].

3.3 BIOGIGA Database

The corpus of the BIOGIGA database consists of synthetic images at 94 GHz of the body of 50 individuals. The images are the result of simulations carried out on corporal models at two types of scenarios (outdoors, indoors) and with two kinds of imaging systems (passive and active). These corporal models were previously generated based on body measurements taken from real subjects.

3.3.1 Generation of the Database

The generation of the database was carried out jointly at the Universidad Autónoma de Madrid (UAM) and Universidad Autónoma de Barcelona (UAB) [12]. The process to generate the images that compose the database can be divided into the following stages:

1. Acquisition of body measures of each person.
2. Generation of the 3D body model of each user based on such measures.
3. Simulation of the images at 94 GHz from each model in the two types of scenarios (indoor/outdoor) and with two types of imaging systems (passive/active).

Corporal Measures

In order to have realistic 3D body models, a set of body measures of each person was taken. These measures are specified in Table 3.2. Some pictures of each subject were also taken in the visible spectrum (with a conventional digital camera).

Main Parameters	**Corporal Measures**	
Gender	Neck circ.	Waist circ.
Age	Height	Nape to waist
Tone	Upper arm circ.	Waist to hip
Weight	Upper arm length	Shoulder to Neck
Height	Lowerarm length	Upperleg height
	Wrist circ.	Lowerleg height
	Front chest dist.	Calf circ.
	Bust circ.	Angle circ.
	Underbust circ.	Thigh circ.
		Hips circ.

Table 3.2: BIOGIGA database: Main parameters and body measures taken from each subject used to create his/her corresponding 3D body model in MakeHuman. The abbreviation *circ.* means circumference.

Corporal Model

The body model of each subject was obtained using the free software MakeHuman[1], which allows to generate images of human bodies in 3D. For each person, his or her main parameters and body measurements (see Table 3.2) were introduced through the menus available for it. Subsequently the 3D model was compared with the picture previously taken to verify that the obtained model corresponds to the body of the concerned person.

[1] http://www.makehuman.org/

Additionally, MakeHuman generates garments adapted to the body of each model. This allows us to generate, in the following stage, images of people with and without clothes at 94 GHz.

Simulation of Images at 94 GHz

The models generated in MakeHuman are exported to Blender[2], which is a free software devoted to modeling, animation and 3D graphics creation. Blender provides a ray tracing engine that treats the radiation at 94 GHz as if it was light interacting with the scene. For a good simulation the properties of materials (skin, clothes...) and light sources should be defined according to their characteristics in the range of 94 GHz [10].

Lastly, the resulting images were postprocessed adding them the typical noise and resolution that the real system to be simulated has [10]. For all the images in BIOGIGA database the spatial resolution was 2 cm and the noise temperature 20 K.

3.3.2 Description of the database

The database consists of images simulated at 94 GHz, of 50 people (25 females and 25 males), with ages between 15 and 55 years old. For each user the database has four sets of images, each of them simulated by:

- A passive system outdoors (PO).
- A passive system indoors (PI).
- An active system outdoors (AO).
- An active system indoors (AI).

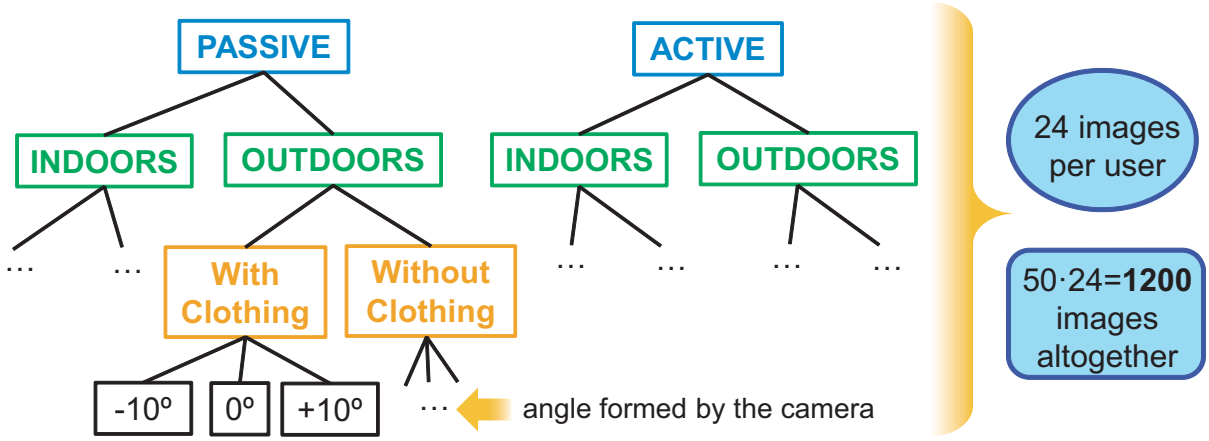

Figure 3.3: BIOGIGA database: Tree showing the different kinds of images simulated for each user.

[2]http://www.blender.org/

For each user and each of the previous sets the following data was generated:

- Images of the human 3D model **with** clothing and an angle formed by the camera of -10°, 0° and +10°.
- Images of the human 3D model **without** clothing and an angle formed by the camera of -10°, 0° and +10°.

According to what is stated above (which is schematically show in Fig. 3.3), for each user the database has 4×2×3=24 images at 94 GHz. Hence, the total number of images in BIOGIGA is 50×24=1200. Fig. 3.4 shows the VIS image and the 3D body models of one subject while Fig. 3.5 and Fig. 3.6 display most of the images simulated at 94 GHz of the same user.

There are certain features of the images at 94 GHz that can be highlighted. These features are related to (i) the influence of clothing and (ii) the contrast and relative level of each image type.

Firstly, regarding the **influence of the clothing**, it is hardly noticeable in the pictures, in fact, the images simulated at 94 GHz from the model with clothes and from the model without clothes are almost the same. The effect of clothing is slightly observed only in some regions, where the fabric is thicker or where there are folds or several layers of clothing. This occurs in the neck of the shirt and the waist, being more noticeable in images simulated with passive systems outdoors.

Secondly, concerning the **contrast in the images**, among the images simulated with passive systems, the simulated outdoors have a higher contrast than the simulated indoors. This is due to the greater temperature difference between the sky (100 K) and the floor (300 K) as it was explained in Sect. 2.4 and Sect. 3.2.1. As it happens in the images of TNO database, the PMMW images of BIOGIGA present a dark color in regions oriented to the floor and light gray color in parts of the body oriented to the sky (see Sect. 3.2.1). However, indoors, the body has a much more uniform color as the surrounding temperature has no major variations. On the other hand, the images simulated with active systems show a higher radiometric temperature level (are darker) because the person is radiated with an external source not natural, collecting the radiation once it has been reflected by the person. For the same reason there is almost no difference between the images simulated indoors and outdoors for active acquisition.

Finally, Fig. 3.7 displays four histograms of different parameters or body measures taken from the subjects that form the database: (i) the age, (ii) the height, (iii) the waist circumference, and (iv) the arm length.

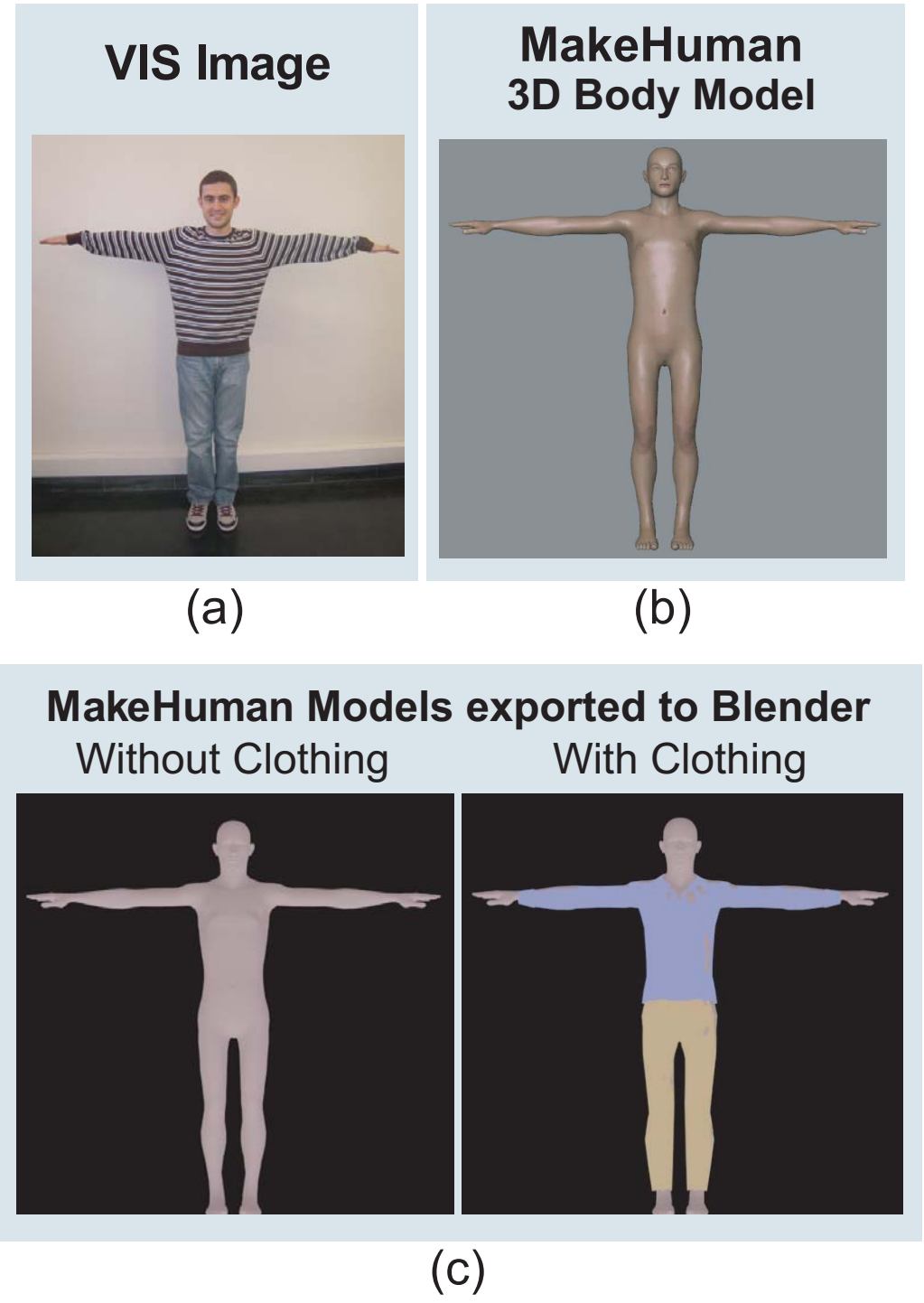

Figure 3.4: BIOGIGA database: (a) Image of a user acquired at VIS spectrum with an ordinary digital camera. (b) 3D body model generated in MakeHuman from the measures of the same user. (c) MakeHuman models exported to Blender (without and with clothing).

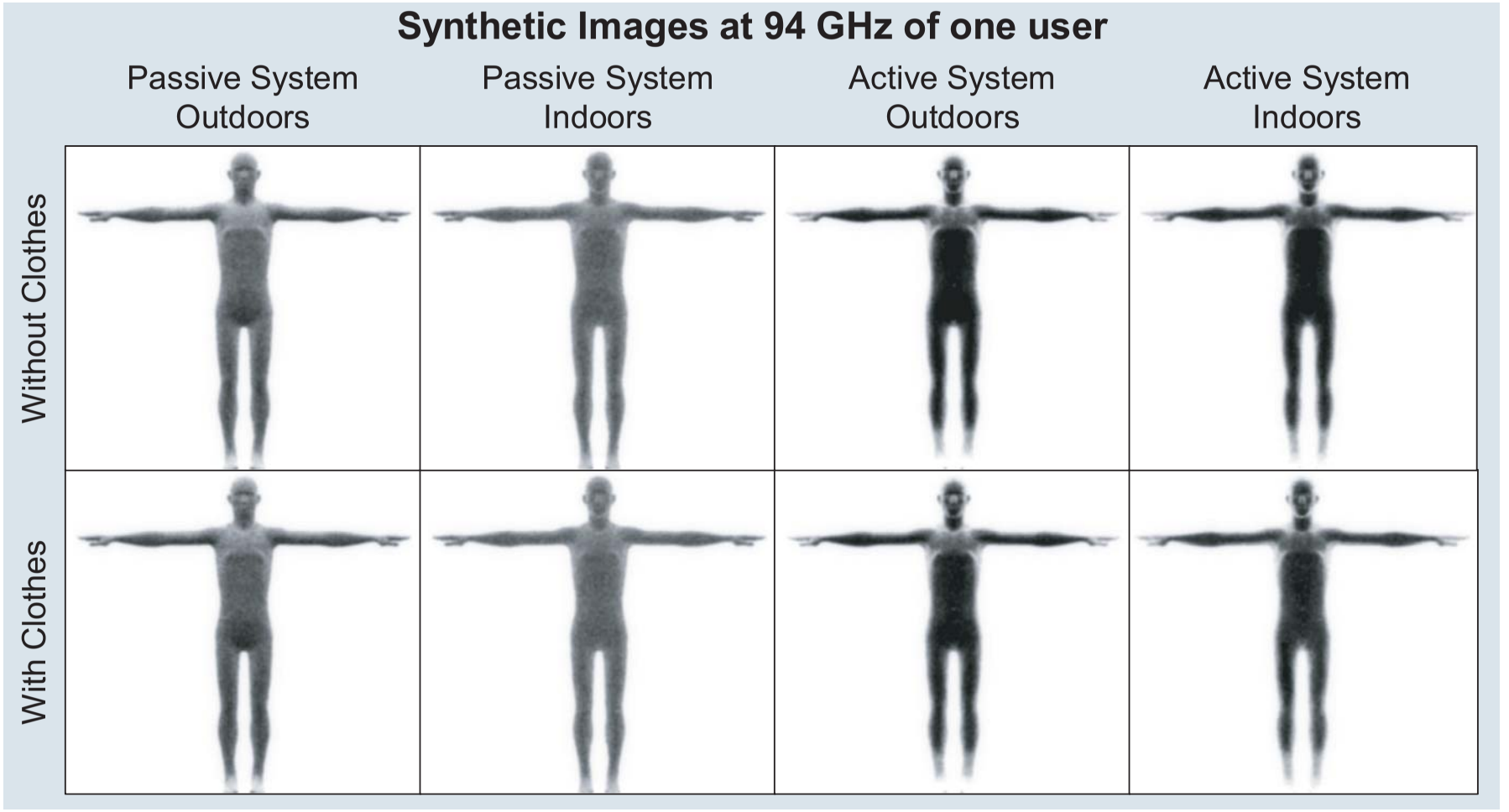

Figure 3.5: BIOGIGA database: Synthetic images of the same user of Fig. 3.4 simulated at 94 GHz with passive and active systems indoors and outdoors, and an orientation angle of the camera of 0°.

Figure 3.6: BIOGIGA database: Synthetic images of the same user of Fig. 3.4 and Fig. 3.5 simulated at 94 GHz with passive and active systems indoors and outdoors, and an orientation angle of $+10^{\circ}$(for images without clothing) and -10°(for images with clothing). In addition to these images and the ones in Fig. 3.5 there are 8 more images for each user in the database (4 without clothing and $-10^{\circ}$and 4 with clothing and $+10^{\circ}$).

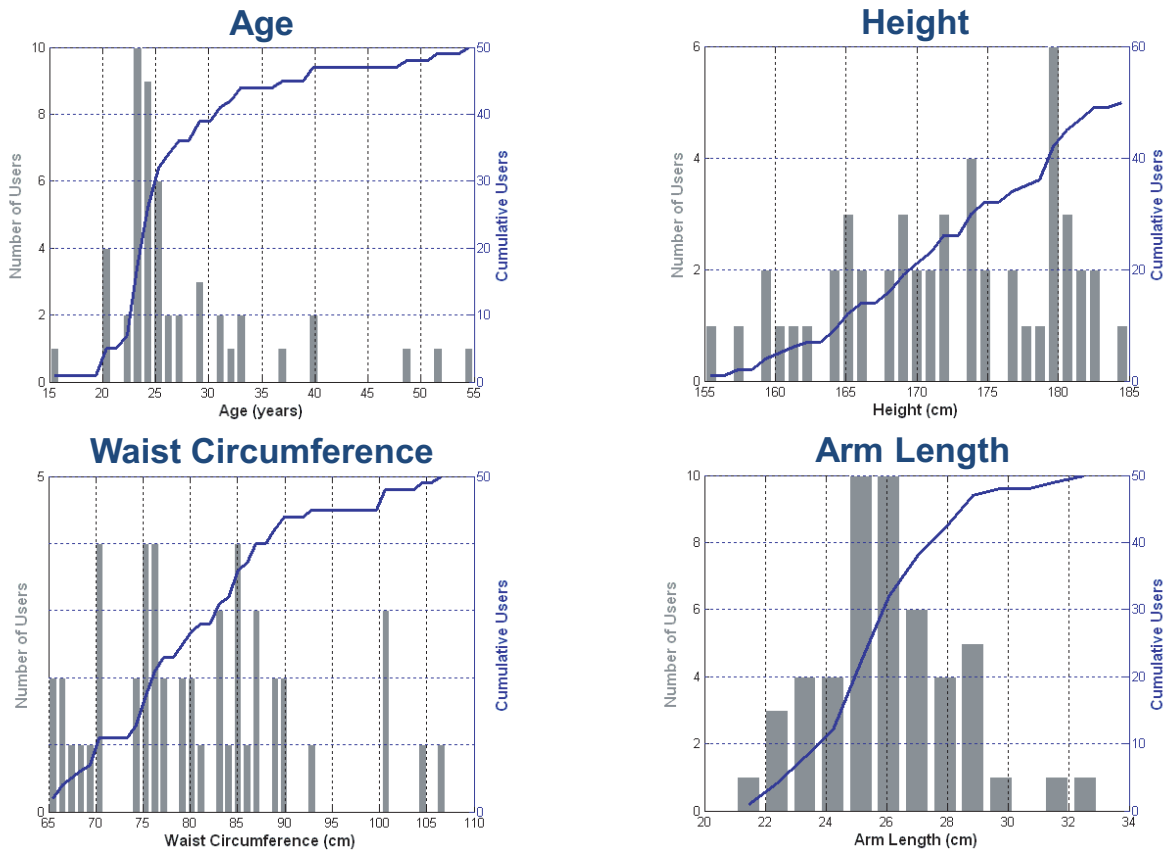

Figure 3.7: BIOGIGA database: Histograms of the age, height, waist circumference and arm length of the users that form BIOGIGA.

4

System, design and development

The aim of this project is the development of a new biometric system based on images acquired at the MMW band. This system has several modules: image processing, most distinctive feature extraction, feature selection, similarity computation and decision maker. After a brief introduction to biometric systems, this chapter describes the modules that constitute the proposed and developed biometric system.

4.1 Introduction to Biometric Systems

A biometric system is the combination of devices, databases and processes that allow the recognition of an individual using one or more of his/her biometric features. The block diagram of a generic biometric system is shown in Fig. 4.1.

Once the user has been enrolled, biometric systems can operate in two modes:

- **Verification Mode.** The user claims an identity and presents his or her biometric trait, then the system determines if the real identity of the user corresponds to the identity claimed by him or her.
- **Identification Mode.** The user only presents his or her biometric trait without claiming any identity, then the system tries to find his or her identity.

In the acquisition stage (see Fig. 4.1) the biometric trait is captured. In our case, the biometric trait is the MMW image of the body. After that, the image is processed obtaining a more suitable image to perform the feature extraction, which is the following step in Fig. 4.1. Next, the vector containing the features of the input image is compared with the feature vector of the claimed user (verification mode) or with all the feature vectors in the database (identification mode). Finally, a decision based on the result of that comparison is made.

The acquisition stage (which, in this work, corresponds to the simulation of the MMW images) was already explained in Sect. 3.3. The rest of the modules of the system are described in the next subsections: the image segmentation (Sect. 4.2) belongs to the preprocessing while the boundary extraction (Sect. 4.3), landmark generation (Sect. 4.4), feature generation (Sect. 4.5)

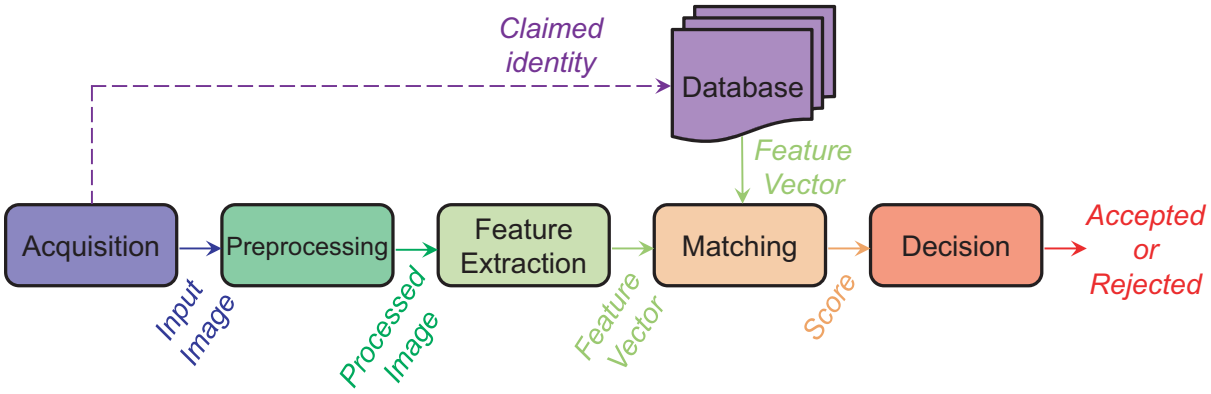

Figure 4.1: Architecture of a generic biometric system working either in verification or identification mode.

and feature selection (Sect. 4.6) are part of the feature extraction module. In Sect. 4.7 (matching) the similarity measure used to perform the comparison between feature vectors is introduced. The value of that similarity measure determines the final decision given by the system (Sect. 4.8).

It is worth mentioning that our system is based on the geometry of the user's body while the system developed by Alefs *et al.* in [9] is based on a holistic approach over the grayscale after various dimensionality reduction techniques. Specifically, in our system, the features extracted from the images are based on distances between points of the silhouette of the body or between points inside the silhouette. In fact, the use of anthropometric indications to recognize people started in the XIX century [46]. Moreover, there are biometric systems based on the geometry of the hand [47]. The process followed to obtain the features is depicted in Fig. 4.2.

4.2 Image Segmentation

The image segmentation is the main step of the image preprocessing module. In this process the input image is binarized, separating the background from the body. A characteristic of the images simulated by passive systems is the different gray level they present in different parts of the body. The ones oriented to the floor (e.g. the abdomen) are much darker than the ones oriented to the sky (e.g. the feet). This fact considerably hinders the segmentation process. This problem was overcome performing the segmentation in two steps:

- Border detection.
- Morphological operations.

The image segmentation comprises several steps, which are shown in Fig. 4.3. After inverting the gray level of the image (see Fig. 4.3(b)), a Canny border detector (whose parameters are previously tuned) is applied to the image (obtaining an image such as the one in Fig. 4.3(c)). Next, various morphological operations are conducted on the resulting border image to close the body boundary. These morphological operations consists of closing operations with different structural elements in different areas of the image (head, arms, from arms to calf, and feet). The resulting image is shown in see Fig. 4.3(d). Finally, the body contour, and any other contour, are filled, obtaining a binary image consisting of a white body, maybe some small white connected components and a black background. An example image after this segmentation process is shown in Fig. 4.3(e).

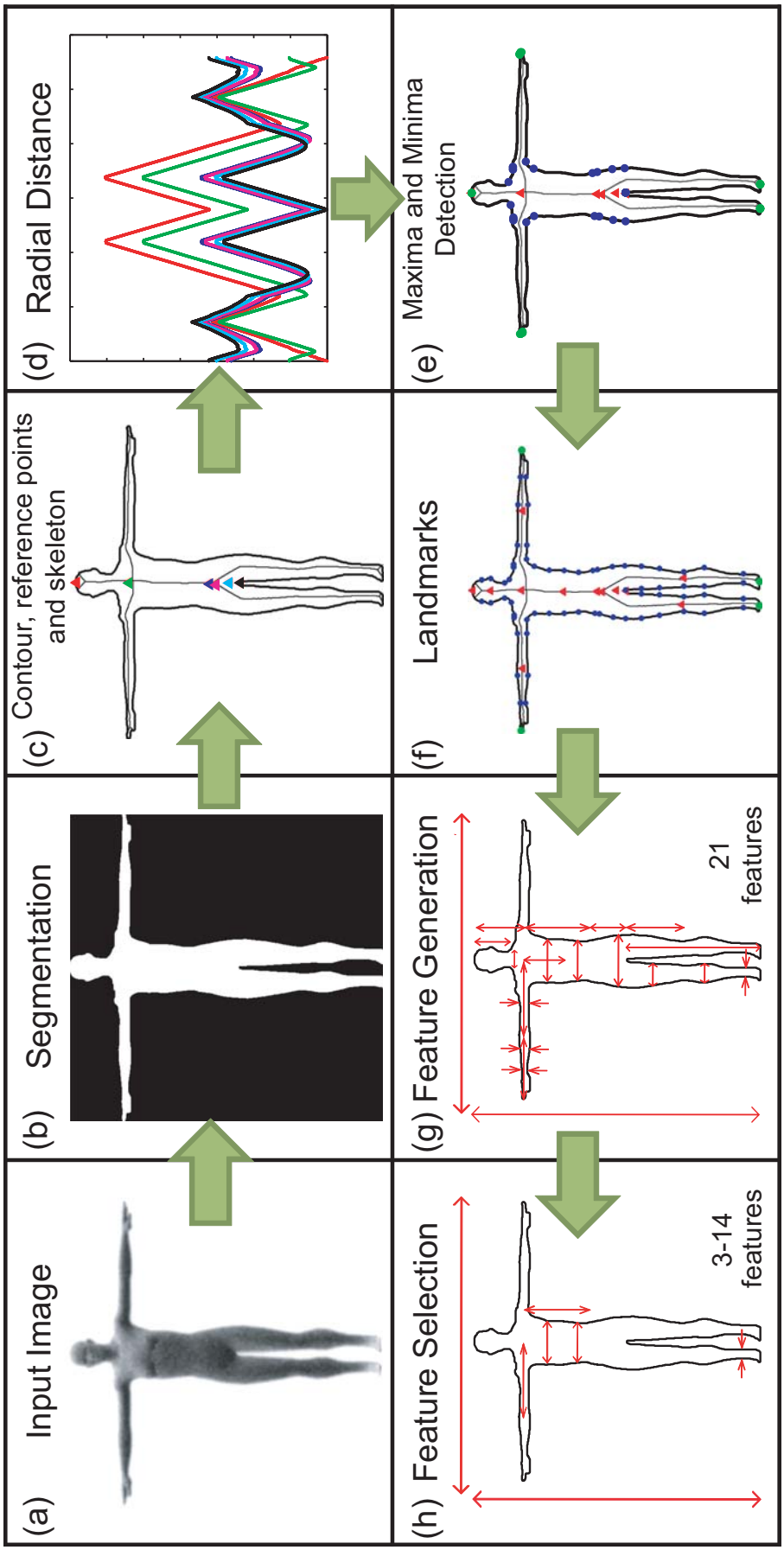

Figure 4.2: Feature extraction in our system: (a) Original image (of a subject with clothing and a camera angle of -10°), (b) segmented image, (c) contour, reference points and basic skeleton, (d) radial distance from each reference point to every point of the contour (one curve per reference point), (e) addition of points with maximum and minimum distance from the reference points, (f) all landmarks, (g) distances used to form the feature vector (with 21 components), and (h) the final selected features after applying the SFFS algorithm (between 3 and 14 components).

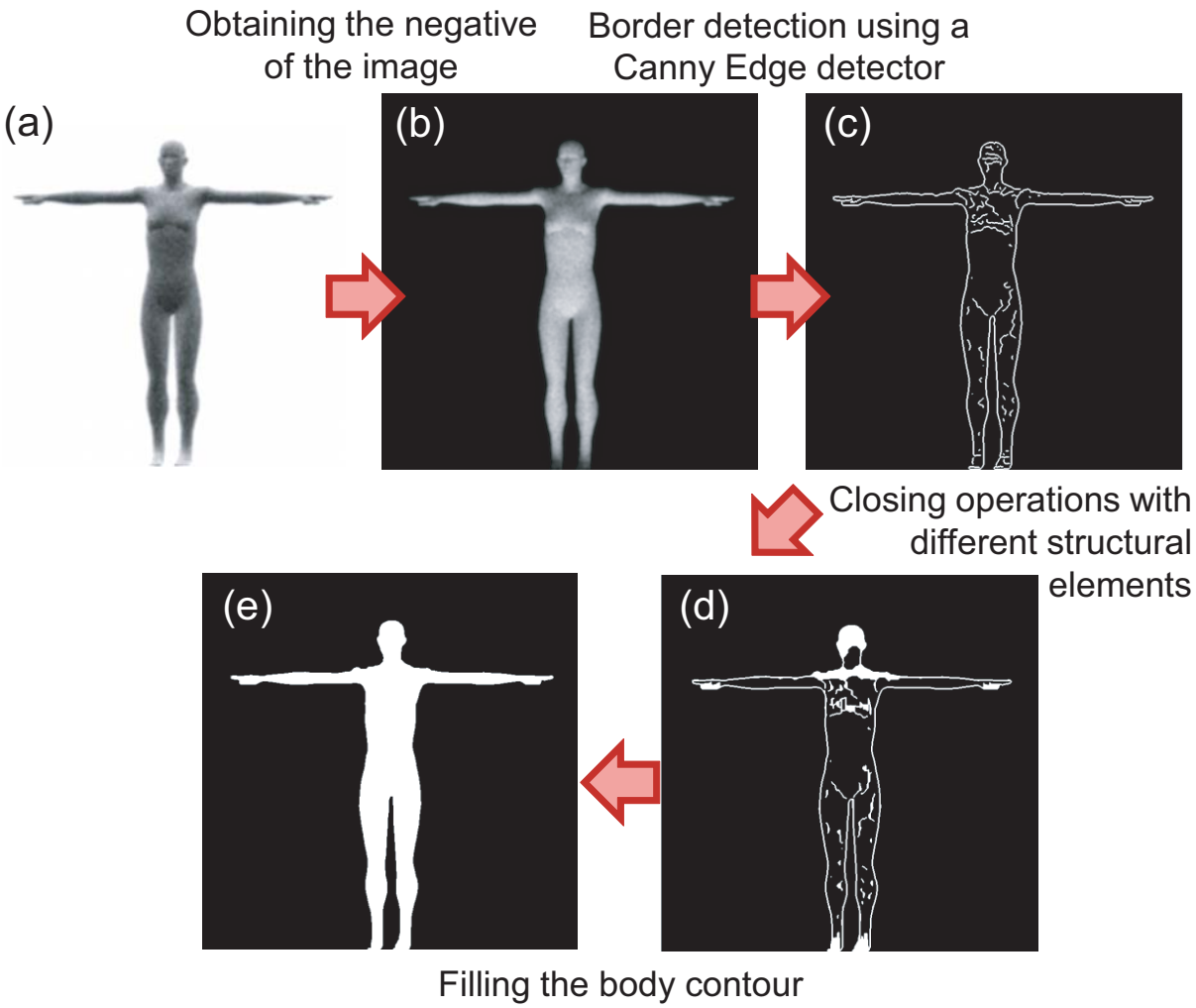

Figure 4.3: Segmentation process in our system: (a) Input image (of a subject with clothing and a camera angle of -10°), (b) negative of the input image, (c) image obtained after the application of the Canny Edge detector, (d) image obtained after closing the contour of the body, and (e) final binary image.

4.3 Boundary Extraction

Once the input image is properly segmented, only the largest connected component is considered, assuming that it is the body. Then, the body boundary is extracted. After that, the middle point of the top of the head is detected. This point is considered to be the first point of the extracted contour. The rest of the coordinates of the boundary are ordered in a clockwise direction. In addition to the boundary of the body, a basic skeleton of the body is obtained by means of morphological operations.

The Fig. 4.4(b) shows the contour of the body and the basic skeleton obtained after this stage.

4.4 Landmark Generation

The generation of the landmarks is composed of several steps, which are described below and shown in Fig. 4.5.

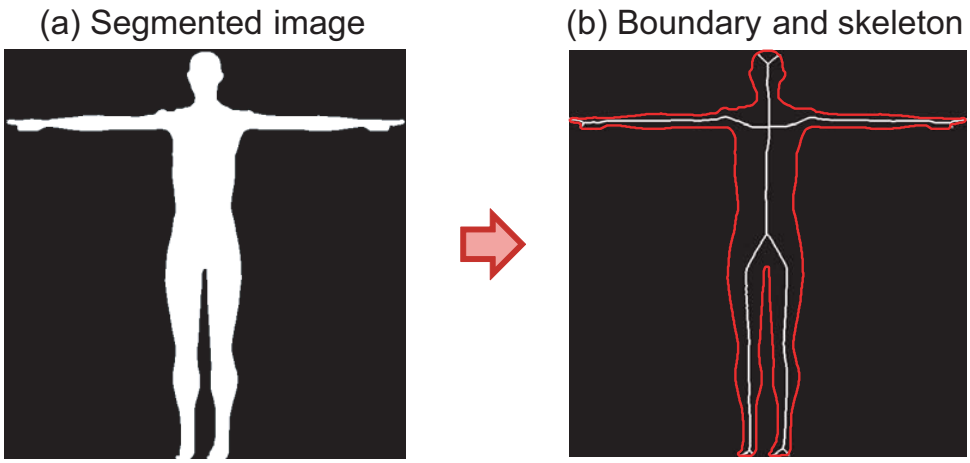

Figure 4.4: Boundary extraction in our system: (a) Segmented binary image and (b) extracted boundary (in red) and basic skeleton (in white).

First of all, six different reference points are considered:

1. The middle point of the top of the head.
2. The crossing point of the arms line and the vertical line of the torso.
3. The centroid of the body.
4. The bifurcation of the skeleton in the abdomen area.
5. The central point of a bounding box including the whole body.
6. The pubis.

An example image obtained after boundary extraction and the reference points detection is depicted in Fig. 4.5(a).

For each reference point, the Euclidean distance between the reference point and every point of the boundary is computed. Therefore, a one-dimensional function, showing the radial distance, is obtained for each reference point. An example of the six resulting radial distance functions is shown in Fig. 4.5(b). Every function is examined to find local maxima and minima. Maxima of the curve correspond to the head, hands, and feet outer points, while the minima correspond to points near the neck, shoulders, axilla, wrist and hips, depending on the considered reference point. Fig. 4.5(c) shows an example boundary together with the reference points and the maximum and minimum distance points.

In order to have enough geometric measures of the body, several extra points are detected inside the area of the body and in its boundary. To summarize, the following points are detected (see Fig. 4.5(d) and (e)):

- The centroid of some parts of the body: head, arms, torso and legs.
- Some points located at the boundary of the above mentioned body parts (for example in case of the torso, the points of the torso boundary located at three different heights are detected: at one quarter, at a half and at three quarters of the torso height.)

The Fig. 4.5(e) shows the complete set of landmarks generated for one user.

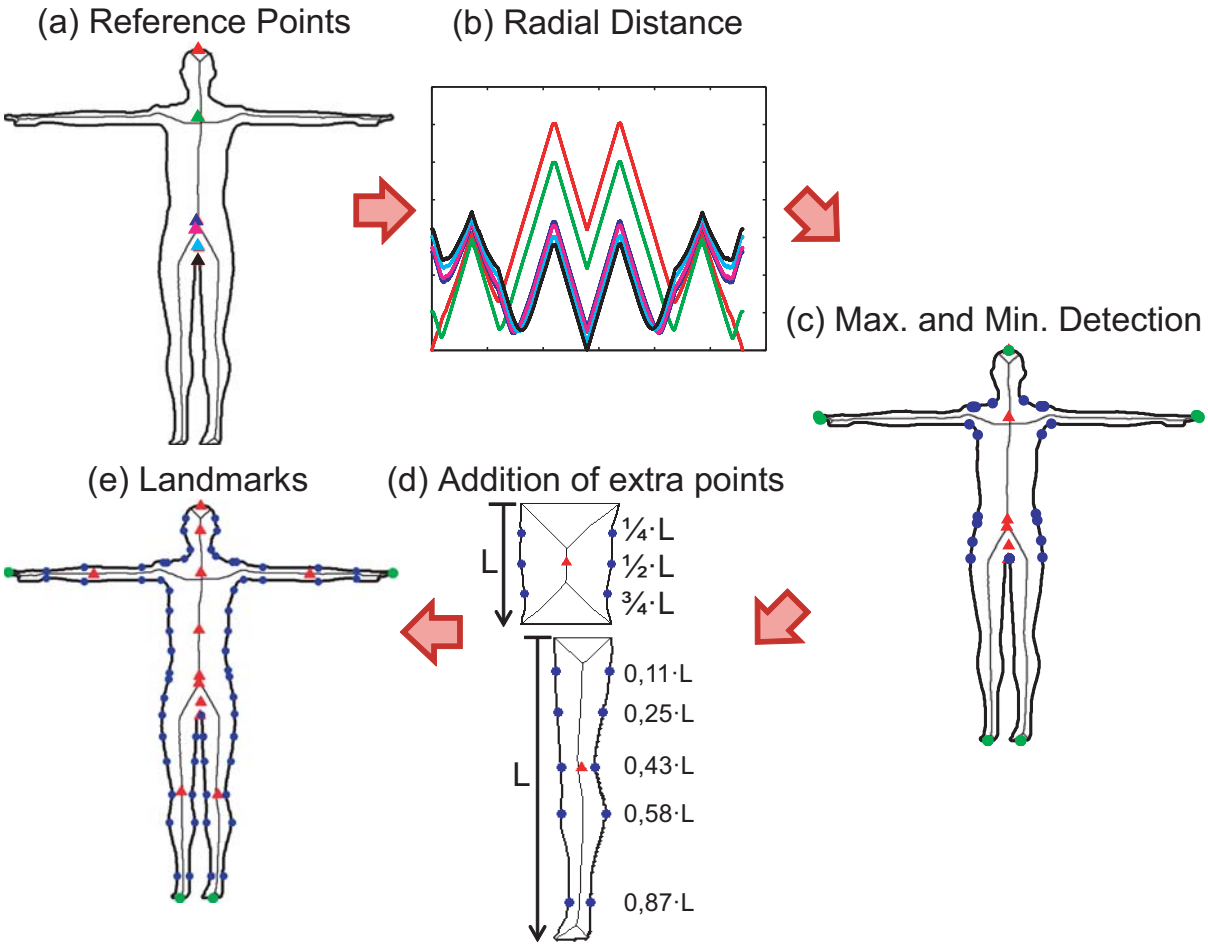

Figure 4.5: Landmark generation in our system: (a) Body contour, basic skeleton and reference points (triangles of different colors), (b) radial distance from each reference point to every point of the body contour (the color of each function matches the color of its corresponding reference point), (c) detection of points with the local maximum and minimum distance from the reference points (maximum distance points are depicted with green circle and minima distance points with blue circles), (d) example of addition of extra points in the torso and in the right leg, and (e) the whole set of landmarks.

4.5 Feature Generation

The Euclidean distance between some of the landmarks is calculated. Specifically, 21 distances are obtained, which constitutes the feature vector. Fig. 4.2(g) and Fig. 4.6 show the considered distances. In Fig. 4.6, next to every distance there is a number that represents the component number in the feature vector (e.g. the height is the first component of the feature vector, it is feature number 1).

4.6 Feature Selection

In order to find the most discriminative set of distance-based features, and therefore increase the performance of the biometric system, a feature selection is performed. In addition, by reducing the number of features the computational cost decreases too.

Among the different feature selection algorithms [48], the one employed in this work is the

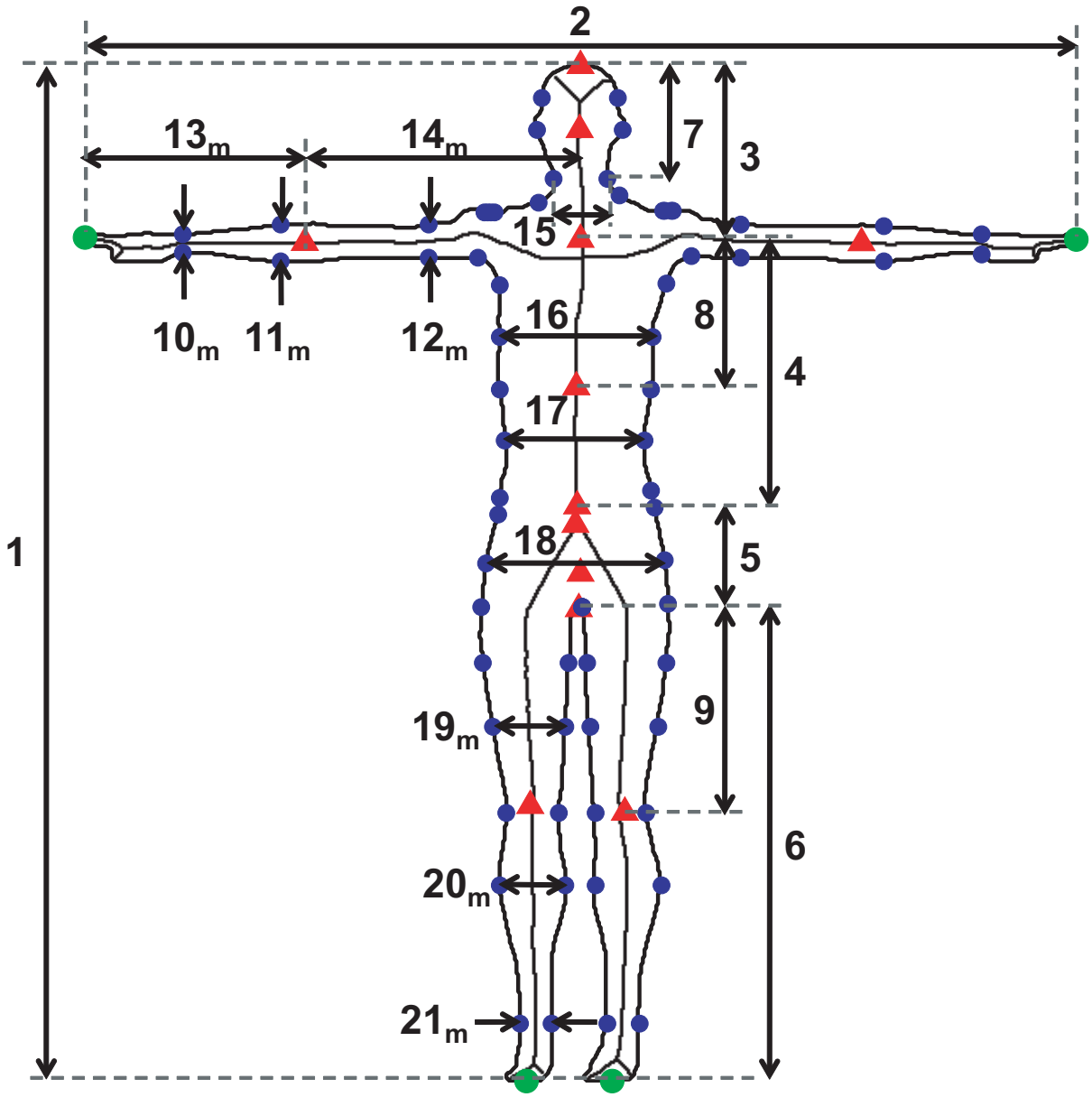

Figure 4.6: Body boundary, landmarks and distances extracted among them of the subject and conditions of Fig. 4.2. These distances form the 21D feature vector. The number next to every distance is the component number in the feature vector. The ones whose number appears with a subindex m are calculated as the average of that distance and the analog one of the right extremity. Red triangles represent the reference points and centroids of head, arms, legs and torso. Blue circles represent landmarks on the silhouette of the body (some of the them have minimum distance to the reference points). Green circles represent landmarks with maximum distance from the reference points.

Sequential Floating Forward Selection (SFFS) [49]. This suboptimal searching technique is an iterative process in which, in each iteration, a new set of features (whose choice is based on the results of previous subsets) is used to compute a certain criterion. This is done until the criterion does not improve. For more details see [48, 49, 50]. In our case the criterion is related to the performance of the system, in particular, is to minimize the value of the EER (Equal Error Rate), magnitude which will be introduced in Sect. 5.1.

Once the features are selected, the feature vector has, depending on the experiment, between

3 and 14 components, having around 6 components in most of the cases. The SFFS algorithm is able to provide the most discriminative set of features with a dimension specified by the user or with the dimension that gives the best value for the criterion (in that case the dimension is not specified). The latter approach was performed in our system. The Fig. 4.2(h) displays some of the most frequently selected features (distances).

4.7 Matching

As it is explained in Chapter 5, several experiments are performed on the developed system. The database is divided into training and test datasets. The training dataset is comprised of the images used to enroll the users in the system, while the test dataset corresponds to the images given by the user to verify his or her identity with the biometric system. For each user, a mathematical model is generated in the training dataset and another one is generated in the test dataset. Each model is simply the arithmetic mean feature vector of the considered images.

Considering one training model and one test model, either containing 21 components or just with the subset of features selected by SFFS, a similarity measure is computed between both of them. This similarity measure is called *matching score*. In our biometric system the matching score is the opposite of the Euclidean distance between the two vectors compared:

$$score(\mathbf{x}, \mathbf{t}) = -d(\mathbf{x}, \mathbf{t}) = -\sqrt{\sum_{i=1}^{L}(x_i - t_i)^2} \tag{4.1}$$

where $d(\mathbf{x}, \mathbf{t})$ is the Euclidean distance, L is the dimension of the feature vectors, x_i the i^{th} component of the vector $\mathbf{x}$, and t_i the i^{th} component of the model of the database $\mathbf{t}$. The reason for using the opposite is to have higher scores for more similar vectors.

4.8 Decision

The obtained scores are used to (i) decide wether the user is who he claims to be (verification) or to (ii) provide a list with the most likely identities (identification). In the verification mode, if the user score is higher than a certain threshold, the user is accepted as a genuine user.

5

Experiments and Results

This chapter is structured as follows. First, the performance evaluation of biometric systems is briefly introduced. Then, in order to have recognition results to compare with, the experiments carried out by *Alefs et al.* in [9] and their results are presented. Next, an analysis of the extracted features in our system is provided. Finally, verification and identification experiments, conducted over the developed system, are described. These experiments are intended to assess different problems. Each experiment includes protocol description, presentation of results and discussion. All the experiments were performed using (i) the 21 features extracted, and (ii) the features selected by the SFFS algorithm.

In the feature analysis, as well as in all the experiments, only images simulated by a passive system indoors and outdoors are considered. The results are shown exclusively for passive outdoors images, for indoors the results are quite similar. The same analysis for images simulated by active systems (indoors and outdoors) will be part of future work, in which a different image segmentation should be followed due to clearly visible differences between the images simulated by passive and active systems (e.g. the last ones present higher contrast).

5.1 Performance Evaluation of Biometric Systems

Once the system is implemented, an evaluation of its performance is desirable. This is done through quantitative measures, obtained from experiments, that reveal how well the system works and allow to compare its performance with the performance of other biometric systems.

5.1.1 Performance Evaluation in Verification Mode

When working in verification mode two main metrics are used to quantify the performance of the biometric system:

- The *False Acceptance Rate* (FAR), which is the probability that an impostor is accepted by the system as a genuine user.
- The *False Rejection Rate* (FRR), that reflects the probability that a genuine user is rejected by the system.

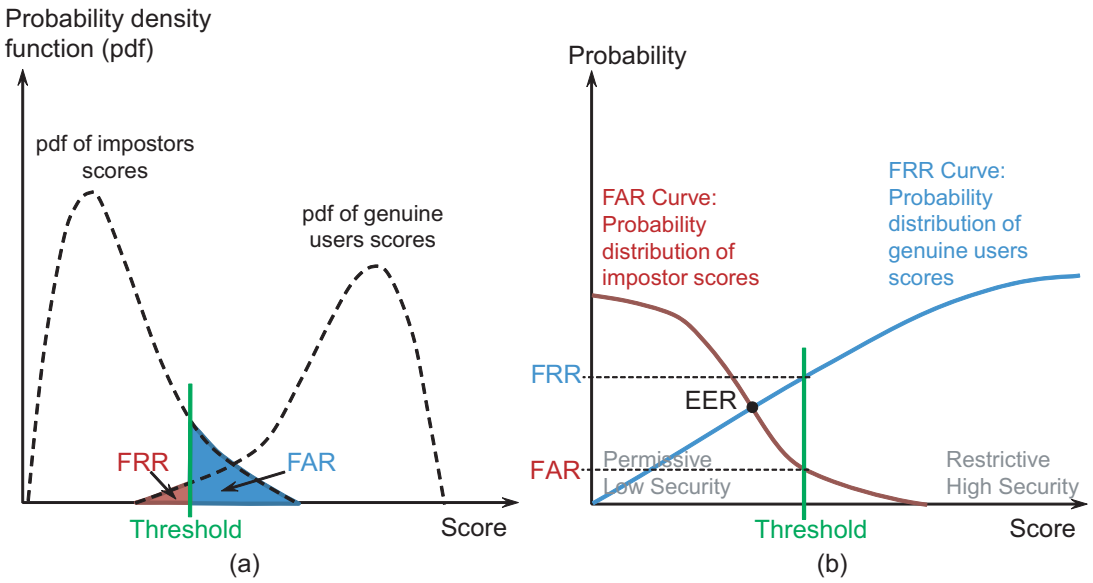

Figure 5.1: (a) Probability density functions and (b) probability distributions of genuine users and impostors. In (a), the shadowed areas are the FRR (the red one) and the FAR (the blue one). In (b), the value of FAR and of the FRR curves at the threshold value corresponds to the FAR an to the FRR respectively. The EER is the crossing point of both curves. The system works in the Permissive Low Security regime when the threshold value is low, and in the Restrictive High Security regime if the threshold value is high.

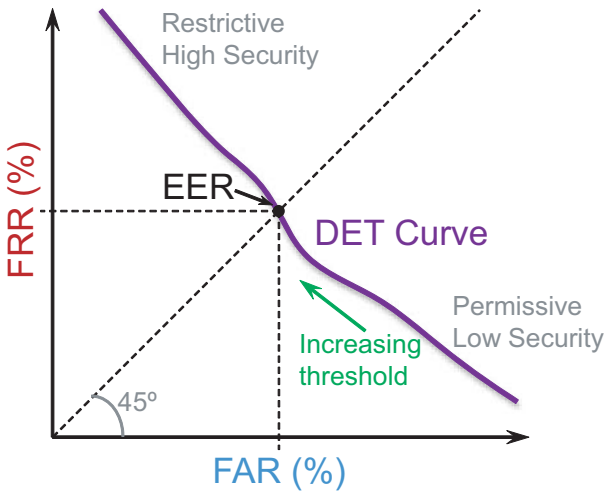

Figure 5.2: A generic DET curve. Both security regimes are shown together with the EER. Notice that it is not possible to simultaneously reduce both error rates, i.e. FAR and FRR. The axes are usually in logarithmic scale giving the value of FAR and FRR in %.

Fig. 5.1 shows the probability density functions and probability distributions of genuine users and impostors and their relationship with the FAR and FRR.

A certain value for the threshold is used to make a decision about the user identity: if the score obtained after the comparison is lower than the threshold, then the user is rejected, and he or she is accepted as a genuine user if it is higher than the threshold. If the selected threshold value increases, the FRR increases too but the FAR decreases. In that case we are in the *Restrictive High Security regime*: the system becomes more secure by rejecting more genuine users and accepting less impostors. The opposite behavior occurs if the threshold is reduced:

the FRR decreases and the FAR increases, being in the *Permissive Low Security regime*: the system becomes less secure accepting more impostors. This is graphically shown in Fig. 5.1(b).

There is a value of the threshold for which the FAR and the FRR coincide. The value of both rates at that threshold is known as the *Equal Error Rate* (EER) and is the most widely used parameter to evaluate the performance of a biometric system working in verification mode. Plotting the FRR versus the FAR for all the different threshold values with logarithmic axes, gives the so-called DET curve (*Detection Error Tradeoff* curve) [51]. This curve is a common way to graphically represent the behavior of a biometric system, where the EER corresponds to the point where the DET curve and the bisector of the first quadrant intersect each other (See Fig. 5.2). The closer the curve is to the origin (and therefore the lower the EER is), the better the system is.

5.1.2 Performance Evaluation in Identification Mode

In identification mode, the sytem compares the model (or feature vector) created from the input data with all the models (or features vectors) stored in the database. Then, a ranked list of candidates is returned. At the top of the list is located the candidate that produces the highest score, followed by the candidate that provides the second highest score, and so on. If the most similar model corresponds to the input identity, then a successful identification has happened.

For this mode, the error measure is computed as the rate of correctly identified users. The *Rank-1 recognition rate* (*R-1*) is the number of users correctly identified with the first candidate of the list over the total number of users, N, the *Rank-n recognition rate* (*R-n*) is the number of users correctly identified with any of the n first candidates of the list, over N. The *R-1* and *R-5* are the most used recognition rates in identification mode.

The performance of a system working in identification mode is graphically shown by means of the so-called CMC (*Cumulative Match Curve*) (See Fig. 5.3). This curve plots the *R-n* versus n (being n the number of the candidates considered at the beginning of the list). The CMC is an increasing function whose value increases from the *R-1* at the beginning (where n=1, only the first user of the list is considered) to 1 at the end (where n=N, all the users are considered, hence the user is one of them). The closer to 1 the CMC is, the better the system is.

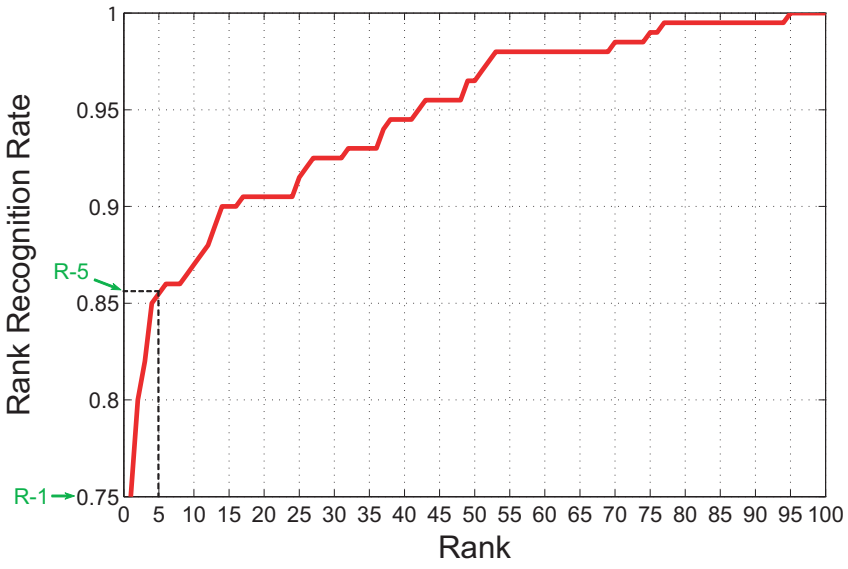

Figure 5.3: A generic CMC curve. The *Rank-1* and *Rank-5 recognition rates* are indicated. In this case the total number of users is 100.

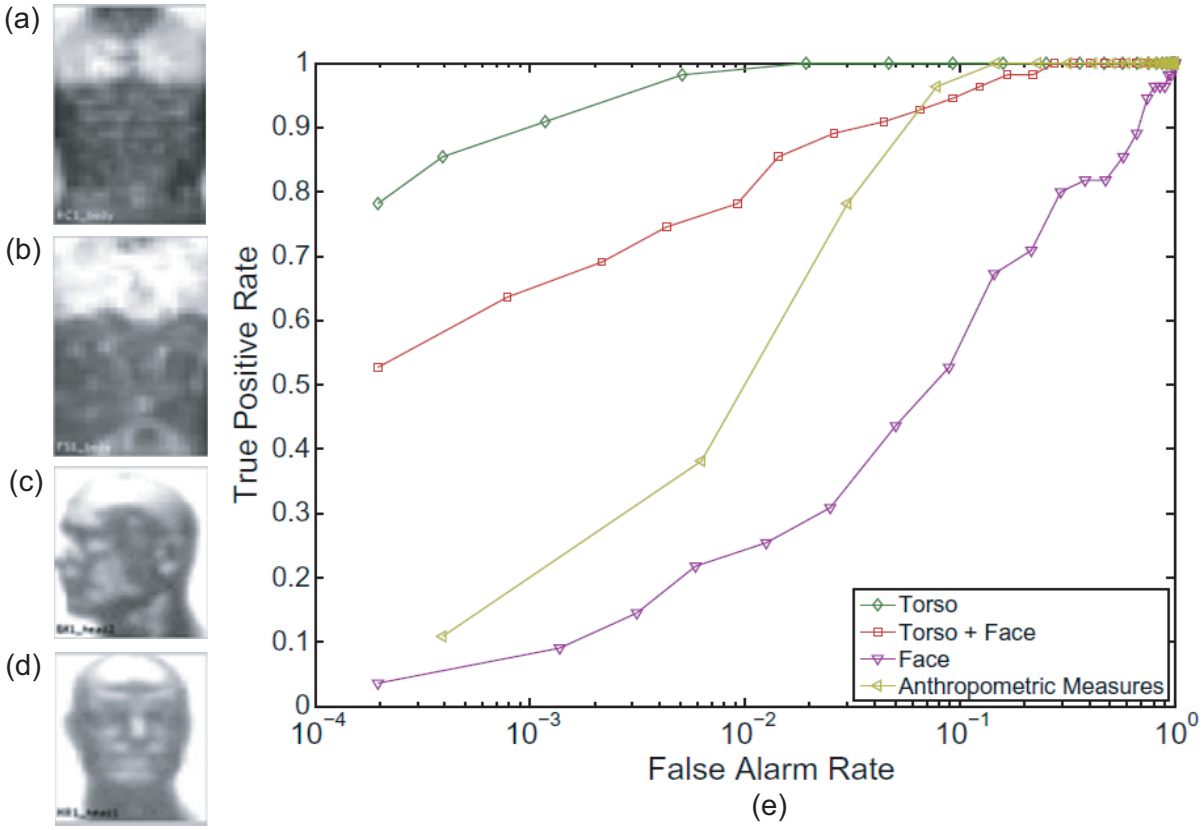

Figure 5.4: MMW images and recognition results obtained in [9] by Alefs *et al.*. (a, b) Thorax images, (c) head image in side view, (d) head image in frontal view, and (e) recognition results as ROC curves for the image regions and anthropometric data.

5.2 Experiments and results obtained by Alefs *et al.*

Alefs *et al.* in [9] conducted recognition experiments using the TNO database described in Sect. 3.2. The work is focused on the use of thorax and face MMW images as biometric traits, applying on them an holistic approach called Multilinear Analysis [52]. Additionally, anthropometric features were also compared to the main approach based on Multilinear Analysis. In total, 11 anthropometric measures were derived from manually annotated characteristic points in the face, torso and arms. The distances include measures such as the hip width, the shoulder width and the head width in frontal and side view.

In their experiments, the training images are recordings without disguise, and the results are presented as *Receiving Operating Characteristics* (ROCs) (See Fig. 5.4). In this kind of representation, the *True Positive Rate* (TPR) is plotted versus the *False Alarm Rate* (FAR). The TPR is the rate of genuine attempts accepted, therefore corresponds to 1-FRR. The False Alarm Rate is the same as the False Acceptance Rate, hence the same abbreviation (FAR) is used.

According to Fig. 5.4, for a 0.98 TPR, the anthropometric measures discriminate with a 0.1 FAR (10%), face discriminates worse, and the thorax region gives the best performance: 0.01 FAR (1%). The combination of face and torso does not improve the performance of the thorax region itself.

In terms of EER, for the case of the torso, we have:

$$\text{TPR} = 0.98 \text{ when FAR} = 0.01 \tag{5.1}$$

then the FRR is:

$$\text{FRR} = 1 - \text{TPR} = 1 - 0.98 = 0.02 \tag{5.2}$$

and therefore, as the EER is the value of FRR and FAR when they coincide, the EER must has a value between 1 and 2%:

$$\text{EER(Thorax)} \in [1, 2]\% \tag{5.3}$$

The exact value of the EER is difficult to obtain from the given graphical results. Finally from Fig. 5.4 we can also observe that the other approaches give worse EERs:

$$\text{EER(Thorax)} < \text{EER(Anthropometric Measures)} < \text{EER(Torso + Face)} < \text{EER(Face)} \tag{5.4}$$

5.3 Feature Analysis

Before computing the recognition capabilities of the developed system, some experimental validations are performed on the extracted features to:

- Determine wether they are discriminative enough.
- Find the most discriminative ones.
- Quantify their discrimination power.

5.3.1 Ranking of features according to their discrimination power

Fig. 5.5(a) represents the mean value and the standard deviation (as an error bar) of each normalized component (distance) of the feature vector, for seven subjects (a different color and symbol for each subject) randomly selected from the 50 available. As it can be seen, some component values are quite different from one subject to another, while others are more similar. Moreover, the error bars overlap in some cases. To determine the most discriminative features, the components of the feature vector are ranked in descending order of degree of discrimination. For this purpose two magnitudes are calculated:

- **The average separation** between the mean values of each component from all subjects.
- **The overlap** between the error bars of the same component among all subjects.

The most discriminative feature will be the one with the largest average separation and the lowest overlap among different users. Hence, the features are ranked in descending order of their discrimination power. This magnitude can be considered as the value of the quotient:

$$\text{discrimination power} = \frac{\text{average separation between mean values}}{\text{overlap of errors bars}} \tag{5.5}$$

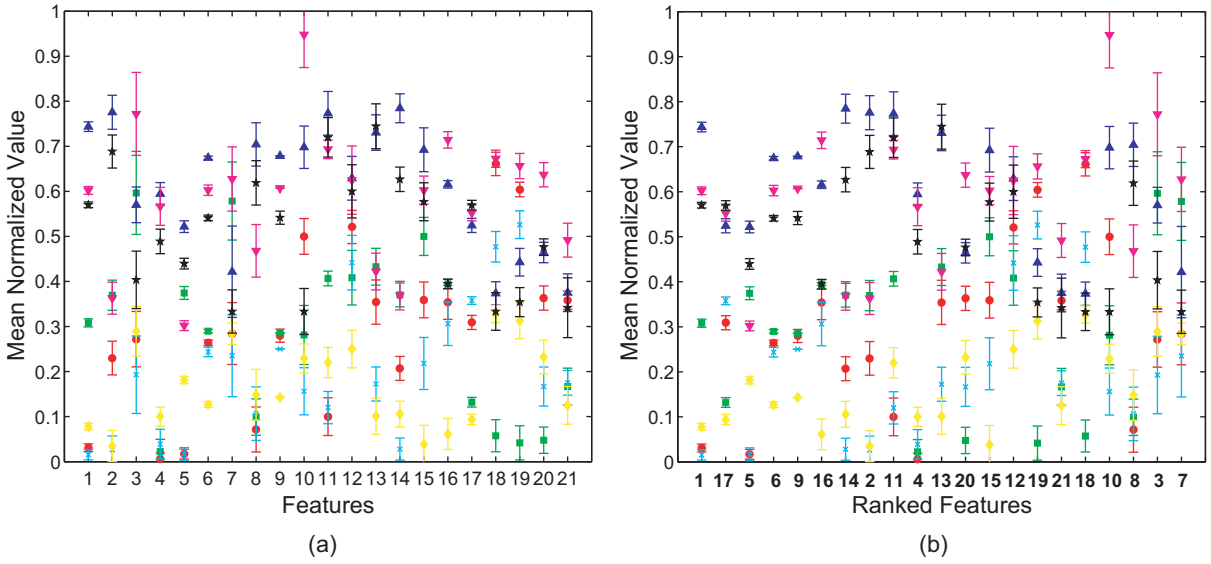

Figure 5.5: Mean normalized value of the feature vector of 7 randomly selected users. Each user vector has a different color and symbol. In (a) the features are ordered according to their number while in (b) they are ranked in descending order of their discrimination power.

Fig. 5.5(b) shows the feature vector for the same seven subjects of Fig. 5.5(a) once its components have been ordered. Although the Fig. 5.5(b) shows the feature vector for 7 users, the ranking was conducted taking into account the vectors from all the 50 subjects. It can be seen the decreasing separation between mean values and the increasing overlap. The initial feature number (the same one as the one in Fig. 4.6) is written below the x axis with bold numbers. It is worth noting that the four most discriminative features (the first four in Fig. 5.5(b)) are:

- Feature #1: the height.
- Feature #17: approximately the waist width.
- Feature #5: the distance between the centroid of the body and the pubis.
- Feature #6: the legs length.

The least discriminative one corresponds to feature #7, which is the height of the head. Furthermore, the three best features and the worst one, obtained for images simulated by passive systems outdoors, are the same ones when using images simulated indoors. It is not surprising that the height of the head is the least discriminating feature due to the process followed to obtain the 3D-body model from the body measures of real subjects. The head height was not considered, so all the models present approximately the same head height in their 3D body model used to simulate MMW images.

5.3.2 Discrimination Power Analysis

With the purpose of better assessing the discrimination power of the features, they are plotted in 2D graphs in Fig. 5.6:

- Fig. 5.6(a) plots the second PCA (*Principal Component Analysis*) component vs the first PCA component of the 300 feature vectors (6 per user), having used all the 21D vectors to obtain the PCA transformation matrix.

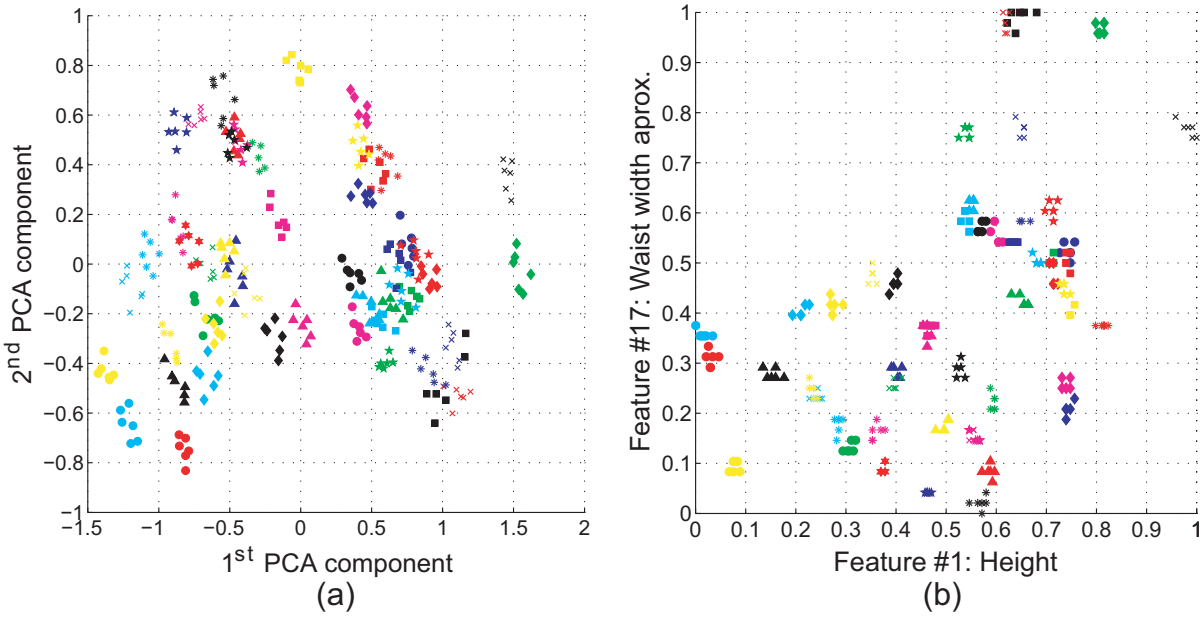

Figure 5.6: Two-dimensional representation of the discrimination power of the extracted features. (a) Second PCA component vs the first PCA component of the 300 feature vectors (6 per user). (b) Second most discriminative feature (waist width aprox.) vs the most discriminative one (the height). In both plots every user has its own color and symbol.

- Fig. 5.6(b) plots the second most discriminative feature (waist width aprox.) vs the most discriminative one (the height).

In both plots every user has its own color and symbol, so every user should be represented by a cluster of symbols with the same color and shape. In both cases, Fig. 5.6(a) and Fig. 5.6(b), it is patent that the clusters are clearly separated. Only in some regions of the 2D subspace some clusters overlap. This fact proves that the selected features are discriminative. Comparing both plots, it seems that the clusters in Fig. 5.6(b) are smaller and more separated among them than in Fig. 5.6(a). This reveals that even with only two features (height and waist width) it would be possible to distinguish different users. It must be noted that this analysis validates the proposed features but does not estimate their practical recognition capabilities. This is done in the following sections, in particular in sections 5.5, 5.6, 5.7 and 5.8.

5.4 Experiments to assess different problems

5.4.1 Effects

The experiments conducted in this project are intended to show how the recognition capabilities of the developed system are affected by different effects. In particular the effects analyzed in the following experiments are the influence of:

- The clothing and camera angle variability between the train and test images.
- Incorporating clothing and angle variability into training.
- The number of training and test images.

The first experiment is carried out to obtain the baseline performance of the system, then three more experiments are conducted to analyze the previous effects (one experiment per effect). The results obtained in each experiment will be compared with the baseline performance, and finally the results will be compared with the other experiments' results.

5.4.2 Notation

For each user, the BIOGIGA database has 6 MMW images simulated with a passive system outdoors:

- 3 images of the user wearing clothing and a camera angle of of -10°, 0° and +10°.
- 3 images of the user without clothing and a camera angle of of -10°, 0° and +10°

With these six kinds of images there is a large casuistry of experiments that can be carried out. We will focus on some relevant cases.

In order to have a compact notation, we will refer to each possible case with these abbreviations:

- **Number of train and test images:** ***#train images : #test images***.
- **Clothing:** Images of a user without clothing will be denoted as ***sr***, and ***cr*** will be used for images of users wearing clothing. (These abbreviations come from the Spanish expressions "sin ropa" (without clothing) and "con ropa" (with clothing)).
- **Angles:** They will be denoted with different letters: $\boldsymbol{a}$, $\boldsymbol{b}$ and $\boldsymbol{c}$, and with an asterisk ($\boldsymbol{*}$). Each letter does not refer to a specific angle, but they will be used only to show whether the considered angle is the same to other angle referred before or not. The asterisk is used to express that the three possible angles are considered. The three letters and the asterisk will appear as subindexes.

For instance:

- For the experiment in which there are two train images, both with clothing, but with different angle, and there is only one test image without clothing having any of the three angles, then, we will have *2:1* and $(cr_a, cr_b) : sr_*$.
- For the experiment in which there are two train images, both with clothing, but with different angle, and there is only one test image with clothing too, having an angle different to the angles of the train images, then, we will have *2:1* and $(cr_a, cr_b) : cr_c$.

5.5 Experiment 1: Baseline Performance

The aim of this initial experiment is to compute the baseline performance of the system. This performance is established as a reference performance to compare with next experiments' behavior.

5.5.1 Protocol Description

To obtain the baseline performance, two different types of experiments are considered, both of them favorable to the system:

1. Experiment 1-1: One train and one test image, both with **the same clothing condition**: both images with clothing, or both without clothing.
2. Experiment 1-2: One train and one test image, both with **the same camera angle**: both with -10°, 0° or +10°.

Notice that due to the scarcity of images, when we consider images both with the same clothing condition, they will have different angle, and viceversa. There will be 12 different combinations for the first case and 6 for the second case:

- For experiment 1-1 (same clothing condition) $cr_a : cr_b$ (gives 6) and $sr_a : sr_b$ (gives other 6)
- For experiment 1-2 (same camera angle): $cr_a : sr_a$ (gives 3) and $sr_a : cr_a$ (gives 3 too).

5.5.2 Results

The identification and verification performances are shown in Table 5.1 as numerical results. The features selected by the SFFS algorithm are also included in the table. In this table, as well as in the tables of the remaining experiments, the selected features appear in the order they were selected. Moreover, the most frequently selected features are presented in bold font. The identification performance is plotted in Fig. 5.7 as CMC curves while the Fig. 5.8 shows the DETs curves (verification).

5.5.3 Discussion

The R-1 and R-5 are higher than 0.99 (99%) in all cases, revealing a very good **identification** performance of the system. Regarding the **verification** performance, the EER is quite low (around 1%) if all the 21 features are considered. When applying the SFFS algorithm, different features are selected in each experiment, providing improved values of the EER (0.33% and 0.03%).

Comparing the results of the experiment with the same clothing condition (exp.1-1) versus the results of the experiment with same angle (exp.1-2), we obtain that:

- When considering **all the features**, the identification as well as the verification performances, are slightly higher with the same clothing condition.
- When considering only the **features selected by the SFFS algorithm**, the identification and the verification performances, are both higher with the same camera angle (specially the EER is much lower: from 0.33% to 0.03%).

Anyway, these behaviors are not completely representative because of (i) the small size of the database, and (ii) the differences in the performances are small.

Concerning the **feature selection**, there are four features that are selected in both experiments: the height (feat.#1), the waist width (feat.#17), the chest width (feat.#16) and the

Experiment 1: Baseline Performance									
			With all features			With features selected by SFFS			
Exp.	Effect	Protocols	R-1	R-5	EER(%)	Selected Features	R-1	R-5	EER(%)
1-1	=Cloth	$cr_a : cr_b$, $sr_a : sr_b$	0.99	0.99	1.00	**1**, **17**, **14**, 4, **16**, 12	0.99	1.00	0.33
1-2	=Angle	$cr_a : sr_a$, $sr_a : cr_a$	0.99	0.99	1.33	2, **1**, **17**, **14**, **16**	1.00	1.00	0.03

Table 5.1: Experiment 1 (Baseline Performance): Identification, verification and SFFS feature selection numerical results. As in the following tables, the most frequently selected features are written in bold fonts.

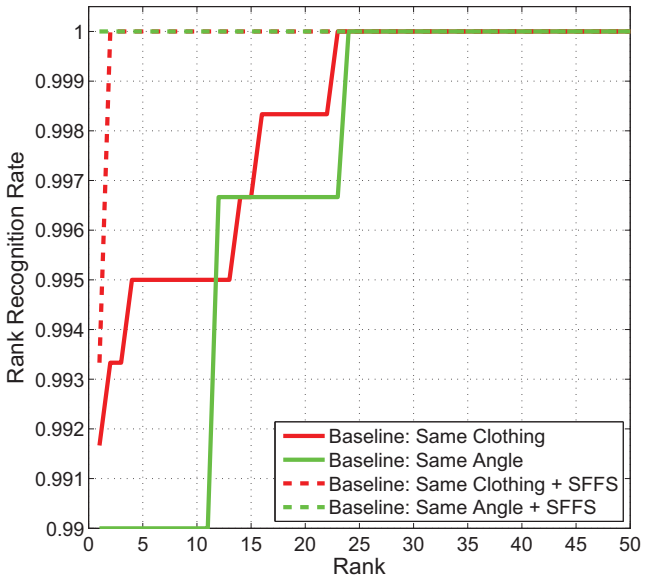

Figure 5.7: Experiment 1 (Baseline Performance): CMC curves.

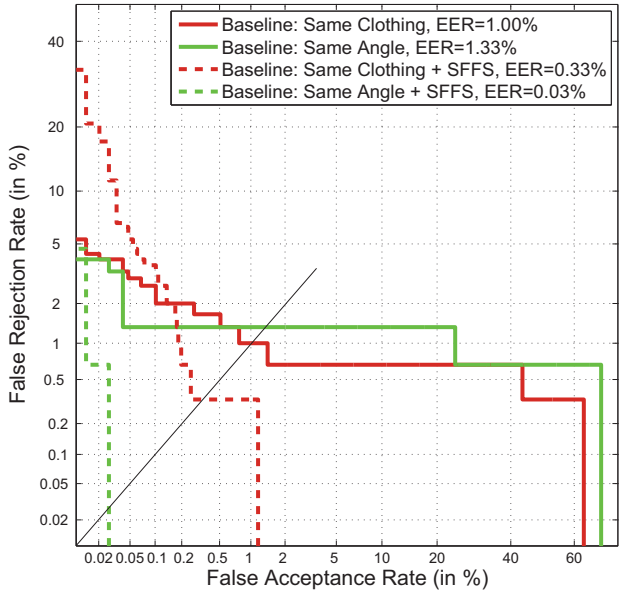

Figure 5.8: Experiment 1 (Baseline Performance): DET curves.

elbow-neck distance (feat.#14). These features are not exactly the same as the four most discriminative ones of Fig. 5.5(b). That is because the SFFS selects the most discriminative *set* of features for each experiment. That is, a group of uncorrelated features that optimizes the verification performance for an specific protocol. This group does not necessarily match the most discriminative features when considering them independently, which are the first four of Fig. 5.5(b): the height (feat.#1), the waist width (feat.#17), the waist-pubis distance (feat.#5) and the leg length (feat.#6).

The obtained results are similar and even better to those obtained by Alefs *et al.* in [9] (with an EER around 1-2%). However, it must be noticed that, in general, the high performance obtained is partially due to the fact that the images are synthetic. In addition, the huge improvement in the verification results when selecting features, can be also due to the fact that the SFFS algorithm uses all the images involved in the experiment and optimizes the EER on them. Rigorously, the SFFS algorithm should be applied to an independent development data set. Due to the small size of the data base, that was not possible in our experiments. Anyway, although the error rates are optimistically biased, the main objective was to identify the most discriminative features, which has been done even without considering that development set.

5.6 Experiment 2: Clothing and Angle Variability between Train and Test

One of the main advantages of using MMWs in biometric recognition is their ability to pass through clothing and other dielectric materials. The first purpose of this experiment is to quantify the **effect of clothing** in the recognition performance using MMW images, which should be very little due to the almost total transparency of clothing in this spectral band.

The second aim of this experiment is to assess the **influence of the camera angle** in the performance of the system. This is a situation very common in the practice because the user does not always stay in front of the imaging system maintaining the same angle.

5.6.1 Protocol Description

For each user the BIOGIGA database counts with 3 images without clothing (and different angles) and 3 more with clothing (and different angles too). Therefore, to compute the effect of the clothing in the recognition performances, the system will be trained with an image with clothing and tested with an image without it, and viceversa. Specifically, this protocol will be used: $cr_a : sr_b$ (6 different combinations) and $sr_a : cr_b$ (other 6 combinations) (see Sect. 5.4.2 for notation).

Notice that the previous protocols are:

- Equal to the ones used in the experiment 1-1 (baseline performance with the same cloth condition): $cr_a : \mathbf{c}r_b$ and $sr_a : \mathbf{s}r_b$, but changing the clothing in the right side of the colon (bold letters).
- Equal to the ones used in the experiment 1-2 (baseline performance with the same camera angles): $cr_a : sr_{\mathbf{a}}$ and $sr_a : cr_{\mathbf{a}}$, but changing the angle in the right side of the colon (bold letters).

Experiment 2: Clothing and Angle Variability between Train and Test									
			With all features			With features selected by SFFS			
Exp.	Effect	Protocols	R-1	R-5	EER(%)	Selected Features	R-1	R-5	EER(%)
2	$\neq$Cloth, $\neq$Angle	$cr_a : sr_b$, $sr_a : cr_b$	0.98	0.99	1.33	**1**, **17**, **16**, **14**, 4	0.97	1.00	0.50

Table 5.2: Experiment 2 (Clothing and Angle Variability between Train and Test): Identification, verification and SFFS feature selection numerical results.

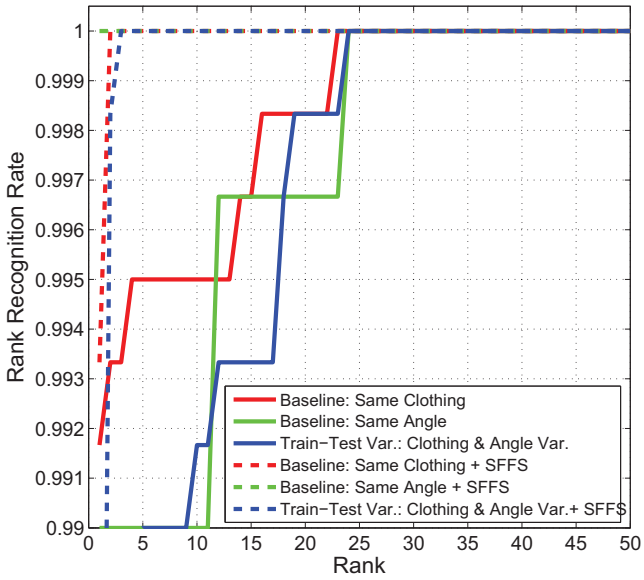

Figure 5.9: Experiment 2 (Clothing and Angle Variability between Train and Test): CMC curves.

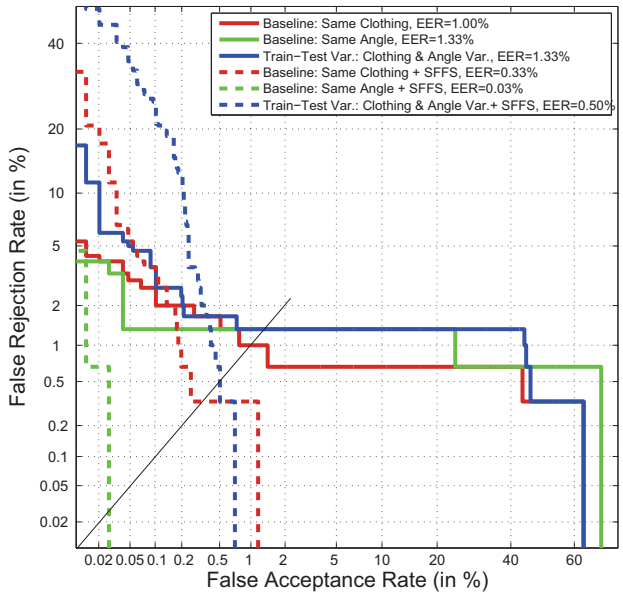

Figure 5.10: Experiment 2 (Clothing and Angle Variability between Train and Test): DET curves.

Exp.1 (Baseline Performance) vs Exp.2 (Clothing and Angle Variability between Train and Test)									
			With all features			With features selected by SFFS			
Exp.	Effect	Protocols	R-1	R-5	EER(%)	Selected Features	R-1	R-5	EER(%)
1-1	=Cloth	$cr_a : \mathbf{c}r_b$, $sr_a : \mathbf{s}r_b$	0.99	0.99	1.00	**1**, **17**, **14**, 4, **16**, 12	0.99	1.00	0.33
1-2	=Angle	$cr_a : sr_{\mathbf{a}}$, $sr_a : cr_{\mathbf{a}}$	0.99	0.99	1.33	2, **1**, **17**, **14**, **16**	<u>1.00</u>	<u>1.00</u>	<u>0.03</u>
2	≠Cloth, ≠Angle	$cr_a : sr_b$, $sr_a : cr_b$	0.98	0.99	1.33	**1**, **17**, **16**, **14**, 4	0.97	1.00	0.50

Table 5.3: Comparison of Experiment 1 (Baseline Performance) vs Experiment 2 (Clothing and Angle Variability between Train and Test): Identification, verification and SFFS feature selection numerical results. The different parameters between the protocols of exp.1-1 and exp.2 and between the exp.1-2 and exp.2 are in bold letters. The underlined results correspond to best results obtained so far. Again, the most frequently selected features are in bold fonts.

Therefore:

- By comparing the results from **exp.2** vs the results from **exp.1-1** we will obtain the influence of the **clothing**.
- By comparing the results from **exp.2** vs the results from **exp.1-2** we will obtain the influence of the **angle**.

5.6.2 Results

The recognition performances of exp.2 are presented in Table 5.2, in a CMC curve (Fig. 5.9) and in a DET curve (Fig. 5.10). In both figures the baseline curves are also plotted for reference.

5.6.3 Discussion

As it was already explained, to assess the influence of the **clothing**, we should compare the results obtained in exp.2 with the ones obtained in the **exp.1-1** (the one with the same cloth condition in Table 5.1). On the other hand, to evaluate the effect of the **camera angle**, the results of exp.2 should be compared with the results of **exp.1-2** (that has the same angle).

To better compare the results see Table 5.3 where the results of experiment 1 (exp.1-1 and exp.1-2) and experiment 2 are summarized. According to these results (exp.1-1 vs exp.2), it can be seen that the **clothing variability** worsens a little the performance of the system, as it was expected: the almost-inappreciable influence of the clothing in the images only slightly reduces the performance of the system. In verification mode the EER increases from 1.00% to 1.33% when all the features are used, and from 0.33% to 0.50% when the SFFS algorithm is applied.

To quantify the effect of the **change in the angle** between the train and the test images, we should compare the results of the experiment 2 with the results of the experiment 1-2 (see Table 5.3). The results show that when having different angle the performance is approximately the same if the 21 features are considered, and decreases significantly when the SFFS-selected features are used (in that case the EER increases from 0.03% to 0.50%). This is not surprising because when the camera angle is different between the train and the test images, then, some features (body measures taken from the silhouette of the body) change, specifically the horizontal measures, reducing the performance of the system. In fact, among all the experiments performed so far, the one that provides the best performance is the one with the same angle in the train and test images using SFFS (recognition rates R-1=R-5=1.00=100%, and EER=0.03%, which are underlined in Table 5.3).

As a result we can conclude that the proposed system is very robust against clothing variability, but no so effective under angle variability.

Finally, the **features selected** by the SFFS algorithm are approximately the same ones as the ones selected in both baseline experiments.

5.7 Experiment 3: Clothing and Angle Variability in Training

Only one training image per user has been used in the previous experiments, however, it is possible to use more than one, if available. Furthermore, these training images can present different properties among them. The aim of this experiment is quantify the effect of incorporating clothing and/or angle variability into and among the training images.

5.7.1 Protocol Description

In order to assess the clothing and/or angle variability in the training images there are many possible protocols that can be taken into account. We will consider the ones below, all of them use two images per user as training set and only one test image:

- Experiment 3-1: **Same clothing condition** and **different angle** in the training images: $(cr_a, cr_b) : cr_c$ and the same without clothing: $(sr_a, sr_b) : sr_c$ (6 combinations in total).
- Experiment 3-2: **Different clothing condition** and **same angle** in the training images: $(cr_a, sr_a) : cr_b$ and $(cr_a, sr_a) : sr_b$ (12 combinations in total).
- Experiment 3-2: **Different clothing condition** and **different angle** in the training images: $(cr_a, sr_b) : cr_{b/c}$ and $(cr_a, sr_b) : sr_{a/c}$ (24 combinations in total).

As explained in Sect. 4.7, in order to generate the model of multiple feature vectors, we just take the mean feature vector.

5.7.2 Results

The Table 5.4 includes the recognition and feature selection numerical results of the experiment 3. To better compare those results with the baseline performances, the results of the baseline are also included in the table. The identification performance of experiment 3 is graphically shown as CMC curves in Fig. 5.11, while verification performance is presented as DET curves in Fig 5.12.

5.7.3 Discussion

The R-1 and R-5 is 0.99 or higher while the EER is lower than 1.50% for all the cases of experiment 3. This proves an excellent performance of the system under these conditions.

When comparing the results with the baseline performance, it can be seen that the **identification** performance of the experiment 3 is quite similar to the baseline's. However, for the **verification** performances, there are different behaviors depending on the use of (i) all the features or (ii) the ones selected by SFFS, and depending on the specific protocol. When **all the features** are considered:

Exp.1 (Baseline Performance) vs Exp.3 (Clothing and Angle Var. in Training)									
			With all features			With features selected by SFFS			
Exp.	Effect	Protocols	R-1	R-5	EER(%)	Selected Features	R-1	R-5	EER(%)
1-1	=Cloth	$cr_a : cr_b$, $sr_a : sr_b$	0.99	0.99	1.00	**1**, **17**, **14**, 4, **16**, 12	0.99	1.00	0.33
1-2	=Angle	$cr_a : sr_a$, $sr_a : cr_a$	0.99	0.99	1.33	2, **1**, **17**, **14**, **16**	1.00	1.00	0.03
3-1	=Cloth	$(cr_a, cr_b) : cr_c$, $(sr_a, sr_b) : sr_c$	0.99	0.99	1.00	**1**,**17**,**4**,16,**13**,**12**,2,**11**,10,8,21	1.00	1.00	0.12
3-2	=Angle	$(cr_a, sr_a) : cr_b$, $(cr_a, sr_a) : sr_b$	0.99	0.99	1.49	**1**,**17**,14,**4**,16,**11**,**13**,**12**	0.99	1.00	0.22
3-3	≠Cloth, ≠Angle	$(cr_a, sr_b) : cr_{b/c}$, $(cr_a, sr_b) : sr_{a/c}$	0.99	0.99	1.42	**17**,14,**4**,6,**1**,**11**,21,**12**,15,**13**,10,7,2,8	0.99	1.00	0.19

Table 5.4: Comparison of Experiment 1 (Baseline Performance) vs Experiment 3 (Clothing and Angle Var. in Training): Identification, verification and SFFS feature selection numerical results.

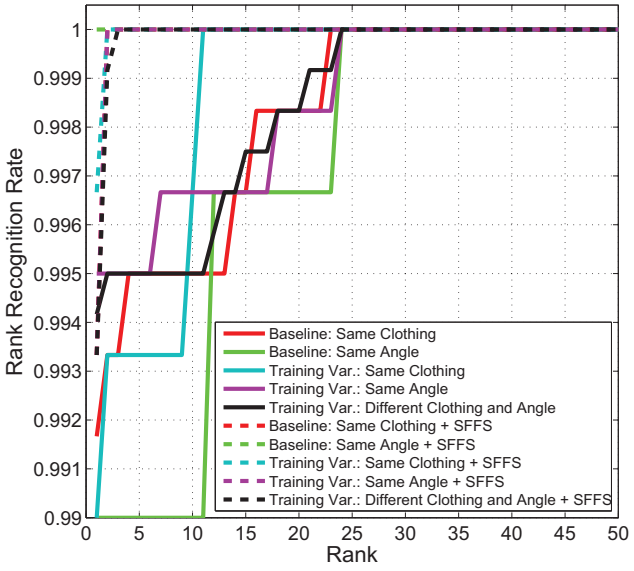

Figure 5.11: Experiment 3 (Clothing and Angle Variability in Training): CMC curves.

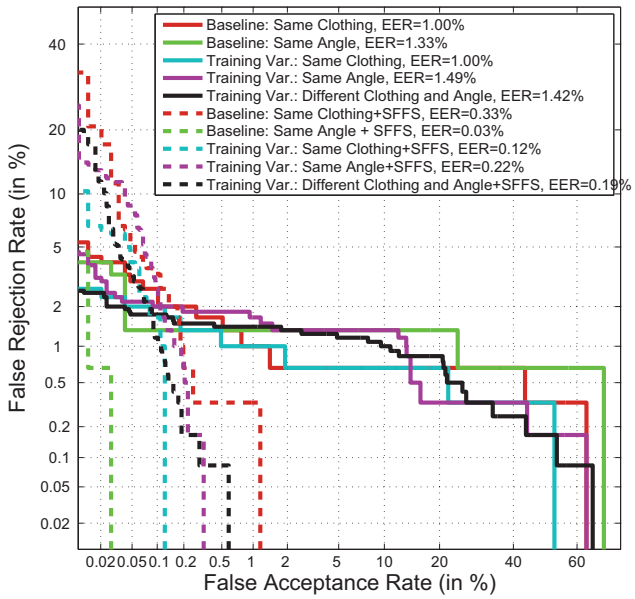

Figure 5.12: Experiment 3 (Clothing and Angle Variability in Training): DET curves.

- The verification performance of exp.3-1 (EER=1.00%) is the same as the baseline's one.
- In exp.3-2 the train images present the same angle (a) but different clothing conditions among them. The effect of the clothing is very low as we have shown in previous experiments (see Sect. 5.6). Although the angle is the same for both train images, is different to the test image's one. This provides an effective angle for the train model, which is more different to the test model's one, and therefore the EER is higher (worse, EER=1.49%) than the EER of the baseline experiments (EER= 1.00% and EER=1.33%). For example, if a=*-10°* and b=*0°* the effective angle of the train model would be ***-10°***, quite different to the test model's one, b=*0°*.
- Finally for the exp.3-3, the train images present different angle and clothing condition among them, and some times different angle and/or clothing condition to the test image. Thus, although this case seems to be the worst one, actually it is an intermediate situation when considering the train and the test model. Both models will be more similar than in the exp.3-2 but much more different than in the exp.3-1. Therefore, the EER has a value slightly lower (better, EER=1.42%) than the exp.3-2's one (EER=1.49%).

If only the **features selected by SFFS** are used, then the results are the following ones:

- The EER for the three cases is approximately an order of magnitude better than the EER obtained considering all the features. This is probably due to the fact that when the most discriminative features are selected, the ones most affected by the angle difference and the clothing, are discarded. As a result the EER is highly improved.
- For the three cases of experiment 3, the EER is lower (EER=0.12%, 0.22%, 0.19%) than the baseline exp.1-1's one (EER=0.33%), and higher than the baseline exp.1-2's one (EER=0.03%). This may be explained taking into account that in exp.1-1 the difference of angle is very high (angle a vs angle b), while in the exp.3-1, 3-2, 3-3 the difference in the angle between the train and test model is not so high. The opposite situation occurs when the comparison is made with exp.1-2 (the train and test model are quite similar due to the same value of angle (a) and there is very little influence due to clothing).

As a result we can conclude that to compensate for the lack of robustness against pose variation, we can incorporate enrollment based on multiple poses.

Regarding the **selection of features**, the higher the angle difference between the train and test model is, the fewer features are selected: in exp.3-3 the difference is between *(a+b)/2* (effective angle of the train model) and b or c having **14** selected features, in exp.3-1 the difference is a little bit higher (between *(a+b)/2* and c), having **11** selected features, and finally, in exp.3-2, the difference in angle is the highest one (between a and b) having only **8** selected features. The features most frequently selected are: feat.#1 (height), feat.#17 (waist width), feat.#11 (lowerarm width), feat.#4 (the distance between the axilla and the centroid of the body), feat.#13 (lowerarm length) and feat.#12 (upperarm width). The height and the waist width are the only features that also belongs to the most discriminative features when considering them independently (feat.#1, #17, #5 and #6, see Fig. 5.5(b)).

5.8 Experiment 4: Number of Train and Test Images

This last experiment is intended to assess the effect of using different number of train images and test images, on the recognition performance.

5.8.1 Protocol Description

With the aim of quantifying this effect, different protocols have been followed, each of them using from 1 to 3 images in both the train and the test set. In all cases, the train images have clothing and the test images do not. Specifically, we will consider these protocols (see Sect. 5.4.2 for notation):

- Experiment 4-1: **1:1**, $cr_* : sr_*$ (9 combinations).
- Experiment 4-2: **1:2**, $cr_* : (sr_*, sr_*)$ (9 combinations).
- Experiment 4-3: **1:3**, $cr_* : (sr_a, sr_b, sr_c)$ (3 combinations).
- Experiment 4-4: **2:1**, $(cr_*, cr_*) : sr_*$ (9 combinations).
- Experiment 4-5: **2:2**, $(cr_*, cr_*) : (sr_*, sr_*)$ (9 combinations).
- Experiment 4-6: **2:3**, $(cr_*, cr_*) : (sr_a, sr_b, sr_c)$ (3 combinations).
- Experiment 4-7: **3:1**, $(cr_a, cr_b, cr_c) : sr_*$ (3 combinations).
- Experiment 4-8: **3:2**, $(cr_a, cr_b, cr_c) : (sr_*, sr_*)$ (3 combinations).
- Experiment 4-9: **3:3**, $(cr_a, cr_b, cr_c) : (sr_a, sr_b, sr_c)$ (1 combination).

Only these 9 protocols were carried out not to have a huge number of cases, and considering that the effect of clothing variability between train and test is very low.

5.8.2 Results

As before, the recognition performance and the feature selection numerical results are presented in a table together with the results of the baseline experiments (Table 5.5).

Exp.1 (Baseline Performance) vs Exp.4 (Number of Train and Test Images)									
			With all features			With features selected by SFFS			
Exp.	Effect	Protocols	R-1	R-5	EER(%)	Selected Features	R-1	R-5	EER(%)
1-1	=Cloth	$cr_a : cr_b$, $sr_a : sr_b$	0.99	0.99	1.00	**1**, **17**, **14**, 4, **16**, 12	0.99	1.00	0.33
1-2	=Angle	$cr_a : sr_a$, $sr_a : cr_a$	0.99	0.99	1.33	2, **1**, **17**, **14**, **16**	1.00	1.00	0.03
4-1	1:1	$cr_* : sr_*$	0.99	0.99	1.33	**1**,**17**,4,**16**,**14**,21,11,8,15,2,12	0.98	1.00	0.44
4-2	1:2	$cr_* : (sr_*, sr_*)$	0.99	0.99	1.56	**1**,**17**,**14**,**16**,4,21	1.00	1.00	0.17
4-3	1:3	$cr_* : (sr_a, sr_b, sr_c)$	0.98	0.99	2.00	**1**,**17**,**14**,**16**,4,21	1.00	1.00	0.08
4-4	2:1	$(cr_*, cr_*) : sr_*$	0.99	0.99	1.33	**1**,**17**,**16**,4,13,**14**	0.99	1.00	0.21
4-5	2:2	$(cr_*, cr_*) : (sr_*, sr_*)$	0.99	0.99	1.78	**1**,**17**,2,**16**,4,21,**14**	1.00	1.00	0.04
4-6	2:3	$(cr_*, cr_*) : (sr_a, sr_b, sr_c)$	0.98	0.99	2.00	**1**,**17**,2,**16**	1.00	1.00	0.00
4-7	3:1	$(cr_a, cr_b, cr_c) : sr_*$	0.99	0.99	1.33	**1**,**17**,**16**,6,**14**,21,10,2,11,8,15,12	0.99	1.00	0.07
4-8	3:2	$(cr_a, cr_b, cr_c) : (sr_*, sr_*)$	0.99	0.99	2.00	**1**,**17**,2,**16**	1.00	1.00	0.00
4-9	3:3	$(cr_a, cr_b, cr_c) : (sr_a, sr_b, sr_c)$	0.98	0.99	2.00	2,**1**,**16**	1.00	1.00	0.00

Table 5.5: Comparison of Experiment 1 (Baseline Performance) vs Experiment 4 (Number of Train and Test Images): Identification, verification and SFFS feature selection numerical results. Note that there are three cases in which R-1=R-5=1.00 and EER=0.00%, these results are underlined.

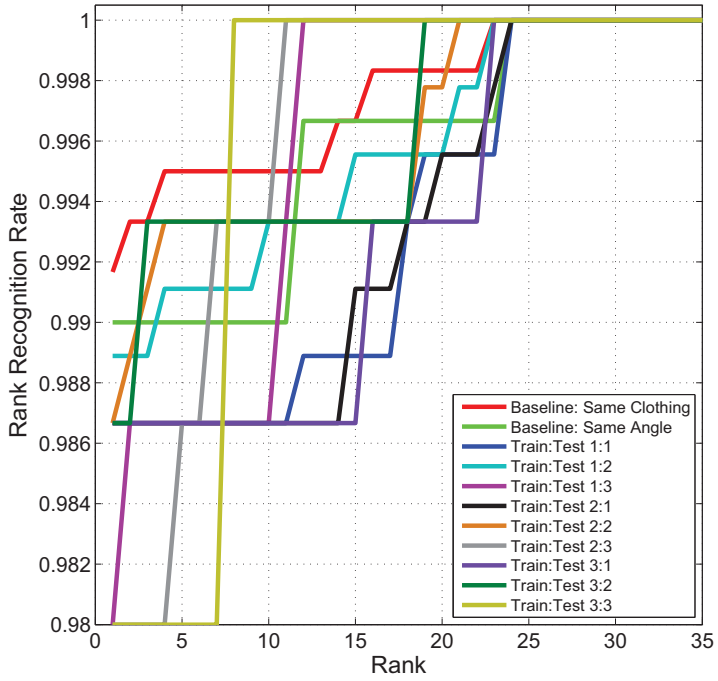

Figure 5.13: Experiment 4 (Number of Train and Test Images): CMC curves, considering all the features.

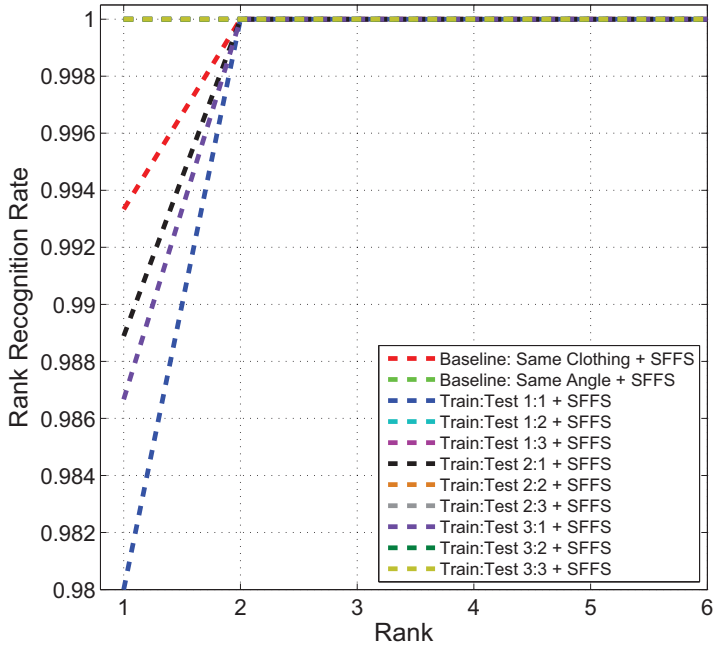

Figure 5.14: Experiment 4 (Number of Train and Test Images): CMC curves, considering SFFS-selected features.

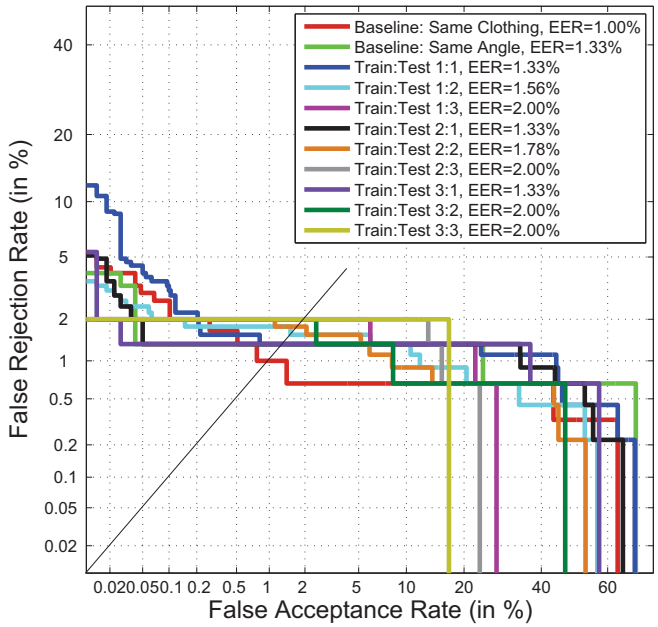

Figure 5.15: Experiment 4 (Number of Train and Test Images): DET curves, considering all the features.

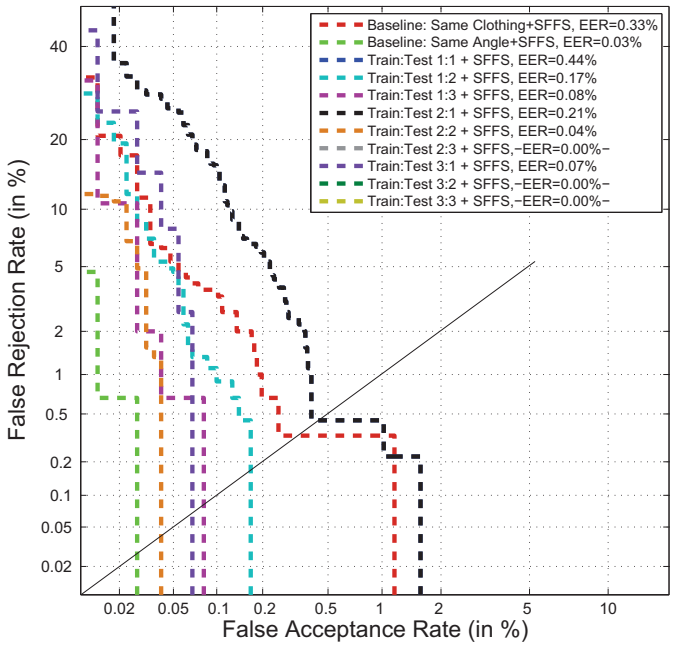

Figure 5.16: Experiment 4 (Number of Train and Test Images): DET curves, considering SFFS-selected features. Note that there are three cases in which EER=0.00% (they are marked with two dashes in the legend), therefore the corresponding DET curves are a point in the origin which is not visible in this plot.

The identification and verification performance is also shown as CMC and DET curves, respectively. In this case two CMC plots (Fig. 5.13 and Fig. 5.14) and two DET plots (Fig. 5.15 and Fig. 5.16) are presented. The Fig. 5.13 shows the CMC curves when all the features are taken into account, while the Fig. 5.14 displays the CMC curves obtained when only the features selected by SFFS algorithm are considered. In the same way, Fig. 5.15 includes the DET curves when the 21 features are used and Fig. 5.16 the DET curves when only the SFFS-selected features are considered.

5.8.3 Discussion

The **identification** results are quite similar to the baseline experiments', with R-1 and R-5 ranging from 0.99 to 1.00. There are only four cases where R-1 is 0.98: the three cases that, considering the 21 features, use three test images (1:3, 2:3 and 3:3), and the case in which, applying the SFFS algorithm, only 1 train and 1 test image are considered (1:1).

The **verification** results obtained using **all the features** are worse (EER=1.33-2.00%) than the baseline experiments' (EER=1.00-1.33%). However, if only the **SFFS-selected features** are considered, the performance of exp.4 (EER=0.07-0.44%) is similar to the baseline experiments' (EER=0.03-0.33%) and even better, reaching 0% of EER in the 2:3, 3:2 and 3:3 protocols. This behavior can be explained taking into account that:

- For the case of using **21 features**, the influence of the clothing between train and test is not negligible , but the influence of the angle it is (as it was showed in the exp.2, see Sect. 5.6). Moreover, there are cases in which the angle is the same between the train and in the test images. Thus the different clothing condition between train and test causes the worsening of the verification performance.
- When only the **features selected by SFFS** are used, the influence of the clothing is lower (as it was explained in Sect. 5.6), but the influence of the angle is higher. However, in many protocols of the experiment 4 the angle between the train and test model is not very different, therefore this effect is not so important, providing very good EERs. Moreover, the EERs become zero when there are at least 5 images involved (2 train and 3 test images or viceversa, and 3 train and 3 test images). This is natural, because as the number of train and test images increases, the models generated should be more realistic, giving excellent error rates. The reason for having a null value in these three cases is due to (i) the specific database used (which does not contain many users, and its images are synthetic) and (ii) the data used to perform the feature selection coincide with the test data.

Another interesting analysis that can be performed on the obtained results is the **evolution of the EER as the number of train and test images changes**. With this purpose the plots of Fig. 5.17 have been produced. Mentioned plots depict the value of the EER vs the number of train images (Fig. 5.17(a)) and the value or the EER vs the number of test images (Fig. 5.17(b)). In both plots:

- When **all the features** are used in the system:
  - For a fixed number of *test* images, the EER **increases** as the number of *train* images increases, except when there is only one test images, case in which the EER=1.33% always (see Fig. 5.17(a), solid lines).
  - For a fixed number of *train* images, the EER also **increases** as the number of *test* images increases (see Fig. 5.17(b), solid lines).

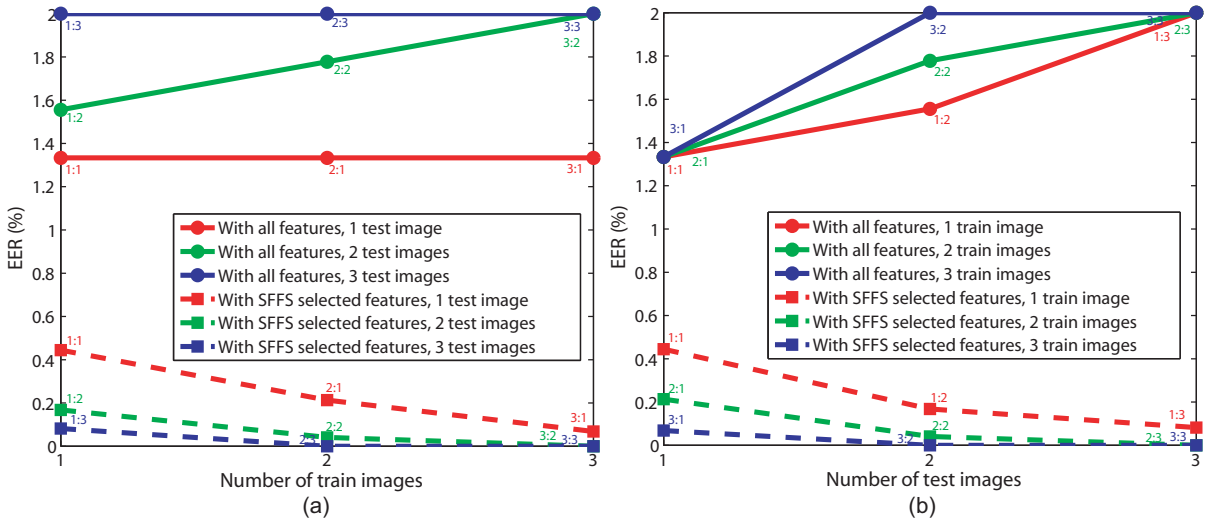

Figure 5.17: Experiment 4 (Number of Train and Test Images): EER values obtained using different number of train and test images: (a) EER vs number of training images, (b) EER vs number of test images.

- If only the **features selected by the SFFS** are considered:
  - For a fixed number of *test* images, the EER **decreases** as the number of *train* images increases (see Fig. 5.17(a), dashed lines).
  - For a fixed number of *train* images, the EER **decreases** as the number of *test* images increases (see Fig. 5.17(b), dashed lines).

This tendency could be due to the fact that, when using **all the features**, the new considered images present different clothing condition and different angle. These images, thus, generate some anthropometric distances that are different between train and test. These distances (features) are considered when performing the comparison, thus, worsening the EER. However, when **applying the SFFS** algorithm, those different distances (affected by the angle and by the clothing) are discarded, improving the verification performance.

In this experiment the **most frequently selected features** are: feat.#1 (the height), feat.#17 (waist width), feat.#16 (chest width) and feat.#14 (elbow-neck distance). They are exactly the same ones as the most frequently selected in exp.1. The height and the waist width are also two of the four most discriminative isolated features (see Fig. 5.5(b)).

Finally, as the number of train or test images increases, there is not a clear tendency of having a bigger or smaller set of selected features. There is only a tendency in the protocols that use 3 train images, and the ones that use 3 test images:

- When using **3 train images** (protocols 3:1, 3:2, and 3:3) the number of selected features decreases as the number of test images increases: **12** features for 3:1, **4** features for 3:2, and **3** features for 3:3.
- When **3 test images** are used (protocols 1:3, 2:3 and 3:3) the number of selected features also decreases as the number of the train images increases: **6** features for 1:3, **4** features for 2:3, and **3** features for 3:3.

Bearing in mind *The Curse of Dimensionality* [53] this behavior is somehow surprising. According to this principle, a higher amount of training data allow to generate a more complex

model (a higher dimension model, or a vector with more features), obtaining a better performance. However, our results show that, when there are more training (or test) data available, we obtain better results by considering less features. This could be due to the fact that, when there are more training (or test) data, the most discriminative features selected by the SFFS algorithm (mainly features #1, #17, #16 and #2 in the five mentioned protocols) become more relevant over the rest, while the rest of features are discarded in the feature selection process.

5.9 Conclusions

The Table 5.6 displays the identification and verification rates of all the performed experiments. The color scale used in the cells that contain the R-1, R-5 and EER, allow to identify the worst results (in red), the best results (in green) and results in between (in yellow and orange). The best results are obtained for experiments 4-6, 4-8 and 4-9 using the SFFS algorithm (R-1=1.00 and EER=0.00%), while the worst ones are obtained for exp.4-3 and 4-6 without SFFS (R-1=0.98 and EER=2.00%).

From the analysis carried out throughout the experiments, and from the Table 5.6, there are some important conclusions that can be drawn. They are stated below.

5.9.1 Effect of Variability between Train and Test, and within Train

The effect of different **clothing condition between train and test** is more noticeable when the 21 features are considered, and it is very low if only the SFFS-selected features are used (see results of exp.1-1 and exp. 2 in Table 5.6).

The effect of the **angle difference between train and test** is just the opposite: it is nearly negligible if all the features are used, and it is higher if the SFFS is applied (see results of exp.1-2 and exp.2 in Table 5.6). Also, the angle difference between train and test degrades much more the performance compared to clothing variability.

Finally, we have seen that, incorporating **various feature vectors** with different poses for **creating the train models**, is a good way to overcome this lack of robustness against pose variation between train and test.

5.9.2 Effect of the Number of Train and Test Images

The use of an increasing number of train and/or test images to perform the recognition experiments, worsens the performance of the system when all the features are considered (which can be explained as more training/test data implies more variability among them in our protocols), but, as expected, it improves the performance if the feature selection is performed (see results of exp.4 in Table 5.6).

5.9.3 Effect of the Feature Selection

The selection of features by means of the SFFS algorithm considerably improves the **EER**, the **R-1** and the **R-5** are also improved, but not so much. This is because the SFFS has the minimization of the EER as optimization criterion.

The **CMC curves** of all the experiments are considerably improved when the feature selection is performed, reaching all of them a R-1 of almost 1.00 after the selection (the exact value has been rounded to two decimals in the tables, but not in the plots).

Exp.	Effect		Protocols	With all features			With features selected by SFFS				Exp.
				R-1	R-5	EER (%)	# Sel. Feat.	Selected Features	R-1	R-5	EER (%)	
1-1	Baseline	=Cloth	cr_a:cr_b, sr_a:sr_b	0,99	1,00	1,00	6	1, 17, 14, 4, 16, 12	0,99	1,00	0,33	1-1
1-2		=Angle	cr_a:sr_a, sr_a:cr_a	0,99	0,99	1,33	5	2, 1, 17, 14, 16	1,00	1,00	0,03	1-2
2	Clothing & angle var. between train and test	≠Cloth, ≠Angle	cr_a:sr_b, sr_a:cr_b	0,99	0,99	1,33	5	1, 17, 14, 4, 16	0,97	1,00	0,50	2
3-1	Clothing & angle variability in training	=Cloth	(cr_a,cr_b):cr_c, (sr_a,sr_b):sr_c	0,99	0,99	1,00	11	1, 17, 4, 16, 13, 12, 2, 11, 10, 8, 21	1,00	1,00	0,12	3-1
3-2		=Angle	(cr_a,sr_a):cr_b, (cr_a,sr_a):sr_b	1,00	1,00	1,49	8	1, 17, 14, 4, 16, 11, 13, 12	0,99	1,00	0,22	3-2
3-3		≠Cloth, ≠Angle	(cr_a,sr_b):$cr_{b/c}$, (sr_a,cr_b):$sr_{b/c}$	0,99	1,00	1,42	14	17, 14, 4, 6, 1, 11, 21, 12, 15, 13, 10, 7, 2, 8	0,99	1,00	0,19	3-3
4-1	Number of train & test images	1:1	cr_*:sr_*	0,99	0,99	1,33	11	1, 17, 4, 16, 14, 21, 11, 8, 15, 2, 12	0,98	1,00	0,44	4-1
4-2		1:2	cr_*:(sr_*,sr_*)	0,99	0,99	1,56	6	1, 17, 14, 16, 4, 21	1,00	1,00	0,17	4-2
4-3		1:3	cr_*:(sr_*,sr_*,sr_*)	**0,98**	**0,99**	**2,00**	6	1, 17, 14, 16, 4, 21	1,00	1,00	0,08	4-3
4-4		2:1	(cr_*,cr_*):sr_*	0,99	0,99	1,33	6	1, 17, 16, 4, 13, 14	0,99	1,00	0,21	5-1
4-5		2:2	(cr_*,cr_*):(sr_*,sr_*)	0,99	0,99	1,78	7	1, 17, 2, 16, 4, 21, 14	1,00	1,00	0,04	5-2
4-6		2:3	(cr_*,cr_*):(sr_*,sr_*,sr_*)	**0,98**	**0,99**	**2,00**	4	1, 17, 2, 16	**1,00**	**1,00**	**0,00**	5-3
4-7		3:1	(cr_a,cr_b,cr_c):sr_*	0,99	0,99	1,33	12	1, 17, 16, 6, 14, 21, 10, 2, 11, 8, 15, 12	0,99	1,00	0,07	6-1
4-8		3:2	(cr_a,cr_b,cr_c):(sr_*,sr_*)	0,99	0,99	2,00	4	1, 17, 2, 16	**1,00**	**1,00**	**0,00**	6-2
4-9		3:3	(cr_a,cr_b,cr_c):(sr_a,sr_b,sr_c)	0,99	0,98	2,00	3	2, 1, 16	**1,00**	**1,00**	**0,00**	6-3

Table 5.6: Experiments 1, 2, 3 and 4: Identification, verification and SFFS feature selection numerical results. The results are presented in shadowed cells with colors ranging from red (worst results) to green (best results), considering separately each type of result (R-1, R-5 and EER). The slightly different color between some cells that contain the same value is due to the fact that the color shadowing does not take into account the decimals rounding. The worst and best results are also written in bold font.

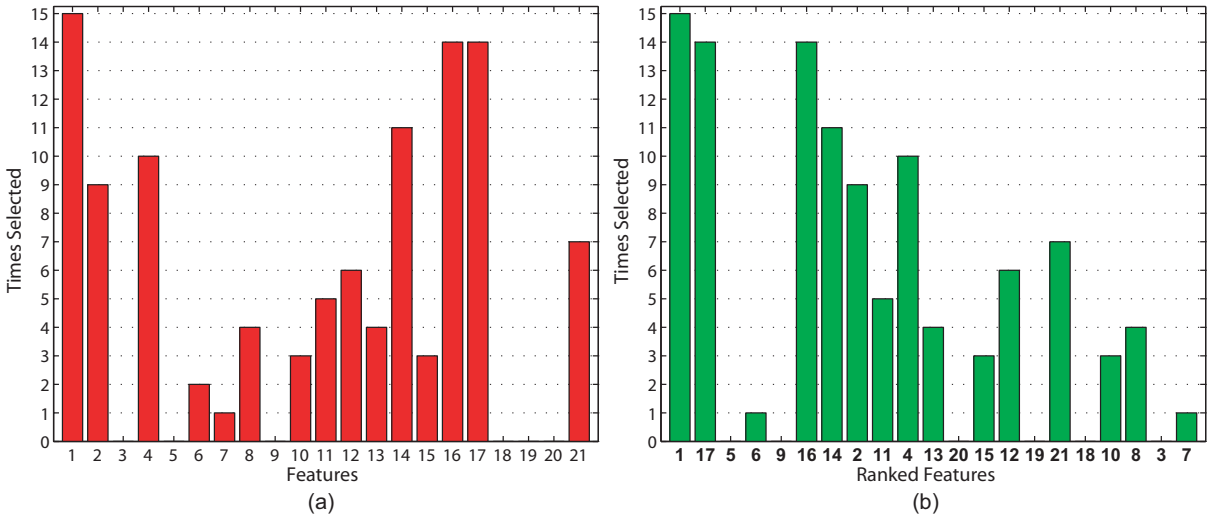

Figure 5.18: Histograms of features selected by the SFFS algorithm.: (a) Histogram with the features regularly ordered, (b) Histogram with the features ordered in the same way as in Fig. 5.5(b) (in decreasing order of the discrimination power of each feature.)

There is an interesting behavior that present all the **DET curves** when the feature selection is applied: they change from having a horizontal appearance to have a vertical one closer to the origin (with a more negative slope, see for example Fig. 5.12). This is a consequence of the minimization of the EER in the feature selection process. This change in the shape of the DET curves provides the system with a higher security: the False Acceptance Rate is reduced while the False Rejection Rate is increased.

5.9.4 Analysis of the Selected Features

In addition to the comments made in each experiment's section about the feature selection, we perform an additional analysis here. The Fig. 5.18(a) is a histogram of the features selected in the experiments. It reveals that the feature most frequently selected corresponds to feat.#1 (the height) selected 15 times, followed by the features #17 (waist width) and #16 (chest width), both selected 14 times. The features #5 (centroid of the body-pubis distance), #9 (thigh length), #18 (hips width), #19 (thigh width) and #20 (calf width) were not selected in any experiment.

The Fig. 5.18(b) displays the same histogram, but the x axis contains, in bold font, the features ranked in decreasing order of their discrimination power (the same order as in Fig. 5.5(b)). If the features were uncorrelated, the bars would gradually decrease as we move along the x axis in the mentioned figure, being the most frequently selected the first ones (the individually most discriminative ones), and the least frequently selected the last ones (the individually least discriminative ones). Although the bars approximately decrease as we move along the x axis, there are some gaps corresponding to features not selected or almost not selected. For instance, features #5 (centroid of the body-pubis distance), #6 (legs length) and #9 (thigh length), which are some of the individually most discriminative features, are not selected by the SFFS algorithm. This reveals that these features, even having a high discrimination power, are not selected because they are correlated with features previously selected during the selection process (they do not add new discriminant information). In particular, it seems obvious that the mentioned features (which are mainly lengths) are highly correlated with the height, which was previously selected.

5.9.5 Final Remarks

We should remark one more time that all the results are not totally representative due to (i) the small size of the database, and (ii) the differences in the performances are small. Moreover, the obtained results are optimistically biased due to three main reasons: (i) the low number of users (only 50) in the database, (ii) the synthetic nature of the images that comprise the database, (iii) the use of the same data to develop the system (in particular to select the most discriminative set of features by means of the SFFS algorithm) and to test it.

In any case, in spite of the previous limitations, it was possible to quantify the influence of the different effects (clothing/angle variability between train and test, in train, and the number of train/test images) and to identify the most discriminative set of features in each case, which was the main objective in this work.

6

Conclusions and Future Work

6.1 Conclusions

Nowadays the security and defense is becoming more and more important in our society. For this reason, many screening portals have been installed in certain places such as airport security checkpoints. One of the latest kind of portals acquires body images in the millimeter waves spectral band (MMW). These portals provide images of the surface of the body revealing if the user conceals arms or drugs under his/her garment. The integration of a biometric system, based on MMW images, in this kind of portals, would also allow to identify people (terrorists among them) previously enrolled in the system. Moreover, the use of this kind of radiation and portals to obtain MMW images presents many advantages (millimeter waves are innocuous, they can penetrate the clothing, these portals are not invasive, they enable the recognition at a distance and/or on the move and also the fusion with other biometrics traits simultaneously acquired, such as the face or the gait).

In this project, firstly, a new method to simulate images of people at 94 GHz (frequency within the MMW band) has been proposed and used to generate a synthetic database. This database, called BIOGIGA, is composed of 1200 images simulated at 94 GHz of 50 users in two types of scenarios with two types of imaging systems.

Secondly, a biometric recognition system, based on certain images of BIOGIGA, has been designed and implemented. In the development of the system we have proposed a feature extraction method based on the detection of relevant points of the body, followed by the measure of 21 distances among them. These distances form the feature vector of every image.

Afterwards, several identification and verification experiments were performed to test the developed system. Each experiment is carried out under different conditions regarding the clothing condition, the camera angle and the number of train and test images used. Each experiment was performed twice: (ii) making use of the 21 features, and (ii) using only the most discriminative *set* of features (obtained by the SFFS algorithm).

The obtained results provide information about the influence of (i) the different conditions, and (ii) the feature selection, on the system performance:

- The effect of different clothing condition between train and test worsens the system performance, being this worsening more noticeable when the 21 features are considered, and

very small if only the SFFS-selected features are used.

- The effect of the camera angle difference between train and test also reduces the performance of the system, but in the opposite way: the worsening is nearly negligible if all the features are used, and it is higher if the SFFS is applied.

- Incorporating various feature vectors with different poses for creating the train models, is a good way to overcome the lack of robustness against pose variation between train and test.

- The use of an increasing number of train and/or test images to perform the recognition experiments, (i) worsens the performance of the system when all the features are considered (due to the fact that more training/test data implies more variability among them in our protocols), and (ii) improves it if the feature selection is performed (as it was expected).

- The selection of features highly improves the verification performance, however, the identification performance is only slightly improved.

- The CMC curves (identification performance plots) are extremely improved when the feature selection is performed.

- When applying feature selection, the DET curves (verification performance plots) become closer to the origin and have a more negative slope, providing the system with a lower (better) EER (verification *Equal Error Rate*) and with higher security (the *False Acceptance Rate* is reduced while the *False Rejection Rate* is increased).

The features more frequently selected in the experiments correspond to: the height, the waist width, the chest width and the elbow-neck distance (in that order). However, the features with the highest discrimination power are the height, the waist width, the distance between the centroid of the body and the pubis, and the legs length (in that order). This mismatch between both sets of features is due to the correlation among some features of the second set (for example the height, the legs length and the distance between the centroid of the body and the pubis are highly correlated).

The recognition performance obtained in the experiments is excellent in both, identification and verification modes: the *Rank-1 recognition rate* has a value between 0.98 and 1.00 (i.e., 98% and 100% respectively), while the EER ranges between 0.00% and 2.00%. These values are similar and even better than the ones obtained by Alefs *et al.* in [9] (the only biometric recognition work based on MMW images published so far). In that work, a EER varying between 1.00% and 2.00% is obtained. Nevertheless, the results obtained in our experiments are not totally representative (due to the small size of the database, 50 users, and the little differences among the obtained performances). In fact, the error rates are optimistically biased. This is caused by (i) the small number of users, (ii) the images are synthetic, and (iii) the selection of features was performed using all the available data (and not exclusively data from a development set).

As stated, the limitations of this work are related to the special characteristics of the database used. The BIOGIGA's images are limited when compared to the real images acquired in practice. However, the synthetic images are very similar to the ones really captured at 94 GHz. Also, the synthetic images used are based on real measures from people. Therefore, the proposed features can be directly applied and are useful for practical MMW images. Moreover, the experiments performed using the BIOGIGA database have provided qualitatively results about the effects of the different conditions and of the feature selection on the system performance, which was one of the main purposes of this project.

6.2 Future Work

As future work, the following research lines are proposed:

- The development of a system similar to the one presented here, that makes use of images simulated with MMW active systems (BIOGIGA also contains this kind of images, but they were not used in this project).
- The generation of a database of real images acquired within the MMW band (and if possible, with images of the same users acquired in the VIS and IR band too, obtaining a *Multispectral Database*).
- The adaptation of the proposed system to be able to operate with real MMW images. In this task, and in the first one, the image segmentation module should be tuned to the new kind of images.
- The design and development of alternative biometric systems that only make use of some parts of the MMW body image (such as the face, the thorax, etc. as it was done in [9]).
- The fusion of different biometric traits acquired at MMW band.
- The fusion of biometric trait(s) acquired at MMW band with (the same or different) trait(s) acquired at other spectral band(s) (i.e. the development of a *Multispectral Biometric System*).
- The use of information extracted from MMW images (such as anthropometric measures) to increase the performance of traditional systems with medium-high recognition performance (*Soft Biometrics).*
- Integration of a biometric system based on real MMW images in a MMW screening portal.

Bibliography

[1] A.K. Jain, A. Ross, and S. Prabhakar. An introduction to biometric recognition. *Circuits and Systems for Video Technology, IEEE Transactions on*, 14(1):4 – 20, jan. 2004.

[2] A.K. Jain, A. Ross, and S. Pankanti. Biometrics: a tool for information security. *Information Forensics and Security, IEEE Transactions on*, 1(2):125–143, june 2006.

[3] National Academy Press, editor. *Airline Passenger Security Screening: New Technologies and Implementation Issues*, chapter Biometrics at a Distance: Issues, Challenges, and Prospects, pages 3–21. National Academy Press, 1996.

[4] Hong Chen and Anil K. Jain. Dental biometrics: Alignment and matching of dental radiographs. *IEEE Transactions on Pattern Analysis and Machine Intelligence*, 27:1319–1326, 2005.

[5] S.Z. Li, RuFeng Chu, ShengCai Liao, and Lun Zhang. Illumination invariant face recognition using near-infrared images. *Pattern Analysis and Machine Intelligence, IEEE Transactions on*, 29(4):627–639, 2007.

[6] R. Appleby and R.N. Anderton. Millimeter-wave and submillimeter-wave imaging for security and surveillance. *Proceedings of the IEEE*, 95(8):1683 –1690, aug. 2007.

[7] L. Yujiri, M. Shoucri, and P. Moffa. Passive millimeter wave imaging. *Microwave Magazine, IEEE*, 4(3):39 – 50, sept. 2003.

[8] J.N. Mait, D.A. Wikner, M.S. Mirotznik, J. van der Gracht, G.P. Behrmann, B.L. Good, and S.A. Mathews. 94-GHz imager with extended depth of field. *Antennas and Propagation, IEEE Transactions on*, 57(6):1713 –1719, june 2009.

[9] B.G. Alefs, R.J.M. den Hollander, F.A. Nennie, E.H. van der Houwen, M. Bruijn, W. van der Mark, and J.C. Noordam. Thorax biometrics from Millimetre-Wave images. *Pattern Recognition Letters*, 31(15):2357–2363, 2010.

[10] Josep Parron, Hector Rossel, Pedro de Paco, Gary Junkin, and Oscar Menendez. Millimeter-Wave Scene Simulation using Blender. In *Proceedings of XXV Simposium Nacional de Union Cientifica Internacional de Radio, URSI 2010*, September 2010.

[11] Rafael C. Gonzalez, Richard E. Woods, and Steven L. Eddins. *Digital Image Processing Using MATLAB*. Prentice-Hall, Inc., Upper Saddle River, NJ, USA, 2003.

[12] Miriam Moreno-Moreno, Julian Fierrez, Pedro Tome, Ruben Vera-Rodriguez, Josep Parron, and Javier Ortega-Garcia. BIOGIGA: Base de datos de imágenes sintéticas de personas a 94 GHz con fines biométricos. In *Proceedings of XXVI Simposium Nacional de Union Cientifica Internacional de Radio*, September 2011.

[13] Miriam Moreno-Moreno, Julian Fierrez, and Javier Ortega-Garcia. Millimeter- and Submillimeter-Wave Imaging Technologies for Biometric Purposes. In *Proceedings of XXIV Simposium Nacional de Union Cientifica Internacional de Radio*, September 2009.

[14] Miriam Moreno-Moreno, Julian Fierrez, and Javier Ortega-Garcia. Biometrics Beyond the Visible Spectrum: Imaging Technologies and Applications. In *Proceedings of BioID-Multicomm 2009*, volume 5707 of *LNCS*, pages 154–161. Springer, September 2009.

[15] Miriam Moreno-Moreno, Julian Fierrez, Pedro Tome, and Javier Ortega-Garcia. Análisis de Escenarios para Reconocimiento Biométrico a Distancia Adecuados para la Adquisición de Imágenes MMW. In *Proceedings of XXV Simposium Nacional de Union Cientifica Internacional de Radio*, September 2010.

[16] Miriam Moreno-Moreno, Julian Fierrez, Ruben Vera-Rodriguez, and Josep Parron. Distance-based Feature Extraction for Biometric Recognition of Millimeter Wave Body Images. In *Proceedings of 45th IEEE International Carnahan Conference on Security Technology*, pages 326–331, October 2011.

[17] Miriam Moreno-Moreno, Julian Fierrez, Ruben Vera-Rodriguez, and Josep Parron. Simulation of Millimeter Wave Body Images and its Application to Biometric Recognition. In *Proceedings of SPIE Defense, Security and Sensing 2012*, volume 8362, April 2012.

[18] Austin Richards. *Alien Vision: Exploring the Electromagnetic Spectrum with Imaging Technology, Second Edition.* SPIE Press, 1st ed. 2010. corr. 2nd printing edition, edition, 2011.

[19] Lior Shamir, Shari Ling, Salim Rahimi, Luigi Ferrucci, and Ilya G. Goldberg. Biometric identification using knee x-rays. *Int. J. Biometrics*, 1(3):365–370, March 2009.

[20] R.H. Bossi, K.D. Friddell, and J.M. Nelson. Backscatter x-ray imaging. *Materials Evaluation*, 46(11):1462–7, Oct. 1988.

[21] Eric Jude L. Morris, Frank A. Dibianca, Hemant Shukla, and Daya Gulabani. A backscattered x-ray imager for medical applications. In *Medical Imaging 2005: Physics of Medical Imaging*, volume 5745, pages 113–120. SPIE, February 2005.

[22] Alex Chalmers. Three applications of backscatter x-ray imaging technology to homeland defense. In *Sensors, and Command, Control, Communications, and Intelligence (C3I) Technologies for Homeland Security and Homeland Defense IV*, volume 5778, pages 113–120. SPIE, March 2005.

[23] Lingyu Wang and Graham Leedham. Near- and far- infrared imaging for vein pattern biometrics. *Advanced Video and Signal Based Surveillance, IEEE Conference on*, 0:52, 2006.

[24] Pradeep Buddharaju, Ioannis T. Pavlidis, Panagiotis Tsiamyrtzis, and Mike Bazakos. Physiology-based face recognition in the thermal infrared spectrum. *IEEE Trans. Pattern Anal. Mach. Intell.*, 29(4):613–626, April 2007.

[25] Chih-Lung Lin and Kuo-Chin Fan. Biometric verification using thermal images of palm-dorsa vein patterns. *Circuits and Systems for Video Technology, IEEE Transactions on*, 14(2):199 – 213, feb. 2004.

[26] Xin Chen, Patrick J. Flynn, and Kevin W. Bowyer. IR and visible light face recognition. *Comput. Vis. Image Underst.*, 99(3):332–358, September 2005.

[27] Andrea Selinger and Diego A. Socolinsky. Face recognition in the dark. *Computer Vision and Pattern Recognition Workshop*, 8:129, 2004.

[28] R.L. Howald, G. Clark, J. Hubert, and D. Ammar. Millimeter waves: The evolving scene. In *Technologies for Homeland Security, 2007 IEEE Conference on*, pages 234 –239, may 2007.

[29] Hai-Bo Liu, Hua Zhong, N. Karpowicz, Yunqing Chen, and Xi-Cheng Zhang. Terahertz spectroscopy and imaging for defense and security applications. *Proceedings of the IEEE*, 95(8):1514 –1527, aug. 2007.

[30] J. E. Bjarnason, T. L. J. Chan, A. W. M. Lee, M. A. Celis, and E. R. Brown. Millimeter-wave, terahertz, and mid-infrared transmission through common clothing. *Applied Physics Letters*, 85(4):519–521, 2004.

[31] M.J. Rosker and H.B. Wallace. Imaging through the atmosphere at terahertz frequencies. In *Microwave Symposium, 2007. IEEE/MTT-S International*, pages 773 –776, june 2007.

[32] G.N. Sinclair, P.R. Coward, R.N. Anderton, R. Appleby, T. Seys, and P. Southwood. Detection of illegal passengers in lorries using a passive millimetre wave scanner. In *Security Technology, 2002. Proceedings. 36th Annual 2002 International Carnahan Conference on*, pages 167 – 170, 2002.

[33] M. Sato, T. Hirose, T. Ohki, H. Sato, K. Sawaya, and K. Mizuno. 94-GHz band high-gain and low-noise amplifier using inp-hemts for passive millimeter wave imager. In *Microwave Symposium, 2007. IEEE/MTT-S International*, pages 1775 –1778, june 2007.

[34] B. Kapilevich, B. Litvak, M. Einat, and O. Shotman. Passive mm-wave sensor for in-door and out-door homeland security applications. In *Sensor Technologies and Applications, 2007. SensorComm 2007. International Conference on*, pages 20 –23, oct. 2007.

[35] D.M. Sheen, D.L. McMakin, and T.E. Hall. Three-dimensional millimeter-wave imaging for concealed weapon detection. *Microwave Theory and Techniques, IEEE Transactions on*, 49(9):1581 –1592, sep 2001.

[36] T. Derham, H. Kamoda, T. Iwasaki, and T. Kuki. Active mmw imaging system using the frequency-encoding technique. In *Microwave Conference, 2007. KJMW 2007. Korea-Japan*, pages 181 –184, nov. 2007.

[37] G.P. Timms, J.D. Bunton, M.L. Brothers, and J.W. Archer. 190 GHz millimetre-wave imaging using mmic-based heterodyne receivers. In *Wireless Broadband and Ultra Wideband Communications, 2007. AusWireless 2007. The 2nd International Conference on*, page 32, aug. 2007.

[38] D.M. Sheen, D.L. McMakin, T.E. Hall, and R.H. Severtsen. Active millimeter-wave stand-off and portal imaging techniques for personnel screening. In *Technologies for Homeland Security, 2009. HST '09. IEEE Conference on*, pages 440 –447, 11-12 2009.

[39] Douglas T. Petkie, Corey Casto, Frank C. De Lucia, Steven R. Murrill, Brian Redman, Richard L. Espinola, Charmaine C. Franck, Eddie L. Jacobs, Steven T. Griffin, Carl E. Halford, Joe Reynolds, Sean O'Brien, and David Tofsted. Active and passive imaging in the thz spectral region: phenomenology, dynamic range, modes, and illumination. *J. Opt. Soc. Am. B*, 25(9):1523–1531, 2008.

[40] A. Luukanen, E.N. Grossman, A.J. Miller, P. Helisto, J.S. Penttila, H. Sipola, and H. Seppa. An ultra-low noise superconducting antenna-coupled microbolometer with a room-temperature read-out. *Microwave and Wireless Components Letters, IEEE*, 16(8):464 –466, aug. 2006.

[41] Xilin Shen, C.R. Dietlein, E. Grossman, Z. Popovic, and F.G. Meyer. Detection and segmentation of concealed objects in terahertz images. *Image Processing, IEEE Transactions on*, 17(12):2465 –2475, dec. 2008.

[42] Arttu Luukanen, Leif Grönberg, Kari Kataja, Mikko Leivo, Tuomas Haarnoja, Anssi Rautiainen, Panu Helistö, Hannu Sipola, , and Heikki Seppä. Stand-off contraband identification using passive thz imaging. In *EDA IEEMT Workshop 2008*, 2008.

[43] K.B. Cooper, R.J. Dengler, N. Llombart, T. Bryllert, G. Chattopadhyay, E. Schlecht, J. Gill, C. Lee, A. Skalare, I. Mehdi, and P.H. Siegel. Penetrating 3-d imaging at 4- and 25-m range using a submillimeter-wave radar. *Microwave Theory and Techniques, IEEE Transactions on*, 56(12):2771 –2778, dec. 2008.

[44] A. Tamminen, J. Ala-Laurinaho, and A.V. Raisanen. Indirect holographic imaging at 310 ghz. In *Radar Conference, 2008. EuRAD 2008. European*, pages 168 –171, oct. 2008.

[45] A.W.M. Lee, B.S. Williams, S. Kumar, Qing Hu, and J.L. Reno. Real-time imaging using a 4.3-thz quantum cascade laser and a 320 /spl times/ 240 microbolometer focal-plane array. *Photonics Technology Letters, IEEE*, 18(13):1415 –1417, july 2006.

[46] Alphonse Bertillon and Gallus Muller. *Alphonse Bertillon's Instructions For Taking Descriptions For The Identification Of Criminals And Others, by Means Of Anthropometric Indications (1889)*. Kessinger Publishing, 1889.

[47] Javier Burgués. Reconocimiento de personas basado en imágenes de la mano. Master's thesis, Universidad Autónoma de Madrid, July 2010.

[48] Luis Carlos Molina, Lluís Belanche, and Àngela Nebot. Feature selection algorithms: A survey and experimental evaluation. In *Proceedings of the 2002 IEEE International Conference on Data Mining*, ICDM '02, pages 306–, Washington, DC, USA, 2002. IEEE Computer Society.

[49] P. Pudil, J. Novovicová, and J. Kittler. Floating Search Methods in Feature Selection. *Pattern Recognition Letters*, 15(11):1119 – 1125, 1994.

[50] Sergios Theodoridis and Konstantinos Koutroumbas. *Pattern Recognition, Third Edition*. Academic Press, 3 edition, March 2006.

[51] A. Martin, G. Doddington, T. Kamm, M. Ordowski, and M. Przybocki. The DET curve in assessment of detection task performance. In *Proceedings of the European Conference on Speech Communication and Technology*, volume 1, pages 1895–1898, 1997.

[52] M. Vasilescu and Demetri Terzopoulos. Multilinear analysis of image ensembles: Tensorfaces. In Anders Heyden, Gunnar Sparr, Mads Nielsen, and Peter Johansen, editors, *Computer Vision ECCV 2002*, volume 2350 of *Lecture Notes in Computer Science*, pages 447–460. Springer Berlin / Heidelberg, 2002.

[53] Christopher M. Bishop. *Pattern Recognition and Machine Learning (Information Science and Statistics)*. Springer, 1st ed. 2006. corr. 2nd printing edition, October 2007.

A

Introducción

A.1 Motivación del proyecto

Se denomina reconocimiento biométrico al proceso que permite asociar una identidad con un individuo de forma automática, haciendo uso de una o varias características físicas o de comportamiento, inherentes al individuo [1, 2]. Son muchas las características que se han venido usando en reconocimiento biométrico: huella dactilar, firma manuscrita, iris, voz, cara, mano, etc. Algunos de estos rasgos biométricos tales como la oreja, la cara, la mano o la forma de andar, se adquieren normalmente con cámaras que trabajan en frecuencias pertenecientes a la banda visible del espectro electromagnético. Tales imágenes se ven afectadas por factores como las condiciones de iluminación y las oclusiones (provocadas por la ropa, el maquillaje, el pelo, etc.).

Con el fin de superar estas limitaciones, impuestas por el uso de imágenes adquiridas en el espectro visible (VIS), investigadores en biometría y seguridad [3] han propuesto el uso de imágenes adquiridas en otros rangos espectrales, a saber: rayos X (RX) [4], infrarrojo (IR) [5], ondas milimétricas (MMW) y submilimétricas (SMW) [6]. Además de solventar hasta cierto punto las limitaciones de las imágenes en el visible, las imágenes tomadas más allá del espectro visible presentan una ventaja extra: son más robustas frente ataques contra sistemas biométricos que otras imágenes o rasgos biométricos.

La banda espectral propuesta en este proyecto para capturar imágenes de rasgos biométricos es la correspondiente a la de las ondas milimétricas (de frecuencia entre 30 y 300 GHz) [7]. La importancia de este tipo de radiación se halla en:

- Su capacidad para atravesar la ropa y otras oclusiones.
- Es inocua para la salud.
- El reciente desarrollo que están experimentando los sistemas de GHz-THz en aplicaciones de captura de imágenes (especialmente en el área de seguridad).

Al contrario de lo que ocurre con la tecnología de captura de imágenes en el visible o infrarrojo, la tecnología de GHz-THz está en pleno desarrollo [8]. Este hecho, junto con los problemas

de privacidad que presentan las imágenes corporales en esa banda, han hecho que hasta la fecha no existan bases de datos públicas con imágenes de personas adquiridas en ese rango de frecuencias. De hecho sólo existe un trabajo publicado hasta el momento sobre reconocimiento biométrico basado en imágenes de GHz [9]. Por todo lo anterior, en el actual proyecto se propone, como una de las tareas fundamentales, la obtención de imágenes simuladas de personas a 94 GHz [10]. A continuación se hará uso de tales imágenes para desarrollar un sistema de reconocimiento biométrico.

El presente proyecto está motivado por las ventajas que presentan las imágenes en la banda de milimétricas y los escenarios de su adquisición:

- La inocuidad de tal radiación. La obtención de imágenes en esa banda se puede realizar de forma pasiva (recogiendo la radiación que de forma natural emite el cuerpo humano en esa banda y que refleja del entorno) o de forma activa (iluminando el cuerpo con fuentes emisoras a esas frecuencia y recogiendo la radiación reflejada). En ningún caso supone riesgo para la salud.
- La transparencia de la vestimenta y otros materiales dieléctricos no polares a esta radiación. Ésta es la principal ventaja para el reconocimiento biométrico ya que evita las oclusiones indeseadas en las imágenes.
- La no invasividad de los sistemas de captura de este tipo de imágenes. La cooperación requerida por el usuario para la adquisición de estas imágenes es mínima.
- La posibilidad de reconocimiento a distancia y/o en movimiento.
- La posibilidad de la integración del sistema de reconocimiento en sistemas de seguridad como portales y otros dispositivos de detección de armas.
- Facilidad de fusión con otros rasgos biométricos como la cara.

Por el contrario, las imágenes adquiridas en esta banda cuentan con algunos inconvenientes como:

- El hecho de requerir de equipos de adquisición extremadamente caros, dado el reciente desarrollo de los mismos.
- Los problemas de privacidad que causan las imágenes que producen (transparentes a la ropa).

A.2 Objetivos

Los objetivos del proyecto se resumen en tres puntos:

- Generación de una base de datos de imágenes simuladas de personas reales en la banda de ondas milimétricas. El primer hito del proyecto es la generación de tales imágenes, como alternativa a la compra de equipos de captura de imágenes a GHz y dada la no existencia de base de datos de libre distribución de este tipo de imágenes.
- Desarrollo de un sistema de reconocimiento biométrico basado en las imágenes anteriores. Dicho sistema contará con varios módulos: procesado de las imágenes, extracción de características más distintivas, medidas de similitud y decisor.

- Evaluación del sistema anterior mediante la realización de diferentes experimentos. El objetivo principal de los experimentos es cuantificar la influencia de las condiciones de cada experimento sobre el rendimiento del sistema. Las condiciones de interés incluyen variabilidad de pose y ropa entre los datos de entrenamiento y de test, y la cantidad de datos de entrenamiento.

A.3 Metodología

La metodología de trabajo se divide en las siguientes etapas:

Etapa de estudio y documentación.

- Como primer paso se realizará un estudio de los diferentes sistemas de adquisición de imágenes fuera del rango visible, en especial de los usados con fines biométricos.
- A continuación se realizará una revisión del estado del arte en sistemas de reconocimiento biométrico basados en imágenes tomadas fuera del rango visible.
- Para completar la fase de documentación se estudiarán las técnicas básicas de procesado digital de imágenes a través del material de la asignatura de Ingeniería de Telecomunicación *Temas Avanzados en Procesado de Señal*, a través del estudio del libro [11] y de la realización de algunos de sus ejemplos prácticos.

Generación de una base de datos sintética de personas reales a 94 GHz. Esto se realizó en colaboración con el grupo AMS de la Universidad Autónoma de Barcelona. Esta etapa cuenta con varios pasos:

- Obtención de medidas corporales de personas reales.
- Generación de modelos corporales a partir de esas medidas usando un software específico para ello.
- Exportación de los anteriores modelos a otra aplicación donde se obtendrán las imágenes de tales modelos en el escenario y a la frecuencia de radiación elegidos.

Desarrollo de un sistema propietario de identificación biométrica. Este sistema utilizará características extraídas de las imágenes generadas en la etapa anterior. Este desarrollo contará con los siguientes pasos:

- Preprocesado de las imágenes.
- Extracción de características.
- Medida de similitud.
- Toma de decisión.

Experimentos para la optimización del sistema. Estos experimentos se centran en la selección de características. Se realizan para obtener un conjunto de características representativo y distintivo de cada usuario que permita incrementar el rendimiento del sistema.

Evaluación del sistema mediante la realización diferentes experimentos.

Evaluación de resultados y extracción de conclusiones.

Documentación del trabajo realizado.

- Descripción de los pasos seguidos.
- Análisis de resultados, evaluación.
- Posible trabajo futuro.

A.4 Organización de la memoria

Este documento está estructurado en 6 capítulos como se describe a continuación:

Capítulo 1: Introducción. Este capítulo presenta el tema del proyecto, las razones principales que nos han llevado a desarrollar este trabajo, los objetivos a alcanzar, la metodología seguida y la organización de la memoria.

Capítulo 2: Estado del Arte en Biometría fuera del Espectro Visible. Este capítulo hace una revisión de algunas de las tecnologías de captura de imágenes del cuerpo humano que operan fuera del espectro visible: tecnología en las bandas de 1) rayos-X, 2) Infrarrojos y de 3) ondas milimétricas y submilimétricas, así como sus aplicaciones biométricas.

Capítulo 3: Bases de datos de imágenes en MMW. En este capítulo se describen dos bases de datos adquiridas en la banda de las ondas milimétricas: 1) la adquirida y usada en [9] y 2) BIOGIGA, que es la base de datos generada en este proyecto y la usada para desarrollar y evaluar el sistema biométrico [12].

Capítulo 4: Sistema propuesto: diseño y desarrollo. El capítulo cuarto, tras una breve introducción a los sistemas biométricos, detalla las diferentes etapas del diseño y desarrollo del sistema biométrico implementado: desde el preprocesado de las imágenes de entrada hasta la decisión sobre la identidad.

Capítulo 5: Experimentos y Resultados. En este capítulo, primero se presenta un resumen de la evaluación de los sistemas biométricos. Después se describen los protocolos experimentales y el clasificador utilizado. Finalmente se presentan y analizan los resultados obtenidos en cada experimento.

Capítulo 6: Conclusiones y Trabajo Futuro. Finalmente se extraen las conclusiones en este capítulo y se propone el posible trabajo futuro.

Por último, las siguientes secciones se hallan al final de la memoria: Bibliografía y los apéndices siguientes: Introducción (traducción obligatoria al español del capítulo 1), Conclusiones y Trabajo Futuro (traducción obligatoria al español del capítulo 6), Presupuesto, Pliego de Condiciones y Publicaciones.

A.5 Contribuciones

Las contribuciones de este proyecto fin de carrera se pueden resumir en los siguientes puntos:

- Resumen del estado del arte sobre los trabajos de investigación de reconocimiento biométrico que hacen uso de imágenes adquiridas fuera del espectro visible.
- Estudio de las principales ventajas e inconvenientes de las imágenes adquiridas en cada banda espectral.
- El uso innovador de imágenes adquiridas en la banda de las ondas milimétricas como rasgo biométrico.
- Generación de una base de datos sintética compuesta de imágenes simuladas de personas a 94 GHz.
- Desarrollo e implementación de un sistema de reconocimiento biométrico basado en las imágenes anteriores.
- Evaluación de los resultados obtenidos con nuestro sistema para extraer conclusiones adecuadas sobre su rendimiento y comportamiento bajo diferentes condiciones.

Durante el desarrollo de este proyecto han sido publicados varios artículos aceptados en congresos nacionales e internacionales:

- Miriam Moreno-Moreno, Julian Fierrez, and Javier Ortega-Garcia. Millimeter- and Submillimeter-Wave Imaging Technologies for Biometric Purposes. In *Proceedings of XXIV Simposium Nacional de Union Científica Internacional de Radio*, September 2009 [13].
- Miriam Moreno-Moreno, Julian Fierrez, and Javier Ortega-Garcia. Biometrics Beyond the Visible Spectrum: Imaging Technologies and Applications. In *Proceedings of BioIDMulticomm 2009*, volume 5707 of LNCS, pages 154-161. Springer, September 2009 [14].
- Miriam Moreno-Moreno, Julian Fierrez, Pedro Tome, and Javier Ortega-Garcia. Análisis de Escenarios para Reconocimiento Biométrico a Distancia Adecuados para la Adquisición de Imágenes MMW. In *Proceedings of XXV Simposium Nacional de Union Científica Internacional de Radio*, September 2010 [15].
- Miriam Moreno-Moreno, Julian Fierrez, Pedro Tome, Ruben Vera-Rodriguez, Josep Parron, and Javier Ortega-Garcia. BIOGIGA: Base de datos de imágenes sintéticas de personas a 94 GHz con Fines Biométricos. In *Proceedings of XXVI Simposium Nacional de Union Científica Internacional de Radio*, September 2011 [12].
- Miriam Moreno-Moreno, Julian Fierrez, Ruben Vera-Rodriguez, and Josep Parron. Distance-based Feature Extraction for Biometric Recognition of Millimeter Wave Body Images. In *Proceedings of 45th IEEE International Carnahan Conference on Security Technology*, pages 326-331, October 2011 [16].
- Miriam Moreno-Moreno, Julian Fierrez, Ruben Vera-Rodriguez, and Josep Parron. Simulation of Millimeter Wave Body Images and its Application to Biometric Recognition. In *Proceedings of SPIE Defense, Security and Sensing 2012*, volume 8362. April 2012 [17].

B

Conclusiones y trabajo futuro

B.1 Conclusiones

Hoy en día, la seguridad y defensa están cobrando cada vez mayor importancia. Por esta razón se han instalado portales de seguridad o escáneres corporales en lugares tales como controles de seguridad de aeropuertos. Uno de los últimos tipos de portales adquiere imágenes del cuerpo de personas en la banda de las ondas milimétricas (MMW). Estos portales proporcionan imágenes de la superficie del cuerpo, revelando si el usuario oculta armas o drogas bajo su vestimenta. La integración de un sistema biométrico basado en imágenes de MMW, en este tipo de portales, permitiría además, identificar personas (entre ellas terroristas) previamente registradas en el sistema. Además, el uso de este tipo de radiación y de portales para obtener imágenes en la banda de MMW presentan muchas ventajas (las ondas milimétricas son inocuas, pueden penetrar la ropa, los portales no son invasivos, permiten el reconocimiento a distancia y/o en movimiento y, adicionalmente, la fusión con otros rasgos biométricos adquiridos simultáneamente, como la cara o forma de andar).

En el presente proyecto, primero, se ha propuesto un nuevo método para simular imágenes de personas a 94 GHz (frencuencia en la banda MMW). Este método se ha usado para generar una base de datos sintética, llamada BIOGIGA, compuesta por 1200 imágenes simuladas a 94 GHz de 50 usuarios en dos tipos de escenarios con dos tipos de sistemas de captura de imagen.

En segundo lugar, se ha diseñado e implementado un sistema biométrico basado en ciertas imágenes de BIOGIGA. En el desarrollo de este sistema se ha propuesto un método de extracción de características basado en la detección de puntos característicos del cuerpo, seguido de la medida de 21 distancias entre dichos puntos. Estas distancias forman el vector de características de cada imagen.

Después, se realizaron diferentes experimentos de identificación y verificación para evaluar el sistema desarrollado. Cara experimento se llevó a cabo bajo diferentes condiciones relativas a la ropa, el ángulo de la cámara y el número de imágenes de train y test. Cada experimento se realizó dos veces: (ii) haciendo uso de las 21 características, y (ii) usando sólo el conjunto de características más discriminativo (obtenido mediante el algoritmo SFFS).

Los resultados obtenidos proporcionan información sobre la influencia que tienen, sobre el rendimiento del sistema, (i) las diferentes condiciones mencionadas, y (ii) la selección de carac-

terísticas:

- El efecto de llevar ropa en las imágenes de train y no en las de test (o viceversa) empeora el rendimiento del sistema, siendo el empeoramiento más notable cuando se consideran las 21 características, y mucho menor si sólo se usan las características seleccionadas por SFFS.
- El efecto de tener diferente ángulo de cámara entre las imágenes de test y de train también reduce el rendimiento del sistema, pero de manera contraria: el empeoramiento es casi despreciable si se consideran todas las características, y es mayor cuando se aplica el algoritmo SFFS.
- Incorporar varios vectores de características con diferentes poses para crear los modelos de entrenamiento, es una forma de superar la falta de robustez frente a la variabilidad de pose entre los datos de entrenamiento y de test
- El uso de un mayor número de imágenes de entrenamiento y/o test al realizar los experimentos de reconocimiento, (i) disminuye el rendimiento del sistema cuando se consideran todas las características (debido al hecho de que tener más datos de entrenamiento/test implica mayor variabilidad entre ellos en nuestros protocolos) y, (ii) lo aumenta si se realiza la selección de características (como es de esperar).
- La selección de características mejora considerablemente la el rendimiento de verificación, sin embargo, el rendimiento de identificación sólo mejora ligeramente.
- Las curvas CMC (representación gráfica del rendimiento de identificación) se ven altamente mejoradas cuando se realiza la selección de características.
- Al aplicar la seleción de características, las curvas DET (gráficas que muestran el rendimiento de verificación) mejoran acercándose al origen y teniendo una pendiente más negativa, dotando al sistema de una menor (mejor) EER (*Equal Error Rate*, tasa de igual error en verificación) y de una mayor seguridad (la probabilidad de falsa aceptación disminuye y la de falso rechazo aumenta).

Las características seleccionadas más frecuentemente corresponden a: la altura, la anchura de la cintura, del pecho y la distancia entre el codo y el cuello (en ese orden). Sin embargo, las características con el mayor poder de discriminación son la altura, la anchura de la cintura, la distancia entre el centroide del cuerpo y el pubis y la longitud de las piernas (en ese orden). La discordancia entre ambos conjuntos de características es debida a la correlación entre algunas características del segundo grupo (por ejemplo la altura, la longitud de las piernas y la distancia desde el centroide del cuerpo y el pubis están altamente correlacionadas).

El rendimiento de reconocimiento obtenido en los experimentos es excelente en ambos modos, identificación y verificación: la tasa *Rank-1 recognition rate* tiene un valor entre 0.98 y 1.00 (0.98% y 100% respectivamente), mientras que la EER varía entre 0.00% y 2.00%. Estos valores son similares e incluso mejores que los obtenidos por Alefs. *et al.* en [9] (el único trabajo publicado hasta ahora sobre reconocimiento biométrico basado en imágenes de MMW). En ese trabajo se obtiene una EER en el rango de 1.00%-2.00%. De todas maneras, los resultados obtenidos en nuestros experimentos no son totalmente representativos (debido al pequeño tamaño de la base de datos, 50 usuarios, y a que las diferencias de rendimiento obtenidas en los diferentes experimentos son pequeñas). De hecho, las tasas de error están sesgadas de forma optimista. Esto es debido a (i) el bajo número de usuarios, (ii) el hecho de que las imágenes son sintéticas, y (iii) que la selección de características se realizó usando todos los datos disponibles (y no usando exclusivamente datos de un conjunto de desarrollo).

Como se ha explicado, las limitaciones de este trabajo están relacionadas con las características especiales de la base de datos usada. Las imágenes de BIOGIGA son limitadas cuando se comparan con las imágenes reales adquiridas en la práctica. Sin embargo, las imágenes sintéticas son muy similares a las realmente capturadas a 94 GHz. Además, las imágenes sintéticas usadas están basadas en medidas reales de las personas. Por tanto, las características propuestas se pueden aplicar directamente y son útiles para imágenes reales en la banda de MMW. Adicionalmente, los experimentos realizados usando la base de datos BIOGIGA han proporcionado resultados cualitativos sobre los efectos de las diferentes condiciones y de la selección de características sobre el rendimiento del sistema, que era uno de los principales objetivos del proyecto.

B.2 Trabajo Futuro

Como trabajo futuro, se proponen las siguientes líneas de investigación:

- El desarrollo de un sistema similar al propuesto aquí, que haga uso de imágenes simuladas con sistemas activos (BIOGIGA también contiene ese tipo de imágenes, pero no fueron usadas en este proyecto).
- La generación de una base de datos de imágenes reales adquiridas en la banda de MMW (y si es posible, también con imágenes de los mismos usuarios capturadas en la banda del VIS y del IR, creando así un *Base de Datos Multiespectral*).
- La adaptación del sistema aquí desarrollado para que opere con imágenes reales en la banda de MMW. En esta tarea, así como en la primera, el módulo de segmentación de la imagen debe ser adaptado al nuevo tipo de imágenes.
- El diseño y desarrollo de sistemas biométricos alternativos que hagan uso sólo de algunas partes de las imágenes de MMW (como la cara, el tórax, etc. como se realizó en [9]).
- La fusión de diferentes rasgos biométricos adquiridos en la banda de MMW.
- La fusión de rasgo(s) biométrico(s) adquirido(s) en la banda MMW con rasgo(s) (iguale(s) o diferente(s)) adquirido(s) en otras bandas (i.e. desarrollo de un *Sistema Biométrico Multiespectral*).
- El uso de información extraída de imágenes en la banda de MMW (como medidas antropométricas) para aumentar el rendimiento de otros sistemas biométricos tradicionales con rendimiento de medio-alto (*Soft Biometrics*).
- La integración de un sistema de reconocimiento biométrico basado en imágenes reales en la banda de MMW en un escáner corporal que trabaje en esa banda espectral.

C

Project Budget

1)	**Ejecución Material**	
	• Compra de ordenador personal (Software incluido)	2.000 €
	• Alquiler de impresora láser	250 €
	• Material de oficina	150 €
	• Total de ejecución material	2.400 €
2)	**Gastos generales**	
	• 16% sobre Ejecución Material	384 €
3)	**Beneficio Industrial**	
	• 6% sobre Ejecución Material	144 €
4)	**Honorarios Proyecto**	
	• 2500 horas a 15 €/ hora	37500 €
5)	**Material fungible**	
	• Gastos de impresión	250 €
	• Encuadernación	100 €
6)	**Subtotal del presupuesto**	
	• Subtotal Presupuesto	40778 €
7)	**I.V.A. aplicable**	
	• 18% Subtotal Presupuesto	7340 €
8)	**Total presupuesto**	
	• Total Presupuesto	48118 €

Madrid, Junio 2012

El Ingeniero Jefe de Proyecto

Fdo.: Miriam Moreno Moreno

Ingeniero Superior de Telecomunicación

D

Schedule of Conditions

Pliego de condiciones

Este documento contiene las condiciones legales que guiarán la realización, en este proyecto, de *Reconocimiento Biométrico Basado en Imágenes simuladas en la banda de Ondas Milimétricas*. En lo que sigue, se supondrá que el proyecto ha sido encargado por una empresa cliente a una empresa consultora con la finalidad de realizar dicho sistema. Dicha empresa ha debido desarrollar una línea de investigación con objeto de elaborar el proyecto. Esta línea de investigación, junto con el posterior desarrollo de los programas está amparada por las condiciones particulares del siguiente pliego.

Supuesto que la utilización industrial de los métodos recogidos en el presente proyecto ha sido decidida por parte de la empresa cliente o de otras, la obra a realizar se regulará por las siguientes:

Condiciones generales.

1. La modalidad de contratación será el concurso. La adjudicación se hará, por tanto, a la proposición más favorable sin atender exclusivamente al valor económico, dependiendo de las mayores garantías ofrecidas. La empresa que somete el proyecto a concurso se reserva el derecho a declararlo desierto.

2. El montaje y mecanización completa de los equipos que intervengan será realizado totalmente por la empresa licitadora.

3. En la oferta, se hará constar el precio total por el que se compromete a realizar la obra y el tanto por ciento de baja que supone este precio en relación con un importe límite si este se hubiera fijado.

4. La obra se realizará bajo la dirección técnica de un Ingeniero Superior de Telecomunicación, auxiliado por el número de Ingenieros Técnicos y Programadores que se estime preciso para el desarrollo de la misma.

5. Aparte del Ingeniero Director, el contratista tendrá derecho a contratar al resto del personal, pudiendo ceder esta prerrogativa a favor del Ingeniero Director, quien no estará obligado a aceptarla.

6. El contratista tiene derecho a sacar copias a su costa de los planos, pliego de condiciones y presupuestos. El Ingeniero autor del proyecto autorizará con su firma las copias solicitadas por el contratista después de confrontarlas.

7. Se abonará al contratista la obra que realmente ejecute con sujeción al proyecto que sirvió de base para la contratación, a las modificaciones autorizadas por la superioridad o a las órdenes que con arreglo a sus facultades le hayan comunicado por escrito al Ingeniero Director de obras siempre que dicha obra se haya ajustado a los preceptos de los pliegos de condiciones, con arreglo a los cuales, se harán las modificaciones y la valoración de las diversas unidades sin que el importe total pueda exceder de los presupuestos aprobados. Por consiguiente, el número de unidades que se consignan en el proyecto o en el presupuesto, no podrá servirle de fundamento para entablar reclamaciones de ninguna clase, salvo en los casos de rescisión.

8. Tanto en las certificaciones de obras como en la liquidación final, se abonarán los trabajos realizados por el contratista a los precios de ejecución material que figuran en el presupuesto para cada unidad de la obra.

9. Si excepcionalmente se hubiera ejecutado algún trabajo que no se ajustase a las condiciones de la contrata pero que sin embargo es admisible a juicio del Ingeniero Director de obras, se dará conocimiento a la Dirección, proponiendo a la vez la rebaja de precios que el Ingeniero estime justa y si la Dirección resolviera aceptar la obra, quedará el contratista obligado a conformarse con la rebaja acordada.

10. Cuando se juzgue necesario emplear materiales o ejecutar obras que no figuren en el presupuesto de la contrata, se evaluará su importe a los precios asignados a otras obras o materiales análogos si los hubiere y cuando no, se discutirán entre el Ingeniero Director y el contratista, sometiéndolos a la aprobación de la Dirección. Los nuevos precios convenidos por uno u otro procedimiento, se sujetarán siempre al establecido en el punto anterior.

11. Cuando el contratista, con autorización del Ingeniero Director de obras, emplee materiales de calidad más elevada o de mayores dimensiones de lo estipulado en el proyecto, o sustituya una clase de fabricación por otra que tenga asignado mayor precio o ejecute con mayores dimensiones cualquier otra parte de las obras, o en general, introduzca en ellas cualquier modificación que sea beneficiosa a juicio del Ingeniero Director de obras, no tendrá derecho sin embargo, sino a lo que le correspondería si hubiera realizado la obra con estricta sujeción a lo proyectado y contratado.

12. Las cantidades calculadas para obras accesorias, aunque figuren por partida alzada en el presupuesto final (general), no serán abonadas sino a los precios de la contrata, según las condiciones de la misma y los proyectos particulares que para ellas se formen, o en su defecto, por lo que resulte de su medición final.

13. El contratista queda obligado a abonar al Ingeniero autor del proyecto y director de obras así como a los Ingenieros Técnicos, el importe de sus respectivos honorarios facultativos por formación del proyecto, dirección técnica y administración en su caso, con arreglo a las tarifas y honorarios vigentes.

14. Concluida la ejecución de la obra, será reconocida por el Ingeniero Director que a tal efecto designe la empresa.

15. La garantía definitiva será del 4

16. La forma de pago será por certificaciones mensuales de la obra ejecutada, de acuerdo con los precios del presupuesto, deducida la baja si la hubiera.

17. La fecha de comienzo de las obras será a partir de los 15 días naturales del replanteo oficial de las mismas y la definitiva, al año de haber ejecutado la provisional, procediéndose si no existe reclamación alguna, a la reclamación de la fianza.

18. Si el contratista al efectuar el replanteo, observase algún error en el proyecto, deberá comunicarlo en el plazo de quince días al Ingeniero Director de obras, pues transcurrido ese plazo será responsable de la exactitud del proyecto.

19. El contratista está obligado a designar una persona responsable que se entenderá con el Ingeniero Director de obras, o con el delegado que éste designe, para todo relacionado con ella. Al ser el Ingeniero Director de obras el que interpreta el proyecto, el contratista deberá consultarle cualquier duda que surja en su realización.

20. Durante la realización de la obra, se girarán visitas de inspección por personal facultativo de la empresa cliente, para hacer las comprobaciones que se crean oportunas. Es obligación del contratista, la conservación de la obra ya ejecutada hasta la recepción de la misma, por lo que el deterioro parcial o total de ella, aunque sea por agentes atmosféricos u otras causas, deberá ser reparado o reconstruido por su cuenta.

21. El contratista, deberá realizar la obra en el plazo mencionado a partir de la fecha del contrato, incurriendo en multa, por retraso de la ejecución siempre que éste no sea debido a causas de fuerza mayor. A la terminación de la obra, se hará una recepción provisional previo reconocimiento y examen por la dirección técnica, el depositario de efectos, el interventor y el jefe de servicio o un representante, estampando su conformidad el contratista.

22. Hecha la recepción provisional, se certificará al contratista el resto de la obra, reservándose la administración el importe de los gastos de conservación de la misma hasta su recepción definitiva y la fianza durante el tiempo señalado como plazo de garantía. La recepción definitiva se hará en las mismas condiciones que la provisional, extendiéndose el acta correspondiente. El Director Técnico propondrá a la Junta Económica la devolución de la fianza al contratista de acuerdo con las condiciones económicas legales establecidas.

23. Las tarifas para la determinación de honorarios, reguladas por orden de la Presidencia del Gobierno el 19 de Octubre de 1961, se aplicarán sobre el denominado en la actualidad "Presupuesto de Ejecución de Contrata" y anteriormente llamado "Presupuesto de Ejecución Material" que hoy designa otro concepto.

Condiciones particulares.

La empresa consultora, que ha desarrollado el presente proyecto, lo entregará a la empresa cliente bajo las condiciones generales ya formuladas, debiendo añadirse las siguientes condiciones particulares:

1. La propiedad intelectual de los procesos descritos y analizados en el presente trabajo, pertenece por entero a la empresa consultora representada por el Ingeniero Director del Proyecto.

2. La empresa consultora se reserva el derecho a la utilización total o parcial de los resultados de la investigación realizada para desarrollar el siguiente proyecto, bien para su publicación o bien para su uso en trabajos o proyectos posteriores, para la misma empresa cliente o para otra.

3. Cualquier tipo de reproducción aparte de las reseñadas en las condiciones generales, bien sea para uso particular de la empresa cliente, o para cualquier otra aplicación, contará con autorización expresa y por escrito del Ingeniero Director del Proyecto, que actuará en representación de la empresa consultora.

4. En la autorización se ha de hacer constar la aplicación a que se destinan sus reproducciones así como su cantidad.

5. En todas las reproducciones se indicará su procedencia, explicitando el nombre del proyecto, nombre del Ingeniero Director y de la empresa consultora.

6. Si el proyecto pasa la etapa de desarrollo, cualquier modificación que se realice sobre él, deberá ser notificada al Ingeniero Director del Proyecto y a criterio de éste, la empresa consultora decidirá aceptar o no la modificación propuesta.

7. Si la modificación se acepta, la empresa consultora se hará responsable al mismo nivel que el proyecto inicial del que resulta el añadirla.

8. Si la modificación no es aceptada, por el contrario, la empresa consultora declinará toda responsabilidad que se derive de la aplicación o influencia de la misma.

9. Si la empresa cliente decide desarrollar industrialmente uno o varios productos en los que resulte parcial o totalmente aplicable el estudio de este proyecto, deberá comunicarlo a la empresa consultora.

10. La empresa consultora no se responsabiliza de los efectos laterales que se puedan producir en el momento en que se utilice la herramienta objeto del presente proyecto para la realización de otras aplicaciones.

11. La empresa consultora tendrá prioridad respecto a otras en la elaboración de los proyectos auxiliares que fuese necesario desarrollar para dicha aplicación industrial, siempre que no haga explícita renuncia a este hecho. En este caso, deberá autorizar expresamente los proyectos presentados por otros.

12. El Ingeniero Director del presente proyecto, será el responsable de la dirección de la aplicación industrial siempre que la empresa consultora lo estime oportuno. En caso contrario, la persona designada deberá contar con la autorización del mismo, quien delegará en él las responsabilidades que ostente.

E

Publications

All publications available at http://atvs.ii.uam.es/

Title: Millimeter- and Submillimeter-Wave Imaging Technologies for Biometric Purposes.
Authors: Miriam Moreno-Moreno, Julian Fierrez, and Javier Ortega-Garcia.
Published in: Proceedings of XXIV Simposium Nacional de Union Científica Internacional de Radio, September 2009.

Title: Biometrics Beyond the Visible Spectrum: Imaging Technologies and Applications.
Authors: Miriam Moreno-Moreno, Julian Fierrez, and Javier Ortega-Garcia.
Published in: Proceedings of BioIDMulticomm 2009, volume 5707 of LNCS, pages 154-161. Springer, September 2009.

Title: Análisis de Escenarios para Reconocimiento Biométrico a Distancia Adecuados para la Adquisición de Imágenes MMW.
Authors: Miriam Moreno-Moreno, Julian Fierrez, Pedro Tome, and Javier Ortega-Garcia.
Published in: Proceedings of XXV Simposium Nacional de Union Científica Internacional de Radio, September 2010.

Title: BIOGIGA: Base de datos de imágenes sintéticas de personas a 94 GHz con Fines Biométricos.
Authors: Miriam Moreno-Moreno, Julian Fierrez, Pedro Tome, Ruben Vera-Rodriguez, Josep Parron, and Javier Ortega-Garcia.
Published in: Proceedings of XXVI Simposium Nacional de Union Científica Internacional de Radio, September 2011.

Title: Distance-based Feature Extraction for Biometric Recognition of Millimeter Wave Body Images.
Authors: Miriam Moreno-Moreno, Julian Fierrez, Ruben Vera-Rodriguez, and Josep Parron.
Published in: Proceedings of 45th IEEE International Carnahan Conference on Security Technology, pages 326-331, October 2011.

Title: Simulation of Millimeter Wave Body Images and its Application to Biometric Recognition.
Authors: Miriam Moreno-Moreno, Julian Fierrez, Ruben Vera-Rodriguez, and Josep Parron.
Published in: Proceedings of SPIE Defense, Security and Sensing 2012, volume 8362. April 2012.

Millimeter- and Submillimeter-Wave Imaging Technologies for Biometric Purposes

M. Moreno-Moreno, J. Fierrez, J. Ortega-Garcia
{miriam.moreno, julian.fierrez, javier.ortega}@uam.es
Dpto. de Ingeniería Informática. Universidad Autónoma de Madrid. C/ Francisco Tomás y Valiente, 11
Cantoblanco – 28049 Madrid, Spain.

***Abstract*- The inherent restrictions of human body images acquired at visible spectrum hinder the performance of person recognition systems built using that kind of information (e.g. scene artifacts under varying illumination conditions). One promising approach for dealing with those limitations is using images acquired out of the visible spectrum. This paper reviews some of the existing human body imaging technologies working beyond the visible spectrum (X-ray, Infrared, Millimeter and Submillimeter Wave imaging technologies). The pros and cons of each technology and their biometric applications are presented, with special attention to Millimeter and Submillimeter Wave imaging.**

I. INTRODUCTION

The ability to capture an image of the whole human body or a part of it has attracted much interest in many areas such as Medicine, Biology, Surveillance and Biometrics. Biometric Recognition, or simply Biometrics, is a technological field in which users are identified through one or several physiological and/or behavioural characteristics [1]. Many biometric characteristics are used to identify individuals: fingerprint, signature, iris, voice, face, hand, etc. Biometric traits such as the ear, face, hand and gait are usually acquired with cameras working at visible frequencies of the electromagnetic spectrum. Such images are affected by, among other factors, lighting conditions and the body occlusion (e.g., clothing, make up, hair, etc.).

In order to circumvent the limitations imposed by the use of images acquired at the visible spectrum (VIS), researchers in biometrics and surveillance areas [2] have proposed acquiring images at other spectral ranges: X-ray (XR), infrared (IR), Millimeter (MMW) and Submillimeter (SMW) waves (see Fig. 1). In addition to overcoming to some extent some of the limitations of visible imaging, the images captured beyond the visible spectrum present another benefit: they are more robust to spoofing than other biometric images/traits.

In this work, we present an overview of the state of the art in body imaging beyond the visible spectrum, with a focus on biometric recognition applications. In particular, we will concentrate on the potential application of images acquired at GHz-THz frequencies for biometric purposes. We stress the importance of this radiation range because of its ability to pass through cloth and other occlusions, its health safety, its low intrusiveness, and the recent deployment and rapid progress of GHz-THz systems in screening applications.

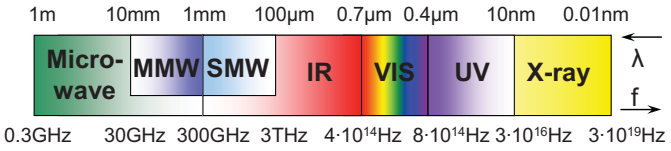

Fig. 1. Electromagnetic spectrum showing the different spectral bands between the microwaves and the X-rays. IR band is sometimes considered to extend to 1 mm including the SMW region.

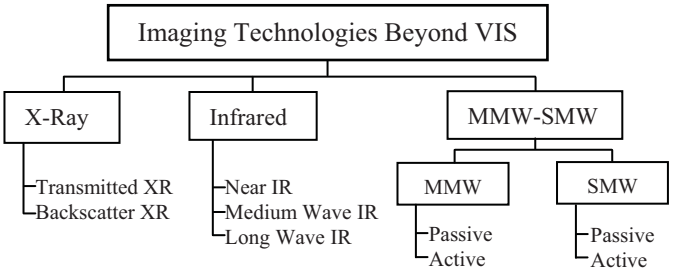

Fig. 2. A taxonomy of imaging technologies beyond visible spectrum. The figure only shows the technologies adequate for biometrics.

II. IMAGING TECHNOLOGIES BEYOND THE VISIBLE SPECTRUM

Many imaging technologies beyond the visible spectrum have been used to capture a body part: IR, magnetic resonance, radioisotope, XR, acoustical-, MMW-, SMW-imaging, etc. Not all of them can be used for biometric purposes because of their high level of intrusiveness. The imaging technologies more adequate for biometric applications are: XR, IR, MMW and SMW imaging. A taxonomy of them is shown in Fig. 2.

Imagery can be classified in two architectures: *passive* or *active*. In the former group the image is generated by receiving natural radiation which has been emitted and reflected from the scene, obtaining a map of brightness temperature. On the other hand, in active imaging the radiation is transmitted to the scene and then collected after reflection to form the image, which is a map of reflectivity.

A. X-ray Imaging

X-radiation has a wavelength in the range of 10-0.01 nm ($3\cdot10^{16}$-$3\cdot10^{19}$ Hz) and enough energy to pass through cloth and human tissues. In addition to cloth penetration, XR imaging provides high image resolution. On the other hand this technology presents some disadvantages: low speed, limitation to very short distances and the health safety concerns it raises because of using ionizing radiation.

The natural background X-radiation is too weak to form an image, therefore active imaging is required in both XR

imaging modalities: *transmission* and *backscatter* X-ray imaging. The first one is the technique used in conventional X-ray radiographic systems, where XR photons transmitted through the body are detected to form the image. In the backscatter XR, the scattered photons are used to construct the image providing mainly a view of the surface of the scanned person [3]. Backscatter XR imaging technology has no tissue penetration.

There are very few works on biometric identification making use of XR imaging: Shamir *et al.* [4] perform biometric identification using knee X-rays while Chen *et al*. [5] present an automatic method for matching dental radiographs. According to our knowledge, there are no works on biometrics using backscatter X-ray images. The application of this technique includes medical imaging [6] and passenger screening at airports and homeland security [7]. There are currently different backscatter X-ray imaging systems available on the market (e.g. AS&E, Rapiscan Systems) to screen people.

B. Infrared Imaging

The infrared band of the electromagnetic spectrum lies between the SMW and VIS regions, its wavelength is in the range of 0.7 μm - 1 mm. The human body emits IR radiation with a wavelength between 3-14 μm, hence both active and passive architectures can be used in IR imaging.

The radiation that is actually detected by an IR sensor depends on the surface properties of the object and of the medium (atmosphere). According to the properties of the medium and the spectral ranges of the currently available IR detectors, the IR spectrum is divided into five parts. However IR imaging systems usually operate in one of the three following IR bands: the near infrared (NIR), the medium wave infrared (MWIR) or the long wave infrared (LWIR), where the high transmissivity atmosphere windows are located. Imaging objects within these IR-bands presents different characteristics. A summary of the properties of these bands is showed in Table 1.

Many biometric research works have been developed using NIR, MWIR and LWIR imaging systems. Face and hand vein pattern recognition are the most important biometric modalities investigated in these three bands (see references in Table 1). Images acquired at any of these bands are, to some extent, environmental illumination invariant. Specifically images at NIR are body condition invariant and can provide good quality vein patterns near the skin surface [9], but external NIR illumination is required. Images acquired at MWIR and LWIR show patterns of radiated heat from the body's surface (often called thermograms). Very few biometric works have been developed in MWIR [10, 11], probably due to the high cost of MWIR cameras. LWIR cameras are much cheaper but, in contrast with NIR, LWIR can only capture large veins. Additionally, most of the LWIR images have low levels of contrast, being also sensitive to ambient and body condition [9].

C. Millimeter and Submillimeter Wave Imaging

MMW and SMW radiation fill the gap between the IR and the microwaves (see Fig. 1). Specifically, millimeter waves lie in the band of 30-300 GHz (10-1 mm) and the SMW regime lies in the range of 0.3-3 THz (1-0.1 mm).

IR Spectral bands	Range (μm)	Archi-tecture	IR camera cost	Image Properties	Applications in Biometrics
Near IR (NIR)	0,7-1	Active	Low, VIS came-ra also sensitive	Good quality, body condition invariant,	Face [8] and Hand Vein [9] Recognition
Medium Wave IR (MWIR)	3 - 5	Passive	High	Good quality, sensiti-ve to body conditions	Face [10] and Hand Vein [11] Recognition
Long Wave IR (LWIR)	8 - 14	Passive	Low	Low contrast, sensiti-ve to body conditions	Face [12] and Hand Vein [9] Recognition

Table 1. Properties of the most important IR bands.

MMW and SMW radiation can penetrate through many commonly used nonpolar dielectric materials such as paper, plastics, wood, leather, hair and even dry walls with little attenuation [13, 14]. Clothing is highly transparent to the MMW radiation and partially transparent to the SMW radiation [15]. Above 30 GHz, the transmission of the atmosphere varies strongly as a function of frequency due to water vapour and oxygen [16, 17]. There are relatively transparent windows centered at 35, 94, 140 and 220 GHz in the MMW range and less transparent windows in the SMW region located at: 0.34, 0.67, 1.5, 2, 2.1, 2.5, 3.4 and 4.3 THz. Atmosphere attenuation is further increased in poor weather. Liquid water extremely attenuates submillimeter waves while MMW radiation is less attenuated (millions of times) in the presence of clouds, fog, smoke, snow, and sand storms than VIS or IR radiation.

Consequently, natural applications of MMW and SMW imaging include security screening, non-destructive inspection, and medical and biometrics imaging. Low visibility navigation is another application of MMW imaging [18]. The detection of concealed weapons has been the most developed application of MMW/SMW imaging systems so far, in contrast to the biometrics area, where no research works have been produced.

Although most of the radiation emitted by the human body belongs to the MWIR and LWIR bands, it emits radiation in the SMW and MMW regions as well. This allows passive imaging. A key factor in MMW and SMW passive imaging is the sky illumination. This makes images acquired in indoor and outdoor environments to have very different contrast when working with passive systems. Outdoors radiometric temperature contrast can be very large, but it is very small indoors. In passive imaging operating indoors the signal to noise ratio (SNR) of the existing cameras is barely enough for coarse object detection, being usually insufficient for identification (as needed for biometrics). There are two solutions to overcome this problem: (i) cooling the detector or alternatively (ii) using active imaging. Cooling the detector improves the sensitivity but it makes the camera more expensive and difficult to use.

In active imaging, the source that illuminates the scene produces much higher power level than the emitted from the scene, so it can be considered as an object at very high temperature. If the source is incoherent and physically large, active imaging is equivalent to passive imaging with the surroundings at very high temperature, and hence results in much greater contrast within the image. If the source is small, active imaging becomes more complicated. In any case, the power level of the radiation source in active imaging strongly affects the detection resolution. In addition to higher resolution than passive imaging, active imaging provides higher SNR, higher signal levels, and the ability to obtain depth information in the scene.

C.1. Millimeter Wave Imaging

- **Passive MMW Imaging**

There have been many research groups working on passive MMW imaging (PMMW) since its early developments. Most of them have constructed prototype radiometers that work at a frequency range centered at 35 GHz [19] or at 94 GHz [13, 20-22].

The images obtained with PMMW imaging systems have low resolution compared to VIS and IR images. This low resolution is a consequence of the longer wavelengths used relative to the aperture size of the sensor's collection optics. Further, images acquired indoors will present less contrast than those acquired outdoors, as it is shown in Fig. 3a and 3b.

The applications of most of the cited works are the detection of concealed weapons or vision under adverse weather conditions. No biometrics applications have been found yet in PMMW imaging in spite of its ability to penetrate cloth and the availability of multiple commerical PMMW cameras (e.g. Quinetiq, Brijot, Alfa Imaging, Sago Systems, Millivision, and View Systems).

- **Active MMW Imaging**

Active MMW imaging (AMMW) has gained more and more attention during the last few years for indoor security applications [23-25]. Sheen *et al.* [23] demonstrated an AMMW imager operating at 27-33 GHz and good quality images were obtained (see Fig. 3c). Derham *et al.* [24] showed the performance of a prototype AMMW imaging system operating at 60 GHz that uses the frequency–encoding technique. Timms *et al.* [25] developed a 190 GHz active imaging system.

An image obtained with AMMW is shown in Fig. 3c together with two PMMW images. The higher quality of the images acquired with active systems is clearly noticeable.

Again, most of AMMW imaging systems are used as security portals. Some AMMW imagers are currently available on the market (Agilent and L3-Communications). Agilent's MMW imaging system works at 30 GHz and has a transverse resolution of 1 cm. L-3 Provision MMW body screening portal has been used since 2007 at some airports. However, no biometric application of AMMW imaging has emerged so far.

C.2. Submillimeter Wave Imaging

The shorter the radiation wavelength is, the better image resolution is available, and hence SMW imaging would provide better resolution than MMW imaging. On the other hand, as the wavelength decreases, the penetration capability decreases. Further, the technology needed in the SMW imaging systems is much less mature than the MMW technology.

- **Passive SMW Imaging**

In passive SMW imaging (PSMW) the contrast in the image depends on the operation frequency: at frequencies below 0.5 THz it will be dominated by the reflectivity of the items, while at frequencies of 0.5 THz and above, it will be dominated by the emissivity of the objects and their physical temperature (similar to thermography).

Some of the more relevant and recent research works on PSMW imaging include [26] and [27]. Luukanen *et al.* [26] developed an imaging system working at 0.1-1 THz. Shen *et al.* [27] performed detection and segmentation of concealed objects in images acquired with the imaging system described in [26]. They obtain good quality images as it can be seen in Fig. 4a. Fig. 4b shows another PSMW image of a man with a spanner hidden under his T-shirt (acquired at 1.5 THz [28]). These two images show that cloth is less transparent to submilliter waves than to MMW radiation (collar and folds of the weave are visible). A passive system required to penetrate all type of clothing should operate below 0.3-0.5 THz [15, 16].

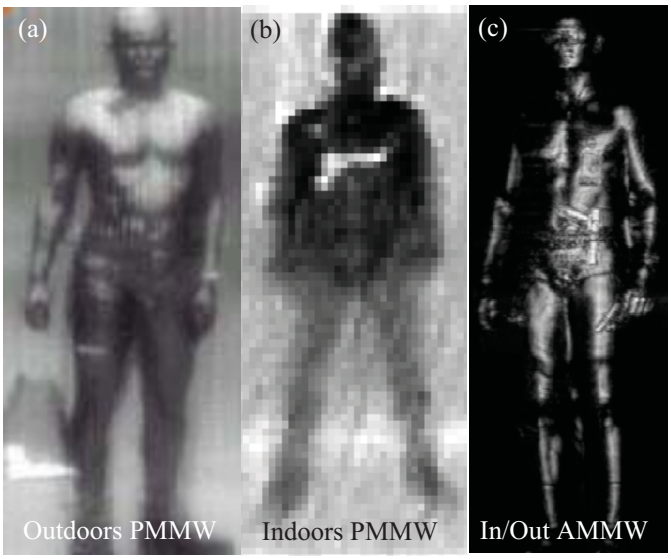

Fig. 3. Images acquired with MMW imaging systems. (a) Outdoors PMMW image (94 GHz) of a man carrying a gun in a bag. (b) Indoors PMMW image (94 GHz) of a man with a gun concealed under clothing. (c) AMMW image of a man carrying two handguns acquired at 27-33 GHz. These figure insets are extracted from: www.vision4thefuture.org (a), www.alfaimaging.com (b) and [23] (c).

The higher resolution of SMW images compared to MMW makes SMW more suitable to biometric recognition applications. However the partial clothing opacity to SMW radiation would hinder the performance of biometric systems. To the best of our knowledge, no biometric works have been performed using PSMW imaging.

Regarding commercial PSMW imaging systems, Thruvision currently produces what it seems to be the only commercially available passive THz imaging system.

- **Active SMW Imaging**

Research works on active SMW imaging (ASMW) have only appeared recently [29-31]. Some of them can image a body part at a distance [29] at 0.6-0.8 THz with a spatial resolution of less than 1 cm, while the rest present much better resolution (< 2 mm) working with relatively close targets at 310 GHz [30], or beyond 1 THz [31].

Fig. 4 c-f shows images acquired at SMW with the active architecture. An image of a man hiding a gun beneath his shirt acquired with a 0.6 THz radar [29] is shown in Fig. 4d while the inset 4c is a full 3-D reconstruction of the same image after some additional smoothing. The two images at the bottom right, insets 4e and 4f, show, respectively, a visible frequency ink thumb print and a reflected terahertz 20-frame average image of the same thumb flattened against a polyethylene wedge [31].

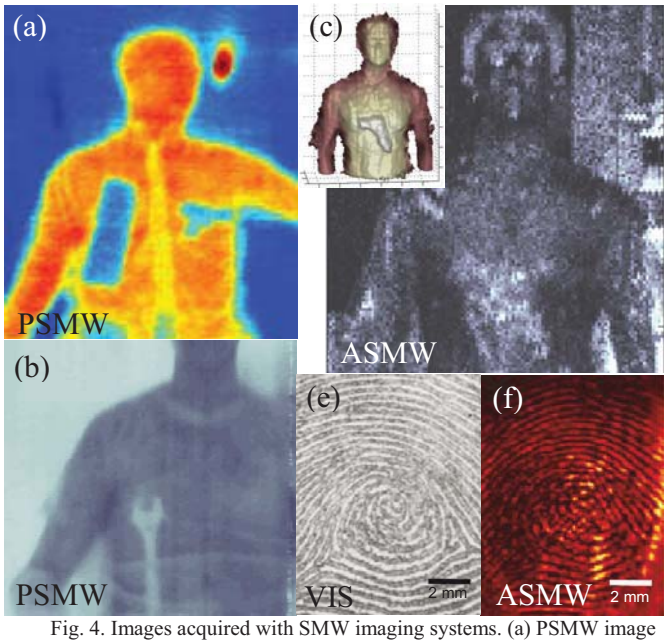

Fig. 4. Images acquired with SMW imaging systems. (a) PSMW image (0.1-1 THz) of a man with concealed objects beneath his jacket. (b) PSMW image (1.5 THz) of a man with a spanner under his T-shirt. (d) ASMW image (0.6 THz) of a man hiding a gun beneath his shirt. (c) Full 3-D reconstruction of the previous described image after smoothing of the back surface. (e) White light image of a thumb print. (f) Terahertz reflection mode image of thumb. These figure insets are extracted from: [27] (a), [28] (b), [29] (c and d) and [31] (e and f).

Although images acquired at a distance with ASMW imaging systems present not very high spatial resolution, extracting signals from the noisy scene clutter is possible [29]. Furthermore, images acquired from targets near the system present a reasonable resolution for biometric applications, as it is shown in Fig. 4f. This fingerprint acquired at 4.3 THz has enough quality to allow the identification of an individual. On the other hand, the imaging system is quite complicated, and it works only in laboratory environments. Active terahertz imaging systems are available providing high resolution (Picometrix) and additional spectroscopic information (Teraview).

III. Conclusions

We have provided a taxonomy of the existing imaging technologies operating at frequencies out of the visible spectrum that can be used for biometrics purposes. Although only X-ray and Infrared spectral bands have been used for biometric applications, we have focused our attention in MMW and SMW bands, which provide interesting advantages over the other kind of radiation (e.g. transmission through common garment, no health hazard and low intrusiveness). However the imaging technology operating at these frequencies (GHz-THz) is not completely mature yet.

Acknowledgments

This work has been supported by Terasense (CSD2008-00068) Consolider project of the Spanish Ministry of Science and Technology. M. M.-M. is supported by a CPI Fellowship from CAM, and J. F. is supported by a Marie Curie Fellowship from the European Commission.

References

[1] A. K. Jain *et al*, "An Introduction to Biometric Recognition", *IEEE Trans. on CSVT*. Vol. 14, No. 1, pp. 4-20, 2004.
[2] National Research Council, *Airline Passenger Security Screening: New Technologies and Implementation Issues*, National Academy Press, Washington, D.C. 1996.
[3] R.H. Bossi *et al*, "Backscatter X-ray imaging", *Materials Evaluation*, Vol.46, No.11, pp. 1462-7, 1988.
[4] L. Shamir *et al*, "Biometric identification using knee X-rays", *Int. J. Biometrics*, Vol. 1, No. 3, pp 365-370, 2009.
[5] H. Chen and A.K. Jain, "Dental Biometrics: Alignment and Matching of Dental Radiographs", *IEEE Transactions on PAMI*, Vol. 27, No. 8, pp. 1319-1326, 2005.
[6] E.J.L. Morris *et al*, "A backscattered x-ray imager for medical applications", *Proc. of the SPIE*, Vol. 5745, pp. 113-120, 2005.
[7] A. Chalmers, "Three applications of backscatter X-ray imaging technology to homeland defense", *Proc. of the SPIE*, Vol. 5778, No.1, pp. 989-93, 2005.
[8] S. Z. Li *et al*, "Illumination Invariant Face Recognition Using Near-Infrared Images", *IEEE Trans. on PAMI*, Vol. 29, No. 4, 2007.
[9] W. Lingyu *et al*, "Near- and Far- Infrared Imaging for Vein Pattern Biometrics", *Proc. of the AVSS*, pp.52-57, 2006.
[10] P. Buddharaju *et al*, "Physiology-Based Face Recognition in the Thermal Infrared Spectrum", *IEEE Trans. on PAMI*, Vol. 29, No. 4, 2007.
[11] C. K. Fann *et al*, "Biometric Verification Using Thermal Images of Palm-dorsa Vein-patterns", *IEEE Trans. on CSVT*, Vol. 14, No. 2, pp. 199-213, 2004.
[12] A. Selinger *et al*, "Face Recognition in the Dark," *Conference on CVPRW*, pp. 129-129, 2004.
[13] R. L. Howald *et al*, "Millimeter Waves: The Evolving Scene", *IEEE Conference on HST*, pp.234-239, 2007.
[14] H. B. Liu *et al*, "Terahertz Spectroscopy and Imaging for Defense and Security Applications", *Proc. of the IEEE*, Vol. 95, No. 8, pp.1514-1527, 2007.
[15] J. E. Bjarnason *et al*, "Millimeter-wave, terahertz, and mid-infrared transmission through common clothing", *Appl. Physics Lett.* Vol. 85, No. 4, 2004.
[16] R. Appleby *et al*, "Millimeter-Wave and Submillimeter-Wave Imaging for Security and Surveillance", *Proc. of the IEEE*, Vol. 95, No. 8, pp. 1683-1690, 2007.
[17] M. J. Rosker, "Imaging Through the Atmosphere at Terahertz Frequencies", *International Microwave Symposium IEEE/MTT-S*, pp.773-776, 2007.
[18] L. Yujiri *et al*, "Passive millimeter wave imaging," *Microwave Magazine, IEEE*, Vol. 4, No. 3, pp. 39-50, 2003.
[19] G. N. Sinclair et al, "Detection of illegal passengers in lorries using a passive millimetre wave scanner", *Proc. International Carnahan Conference on Security*, pp. 167-170, 2002.
[20] M. Sato *et al*,"94-GHz Band High-Gain and Low-Noise Amplifier Using InP-HEMTs for Passive Millimeter Wave Imager," *International Microwave Symposium IEEE/MTT-S*, pp.1775-1778, 2007.
[21] Kapilevich *et al*, "Passive mm-wave Sensor for In-Door and Out-Door Homeland Security Applications", *SensorComm 2007*, pp.20-23, 2007.
[22] C. Sklarczyk *et al*, "94 GHz Radar Sensor for Process Control and Imaging", *9th European Conference on NDT*, 2006.
[23] D. M. Sheen *et al*, "Three-dimensional millimeter-wave imaging for concealed weapon detection", *IEEE Trans. on Microwave Theory and Techniques*, Vol.49, No.9, pp.1581-1592, 2001.
[24] T. Derham *et al*, "Active MMW Imaging System using the Frequency-Encoding Technique," *Microwave Conference*, pp.181-184, 2007.
[25] G.P. Timms *et al*, "190 GHz Millimetre-wave Imaging using MMIC-based Heterodyne Receivers," *Conference on AusWireless* 2007, pp.32-32, 2007.
[26] A Luukanen *et al*, "An Ultra-Low Noise Superconducting Antenna-Coupled Microbolometer With a Room-Temperature Read-Out", *IEEE Microwave and Wireless Components Lett.*, Vol. 16, No. 8, 2006.
[27] X. Shen *et al*, "Detection and Segmentation of Concealed Objects in Terahertz Images", *IEEE trans. on IP*, Vol. 17, No. 12, 2008.
[28] A. Luukanen *et al*, "Stand-off Contraband Identification using Passive THz Imaging", *EDA IEEMT Workshop*, 2008.
[29] K. B. Cooper *et al*, "Penetrating 3-D Imaging at 4- and 25-m Range Using a Submillimeter-Wave Radar", *IEEE Trans. on Microwave Theory and Techniques*, Vol. 56, No. 12, 2008.
[30] A. Tamminen, "Indirect Holographic Imaging at 310 GHz", *Proc. of EuMC*, pp. 168-17, 2008.
[31] A. W. Lee *et al*, "Real-time imaging using a 4.3-THz Quantum Cascade Laser and a 320 x 240 Microbolometer Focal-Plane Array," *IEEE Photonics Technology Letters*, Vol. 18, No.13, pp.1415-1417, 2006.

Biometrics Beyond the Visible Spectrum: Imaging Technologies and Applications

Miriam Moreno-Moreno, Julian Fierrez and Javier Ortega-Garcia

Escuela Politécnica Superior. Universidad Autónoma de Madrid.
C/ Francisco Tomás y Valiente, 11 – Cantoblanco – 28049 Madrid, Spain.
{miriam.moreno, julian.fierrez, javier.ortega}@uam.es

Abstract. Human body images acquired at visible spectrum have inherent restrictions that hinder the performance of person recognition systems built using that kind of information (e.g. scene artefacts under varying illumination conditions). One promising approach for dealing with those limitations is using images acquired beyond the visible spectrum. This paper reviews some of the existing human body imaging technologies working beyond the visible spectrum (X-ray, Infrared, Millimeter and Submillimeter Wave imaging technologies). The benefits and drawbacks of each technology and their biometric applications are presented.

Keywords: Imaging Technologies, X-ray, Infrared, Millimeter Waves, Submillimeter Waves, Thermograph, Passive Imaging, Active Imaging, Terahertz Imaging, Biometrics, Face Recognition, Hand Vein Recognition.

1 Introduction

The ability to capture an image of the whole human body or a part of it has attracted much interest in many areas such as Medicine, Biology, Surveillance and Biometrics. Biometric Recognition, or simply Biometrics, is a technological field in which users are identified through one or more physiological and/or behavioural characteristics [1]. Many biometric characteristics are used to identify individuals: fingerprint, signature, iris, voice, face, hand, etc. Biometric traits such as the ear, face, hand and gait are usually acquired with cameras working at visible frequencies of the electromagnetic spectrum. Such images are affected by, among other factors, lighting conditions and occlusions (e.g., clothing, make up, hair, etc.)

In order to circumvent the limitations imposed by the use of images acquired at the visible spectrum (VIS), researchers in biometrics and surveillance [2] have proposed acquiring images at other spectral ranges: X-ray (XR), Infrared (IR), Millimeter (MMW) and Submillimeter (SMW) waves (see Fig. 1). In addition to overcoming to some extent some of the limitations of visible imaging, the images captured beyond the visible spectrum present another benefit: they are more robust to spoofing than other biometric images/traits [3].

In this work, we present an overview of the state of the art in body imaging beyond the visible spectrum, with a focus on biometric recognition applications. In particular,

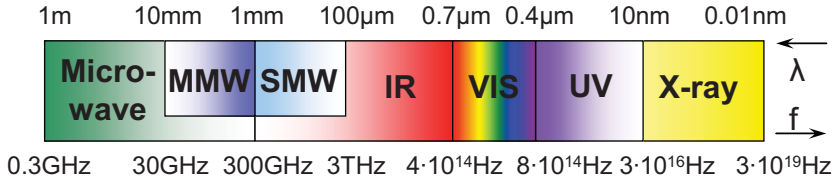

Fig. 1. Electromagnetic spectrum showing the different spectral bands between the microwaves and the X-rays. The IR band is sometimes considered to extend to 1 mm including the SMW region.

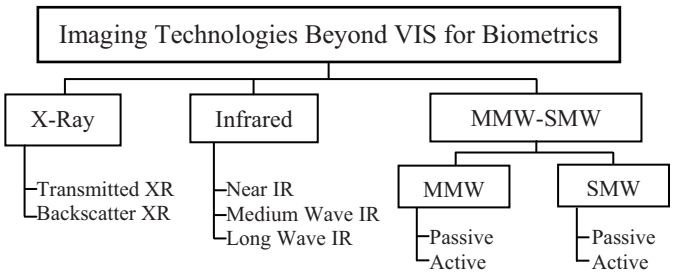

Fig. 2. A taxonomy of imaging technologies beyond visible spectrum. The figure only shows the technologies adequate for biometrics.

a taxonomy followed by the properties and the biometric applications of each imaging technology beyond the visible spectrum is presented.

2 Fundamentals and Taxonomy of Imaging Technologies beyond the Visible Spectrum

Many imaging technologies beyond the visible spectrum have been used to capture a body part: IR, magnetic resonance, radioisotope, XR, acoustical, MMW- and SMW-imaging, etc. Not all of them can be used for biometric purposes because of their high level of intrusiveness. The imaging technologies more adequate for biometric applications are: XR, IR, MMW and SMW imaging. A taxonomy of them is shown in Fig. 2.

Imagery can be classified in two architectures: *passive* or *active*. In the former group the image is generated by receiving natural radiation which has been emitted and reflected from the scene, obtaining a map of brightness temperature. On the other hand, in active imaging the radiation is transmitted to the scene and then collected after reflection to form the image, which is a map of reflectivity.

The contrast in the scene in any part of the spectrum is a function of the optical properties of the object being imaged and its background. In particular, the apparent temperature of an object T_0 is defined by:

$$T_0 = T\varepsilon + T_s r + T_b t \quad \textbf{(1)}$$

where T is the physical temperature of the object, ε its emissivity, T_s is the temperature of the background which is reflected by the object with reflectivity r, T_b is the temperature of the background behind the object and t the object's transmissivity [4].

3 X-ray Imaging

X-radiation have a wavelength in the range of 10-0.01 nm ($3 \cdot 10^{16}$-$3 \cdot 10^{19}$ Hz) and enough energy to pass through cloth and human tissues. In addition to cloth penetration, XR imaging provides high image resolution. On the other hand, this technology presents some disadvantages: low speed, limitation to very short distances and the health safety concerns it raises because of using ionizing radiation.

The natural background X-radiation is too weak to form an image, therefore active imaging is required in both XR imaging modalities: *transmission* and *backscatter* X-ray imaging. X-rays are commonly produced by accelerating charged particles.

Transmission X-ray Imaging. Conventional X-ray radiographic systems used for medical purposes produce images relying on this kind of imaging: a uniform X-ray beam incident on the patient interacts with the tissues of the body, producing a variable transmitted X-ray flux dependent on the attenuation along the beam paths. An X-ray-sensitive detector captures the transmitted fraction and converts the X-rays into a visible projection image.

Only a few works on biometric identification making use of the conventional X-rays can be found: Shamir *et al.* [5] perform biometric identification using knee X-rays while Chen *et al.* [6] present an automatic method for matching dental radiographs (see Fig. 3a-c). These knee or dental X-rays are difficult to forge and present additional advantages: they can be used in forensic identification where the soft tissues are degraded.

Backscatter X-ray Imaging. In this technique the XR scattered photons, instead of transmitted photons, are used to construct the image [7]. This technology utilizes high energy X-rays that are more likely to scatter than penetrate materials as compared to lower-energy X-ray used in medical applications. However, this kind of radiation is able to penetrate some materials, such as cloth.

A person is scanned by moving a single XR beam over her body. The backscattered beam from a known position allows a realistic image to be reconstructed. As only scattered X-rays are used, the registered image is mainly a view of the surface of the scanned person, i.e. her nude form. As the image resolution is high, these images present privacy issues. Some companies (e.g. AS&E) ensure privacy by applying an algorithm to the raw images so that processed images reveal only an outline of the scanned individual. Raw and processed backscatter XR images are shown in Fig. 3d and e.

According to our knowledge, there are no works on biometrics using backscatter X-ray images. The application of this technique includes medical imaging [8] and passenger screening at airports and homeland security [9]. There are currently

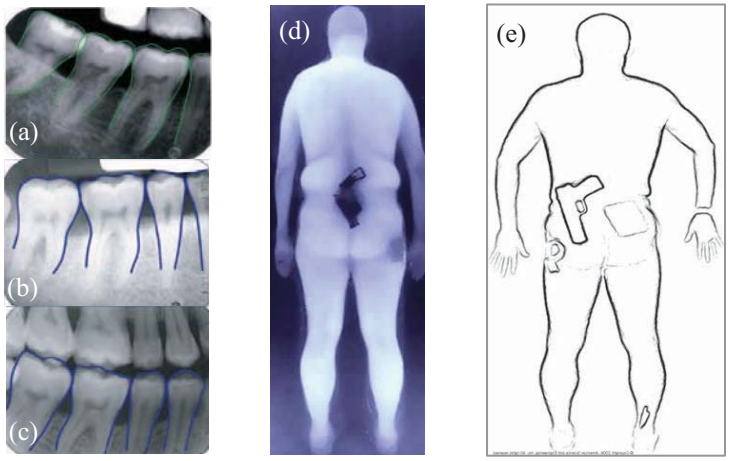

Fig. 3. (a-c) Dental radiographs used for human identification. (d) A backscatter XR image of a man, it shows the skin surface and objects hidden by clothing. (e) A backscatter XR image processed to ensure privacy. These figure insets are extracted from: [6] (a-c), [http://www.elpais.com] (d) and [http://www.as-e.com/] (e).

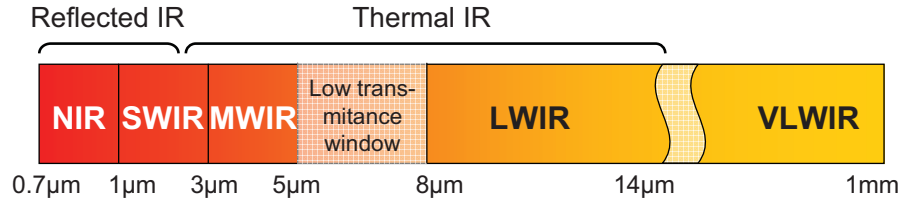

Fig. 4. Infrared band of the electromagnetic spectrum showing the different IR sub-bands.

different backscatter X-ray imaging systems available on the market to screen people (e.g. AS&E, Rapiscan Systems).

4 Infrared Imaging

The infrared band of the electromagnetic spectrum lies between the SMW and VIS regions, with wavelengths in the range of 0.7 μm - 1 mm (see Fig. 1). The human body emits IR radiation with a wavelength between 3-14 μm, hence both active and passive architectures can be used in IR imaging.

As indicated in Eq. (1), the radiation that is actually detected by an IR sensor depends on the surface properties of the object (ε, r, t) and on the trasmissivity of the medium (atmosphere). According to the properties of the medium and the spectral ranges of the currently available IR detectors, the IR spectrum is divided into five sub-bands, summarized in Fig. 4. The limits of these sub-bands are not completely fixed and depend on the specific application. In practice, IR imaging systems usually operate in one of the three following IR sub-bands: the near infrared (NIR), the medium wave infrared (MWIR) or the long wave infrared (LWIR), where the windows of high atmosphere transmissivity are located.

Table 1. Properties of the most important IR sub-bands.

IR Spectral bands	Range (μm)	Architecture	IR camera cost	Image Properties	Applications in Biometrics
Near IR (NIR)	0,7-1	Active	Low, VIS camera also sensitive	Good quality, body condition invariant	Face [10] and Hand Vein [11] Recognition
Medium Wave IR (MWIR)	3 - 5	Passive	High	Good quality, sensitive to body conditions	Face [12] and Hand Vein [13] Recognition
Long Wave IR (LWIR)	8 - 14	Passive	Low	Low contrast, sensitive to body conditions	Face [14] and Hand Vein [11] Recognition

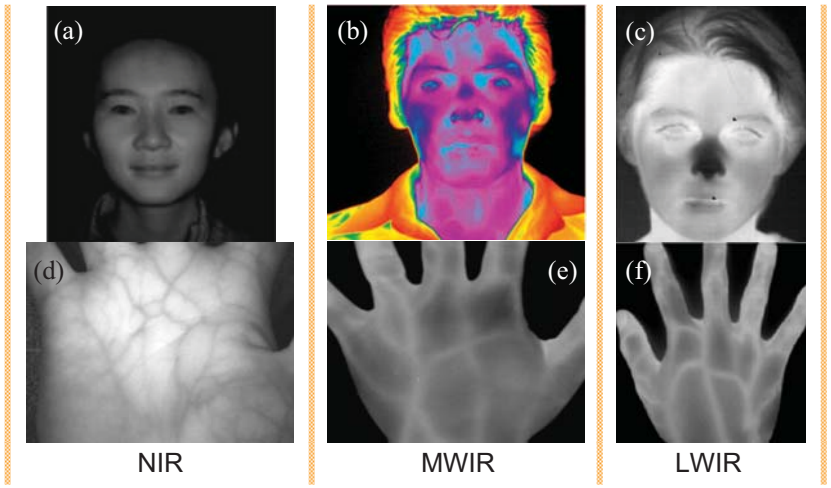

Fig. 5. Face and hand images acquired at NIR, MWIR and LWIR: (a) face at NIR, (b) face at MWIR, (c) face at LWIR, (d) palm at NIR, back of the hand at MWIR (e) and at LWIR (f). The images are extracted respectively from [10], [12], [14], [11]. [13] and [11].

In Fig. 4 the IR band is split in two sub-bands: *Reflected IR* band (0.7-2.4 μm) and *Thermal IR* band (beyond 2.4 μm). The Reflected IR band is associated with reflected solar radiation that contains no information about the thermal properties of materials. The Thermal IR band is associated with the thermal radiation emitted by the objects. This division in two bands is also related to the two kind of imaging architectures: active and passive imaging. In the Reflected IR band external illumination is needed while in the Thermal IR band passive imaging is preferred (natural IR radiation emitted by the person is captured).

The three mentioned practical IR sub-bands (i.e. NIR, MWIR and LWIR) present different characteristics. A summary of the properties of these sub-bands is given in Table 1 while Fig. 5 shows face and hand images acquired at NIR, MWIR and LWIR.

Many research works have been developed using NIR, MWIR and LWIR imaging systems for biometrics. Face and hand vein pattern recognition are the most important biometric modalities investigated in these three bands (see references in Table 1). Images acquired at any of these bands (see Fig. 5) are, to some extent, environmental illumination invariant. Specifically, images at NIR are body condition invariant and can provide good quality vein patterns near the skin surface [11], but external NIR illumination is required. Images acquired at MWIR and LWIR show patterns of

radiated heat from the body's surface (often called thermograms). Very few biometric works have been developed in MWIR [12, 13], probably due to the high cost of MWIR cameras. LWIR cameras are much cheaper but, in contrast with NIR, LWIR can only capture large veins. Additionally, most of the LWIR images have low levels of contrast, being also sensitive to ambient and body condition [11].

5 Millimeter and Submillimeter Wave Imaging

MMW and SMW radiation fill the gap between the IR and the microwaves (see Fig. 1). Specifically, MMW band spreads from 30 to 300 GHz (10-1 mm) while the SMW band lies in the range of 0.3-3 THz (1-0.1 mm) [4].

The use of MMW/SMW of radiation within imaging systems is currently an active field of research due to some of its interesting properties [15-20]. The penetration through clothing and other nonpolar dielectric materials even at stand off ranges is one of the most important MMWs and SMWs abilities. Hence, security screening (detection of concealed weapons under clothing), nondestructive inspection and medical and biometric imaging are the most relevant applications of MMW/SMW imaging. Another application of MMW imaging is low visibility navigation (due to the low attenuation of MMWs under adverse weather).

Images acquired at MMW/SMW frequencies have lower resolution than IR or VIS images due to larger wavelength. Further, MMW and, specially, SMW imaging technologies are not as mature as the IR or VIS imaging technologies, which restricts the quality of the resulting images. On the other hand, SMW images have better spatial resolution than MMW images (SMW wavelength is smaller), but SMW clothing penetration is lower compared to MMW. In any case, images acquired with passive or with active systems present different characteristics (see Table 2). Different Passive MMW (PMMW), Active MMW (AMMW), Passive SMW (PSMW) and Active SMW (ASMW) images are shown in Fig. 6. As MMW and SMW images

Table 2. Properties of MMW and SMW imaging operating with passive or active architecture. The spatial resolution depends on some conditions such as the distance between the target and the detector, the given resolution corresponds to a target-detector distance of some meters.

Radiation	Architecture	Image Properties	Relative Spatial Resolution	Operating Frequencies	Commercial Systems
MMW	Passive	▪ Low resolution compared to VIS and IR ▪ Highly affected by sky illumination	Very Low (indoors) Low-Medium (outdoors)	▪ 35 GHz ▪ 94 GHz	▪ Qinetiq ▪ Brijot ▪ Alfa Imaging ▪ Sago Systems
	Active	▪ Higher quality than Passive MMW images	Medium	▪ 30 GHz ▪ 60 GHz ▪ 190 GHz	▪ Agilent ▪ L-3 Communications
SMW	Passive	▪ Good quality ▪ Partial clothing opacity	Medium-High	▪ 0.1-1 THz ▪ 1.5 THz	▪ Thruvision
	Active	▪ Higher quality than Passive SMW images ▪ Partial clothing opacity	High (at a distance) Very high (near)	▪ 0.6-0.8 THz ▪ 310 GHz ▪ > 1 THz	▪ Picometrix ▪ Teraview

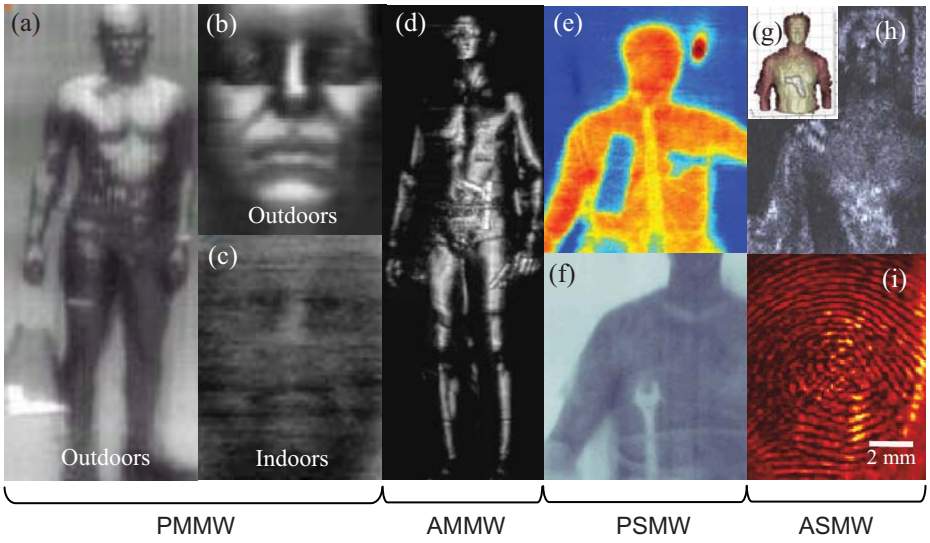

Fig. 6. Images acquired with MMW and SMW imaging systems. (a) Outdoors PMMW image (94 GHz) of a man carrying a gun in a bag. (b-c) Indoors and outdoors PMMW image of a face. (d) AMMW image of a man carrying two handguns acquired at 27-33 GHz. (e) PSMW image (0.1-1 THz) of a man with concealed objects beneath his jacket. (f) PSMW image (1.5 THz) of a man with a spanner under his T-shirt. (h) ASMW image (0.6 THz) of a man hiding a gun beneath his shirt. (g) Full 3-D reconstruction of the previous image after smoothing of the back surface and background removal. (i) Terahertz reflection mode image of a thumb. These figure insets are extracted from: www.vision4thefuture.org (a-c), [16] (d), [17] (e), [18] (f), [19] (g-h) and [20] (i).

measure the different radiometric temperatures in the scene, see Eq. (1), images acquired indoors and outdoors have very different contrast when working in passive mode, specially with MMW (see Fig. 6b and c).

In spite of the significant advantages of MMW and SMW radiation for biometric purposes (cloth penetration, low intrusiveness, health safety), no biometric applications have been developed yet.

3 Conclusions

We have provided a taxonomy of the existing imaging technologies operating at frequencies beyond the visible spectrum that can be used for biometrics purposes. The advantages and challenges of each imaging technology, as well as their image properties have been presented. Although only X-ray and Infrared spectral bands have been used for biometric applications, there is another kind of radiation with promising applications in the biometric field: millimeter and submillimeter waves. However MMW and SMW technology is not completely mature yet.

Acknowledgments. This work has been supported by Terasense (CSD2008-00068) Consolider project of the Spanish Ministry of Science and Technology. M. M.-M. is supported by a CPI Fellowship from CAM, and J. F. is supported by a Marie Curie Fellowship from the European Commission.

References

1. Jain, A. K. *et al.*: An Introduction to Biometric Recognition*,* IEEE Trans. on CSVT. Vol. 14, No. 1, pp. 4-20 (2004).
2. National Research Council, Airline Passenger Security Screening: New Technologies and Implementation Issues, National Academy Press, Washington, D.C. (1996).
3. Galbally, J. *et al.*: Fake Fingertip Generation from a Minutiae Template, in Proc. Intl. Conf. on Pattern Recognition, ICPR, IEEE Press, (2008).
4. Appleby, R. *et al.*: Millimeter-Wave and Submillimeter-Wave Imaging for Security and Surveillance, Proc. of the IEEE, Vol. 95, No. 8, pp. 1683-1690 (2007).
5. Shamir, L. *et al.*: Biometric identification using knee X-rays, Int. J. Biometrics, Vol. 1, No. 3, pp 365-370 (2009).
6. Chen, H. and Jain, A.K.: Dental Biometrics: Alignment and Matching of Dental Radiographs, IEEE Transactions on PAMI, Vol. 27, No. 8, pp. 1319-1326 (2005).
7. Bossi, R.H. *et al*.: Backscatter X-ray imaging, Materials Evaluation, Vol.46, No. 11, pp. 1462-7 (1988).
8. Morris, E.J.L. *et al*.: A backscattered x-ray imager for medical applications*,* Proc. of the SPIE, Vol. 5745, pp. 113-120 (2005).
9. Chalmers, A.: Three applications of backscatter X-ray imaging technology to homeland defense, Proc. of the SPIE, Vol. 5778, No. 1, pp. 989-93 (2005).
10. Li, S. Z. *et al.*: Illumination Invariant Face Recognition Using Near-Infrared Images, IEEE Trans. on PAMI, Vol. 29, No. 4, pp.627-639 (2007).
11. Lingyu, W. *et al.*: Near- and Far- Infrared Imaging for Vein Pattern Biometrics, Proc. of the AVSS, pp.52-57 (2006).
12. Buddharaju, P. *et al.*: Physiology-Based Face Recognition in the Thermal Infrared Spectrum, IEEE Trans. on PAMI, Vol. 29, No. 4, pp.613-626 (2007).
13. Fann, C. K. *et al.*: Biometric Verification Using Thermal Images of Palm-dorsa Vein-patterns, IEEE Trans. on CSVT, Vol. 14, No. 2, pp. 199-213 (2004).
14. Chen, X. *et al.*: IR and visible light face recognition, Computer Vision and Image Understanding, Vol. 99, No. 3, pp. 332-358, (2005).
15. Kapilevich, B. *et al.*: Passive mm-wave Sensor for In-Door and Out-Door Homeland Security Applications, SensorComm 2007, pp.20-23 (2007).
16. Sheen, D. M. *et al.*: Three-dimensional millimeter-wave imaging for concealed weapon detection, IEEE Trans. on Microwave Theory and Techniques, Vol.49, No. 9, pp.1581-1592, (2001).
17. Shen, X. *et al.*: Detection and Segmentation of Concealed Objects in Terahertz Images, IEEE trans. on IP, Vol. 17, No. 12, (2008).
18. Luukanen, A. *et al.*: Stand-off Contraband Identification using Passive THz Imaging, EDA IEEMT Workshop, (2008).
19. Cooper, K. B. *et al.*: Penetrating 3-D Imaging at 4- and 25-m Range Using a Submillimeter-Wave Radar, IEEE Trans. on Microwave Theory and Techniques, Vol. 56, No. 12 (2008).
20. Lee, A. W. *et al.*: Real-time imaging using a 4.3-THz Quantum Cascade Laser and a 320 x 240 Microbolometer Focal-Plane Array, IEEE Photonics Technology Letters, Vol. 18, No. 13, pp.1415-1417 (2006).

ANÁLISIS DE ESCENARIOS PARA RECONOCIMIENTO BIOMÉTRICO A DISTANCIA ADECUADOS PARA LA ADQUISICIÓN DE IMÁGENES MMW

M. Moreno-Moreno, J. Fierrez, P. Tome, J. Ortega-Garcia.
{miriam.moreno, julian.fierrez, pedro.tome, javier.ortega}@uam.es
Avda. Francisco Tomás y Valiente, 11 - Campus de Cantoblanco - 28049 Madrid, Spain

***Abstract*— Con objeto de analizar en qué medida puede ayudar el uso de imágenes adquiridas en el rango de ondas milimétricas (MMW) al reconocimiento biométrico de personas a distancia, se presenta un análisis experimental de tres escenarios con diferentes distancias de captura adecuadas para la adquisición de imágenes MMW. En concreto se realizan experimentos de reconocimiento facial a corta, media y larga distancia entre la cámara y el sujeto a identificar, siendo los escenarios de media y larga distancia los más adecuados para las capturas en MMW. Los tres escenarios consideran plantillas registradas en condiciones controladas, y para su estudio se usan datos del NIST Multiple Biometric Grand Challenge. Este enfoque permite:** 1) **aproximarnos al problema del reconocimiento biométrico de imágenes en MMW como complemento a biometrías tradicionales como es el reconocimiento facial, y** 2) **entender los factores de mayor variabilidad que afectan al reconocimiento de personas a distancia, que serán los factores a compensar con las tecnologías complementarias al reconocimiento, como MMW. El análisis de escenarios se realiza cuantitativamente de dos maneras. Primero se analiza el contenido de información en caras segmentadas en los diferentes escenarios. A continuación se evalúa el rendimiento en cada escenario de tres comparadores, uno comercial, y dos aproximaciones estándar usando características (PCA y DCT) y comparadores (SVM y GMM) tradicionales. Los resultados muestran hasta qué punto las características de la adquisición influyen en el rendimiento de la verificación del reconocimiento facial a distancia, y esto sirve de punto de partida para comprender en qué medida pueden ayudar al reconocimiento tecnologías complementarias como MMW.**

I. INTRODUCCIÓN

Las imágenes adquiridas a frecuencias de milimétricas (MMW) presentan propiedades únicas, que permiten su aplicación en diferentes ámbitos (seguridad, inspección no intrusiva, medicina y biometría entre otras) [1], [2]. A pesar del actual desarrollo de los sistemas de adquisición de este tipo de imágenes [3], [4], no existe ninguna base de datos de imágenes de personas en este rango espectral. Ello es debido, en parte, a los problemas de privacidad que presentan dichas imágenes. Este hecho limita considerablemente el desarrollo de sistemas biométricos basados en imágenes adquiridas en este rango espectral, los cuales necesitan un número suficiente de imágenes de diferentes usuarios. Dado que la adquisición de estas imágenes se realiza a diferentes distancias y puesto que no existe ninguna base de datos de imágenes en MMW, el trabajo presentado se aproxima al problema del reconocimiento biométrico de personas con imágenes en MMW, pero usando imágenes adquiridas en el visible en un escenario similar al de la adquisición de imágenes en MMW. En concreto el artículo realiza un análisis de tres escenarios para reconocimiento facial a distancia.

La cara y el iris son dos de los rasgos biométricos usados actualmente en muchas aplicaciones de reconocimiento de usuario a distancia [5], [6]. Una nueva línea de investigación que está ganando popularidad se centra en el uso de estos rasgos biométricos en escenarios menos controlados de una manera no-invasiva incluyendo adquisición en movimiento ("On the Move") y a distancia ("At a Distance") [7]. Este tipo de escenarios está todavía en su infancia y se necesita mucha investigación y desarrollo para alcanzar los niveles de precisión y de rendimiento que requieren las aplicaciones prácticas.

El nuevo campo de la biometría a distancia se ha hecho posible primordialmente gracias a: 1) los recientes avances en los sensores, y 2) los nuevos algoritmos y métodos para tratar con factores variables (e.g. iluminación, movimiento, pose, distancia a la cámara), que en este caso están menos controlados que en las situaciones consideradas comúnmente en biometría.

Como resultado del interés en estas aplicaciones biométricas a distancia, hay un número creciente de trabajos de investigación que estudian cómo compensar las principales degradaciones encontradas en escenarios no controlados [8]. Sin embargo, apenas existe conocimiento experimental sobre los factores de variabilidad en escenarios específicos, que puedan ayudar en la creación de métodos robustos para la biometría a distancia (diseñada para aplicaciones específicas de importancia práctica). La contribución de este artículo es hacia este fin, analizando cuantitativamente tres escenarios del reconocimiento facial a distancia, a saber: corta, media y larga distancia entre el usuario y la cámara; siendo los escenarios de media y larga distancia los más adecuados para incorporar imágenes del cuerpo en MMW. Este análisis se realiza a dos niveles: 1) los principales datos estadísticos de

Fig. 1. Ejemplo de imágenes de los tres escenarios: a) corta distancia, b) media distancia, y c) larga distancia.

la información de contenido, y 2) el rendimiento de varios sistemas de reconocimiento: uno comercial, y dos basados en características (PCA, DCT) y comparadores tradicionales (SVM, GMM).

Los escenarios bajo estudio han sido extraídos de NIST Multiple Biometric Grand Challenge [9], el cual se centra en el reconocimiento biométrico a distancia usando el iris y la cara. En particular, usamos un subconjunto de estos datos compuesto de imágenes de un total de 112 usuarios adquiridos a diferentes distancias y condiciones variables de iluminación, pose/ángulo de la cara, y expresión facial.

Este análisis de escenarios para una biometría tradicional, como es el reconocimiento facial, permite comprender las limitaciones de la tecnología actual y sirve de punto de partida para ver en qué medida la tecnología MMW puede solventar dichas limitaciones.

El artículo se estructura como sigue. La Sec. II describe los conjuntos de datos y escenarios bajo estudio. La Sec. III analiza los principales datos estadísticos de los escenarios. La Sec. IV estudia el rendimiento de los tres sistemas de reconocimiento considerados en los diferentes escenarios. Finalmente la Sec. V muestra los resultados experimentales y esboza el trabajo futuro.

II. DEFINICIÓN DE LOS ESCENARIOS

Los tres escenarios considerados son: 1) "corta" distancia, en la que los hombros pueden estar presentes; 2) "media" distancia, incluyendo la parte superior del cuerpo; y 3) "larga" distancia, incluyendo el cuerpo entero (ver Fig. 1). En esta figura, además de un par de imágenes en cada escenario en el rango visible, se muestran dos imágenes adquiridas en el rango de MMW mediante un radiómetro trabajando a 94 GHz, cortesía de AlfaImaging[1]. Una de ellas (a media distancia) se adquirió en exteriores y la otra (a larga distancia) en interiores. Se comprueba el parecido de ambos tipos de imágenes (en visible y en MMW) en los escenarios de media y larga distancia, de ahí el interés en el análisis del reconocimiento biométrico usando imágenes en el visible en estos escenarios, como base sobre la que comparar en qué medida puede ayudar al reconocimiento clásico la incorporación de imágenes adquiridas en el rango de los GHz.

Usando estos tres escenarios generales, hemos marcado manualmente las 3482 imágenes de los 147 usuarios presentes en la base de datos NISR MBGC v2.0 Face Stills [9]. Algunas se muestran en la Fig. 1. Una porción del conjunto de imágenes fue desechada (360 imágenes de 89 usuarios), porque la cara estaba ocluída o la iluminación degradaba completamente la imagen de la cara. Además, aunque esta información no se usa en el presente artículo, todas las imágenes fueron marcadas como adquiridas en interiores o exteriores.

Finalmente, para posibilitar experimentos de verificación considerando el registro con imágenes adquiridas a corta distancia y realizando experimentos de evaluación en escenarios a corta, media y larga distancia, mantenemos sólo los usuarios con al menos dos imágenes a corta y al menos una imagen en los otros dos escenarios. El proceso de selección de datos está resumido en la Tabla I, donde se puede observar que los tres escenarios considerados resultan en 112 usuarios y 2964 imágenes.

III. ANÁLISIS DE ESCENARIOS: DATOS ESTADÍSTICOS

Primero se segmentan y se localizan las caras (áreas rectangulares) en los tres escenarios usando el software VeriLook SDK (ver Sec. IV-A). Los resultados de la segmentación se muestran en la Tabla II, donde los errores de segmentación crecen significativamente según la distancia cara-cámara aumenta, desde sólo un 1.43% en corta distancia a un 82.57% en larga distancia. Los errores de segmentación en este caso significan que el software VeriLook no puede encontrar la cara en la imagen. Para todas las caras detectadas por VeriLook, llevamos a cabo una comprobación visual, donde se observaron 3 y 10 errores de segmentación para media y larga distancia respectivamente.

Estos errores de segmentación fueron corregidos manualmente marcando los ojos. El área de la cara se estimó basándose en la distancia marcada entre los ojos.

[1] http://www.alfaimaging.com/

Núm. usuarios	Corta distancia	Media distancia	Larga distancia	Imágenes Rechazadas	Total
147	1539	870	713	360	**3482**
	*Al menos **2** imágenes por usuario*	*Al menos **1** imagen por usuario*			
112	1468	836	660		**2964**

TABLE I

NÚMERO DE IMÁGENES DE CADA ESCENARIO DEFINIDAS DEL NIST MBGC V2.0 FACE VISIBLE STILLS.

	Corta distancia	Media distancia	Larga distancia	Imágenes Rechazadas	Total
Núm. Imágenes	1468	836	660	360	**3324**
Errores	21	151	545		**848**
Errores(%)	1.43%	18.06%	**82.57%**		

TABLE II

RESULTADOS DE SEGMENTACIÓN BASADOS EN ERRORES PRODUCIDOS POR EL EXTRACTOR DE CARAS DE VERILOOK SDK.

Se comprobó que el tamaño de las caras segmentadas decrece con la distancia de adquisición. En concreto el tamaño promedio de la cara (en píxeles) para cada escenario es: 988 $\times$ 988 para corta, 261 $\times$ 261 para media, y 78 $\times$ 78 para larga distancia.

Otro dato estadístico que calculamos para los tres escenarios es el promedio del índice de calidad proporcionado por VeriLook (0 = mínima, 100 = máxima): 73.93 para corta, 68.77 para media, y 66.50 para larga distancia (ver Fig. 2, calculados sólo para las caras correctamente segmentadas por VeriLook). Como afirman los proveedores de VeriLook, este índice de calidad considera factores como la iluminación, pose y expresión.

IV. ANÁLISIS DE ESCENARIOS: EVALUACIÓN DE RENDIMIENTO DE VERIFICACIÓN

A. Sistemas de Reconocimiento Facial

- **VeriLook SDK**. Sistema de reconocimiento facial comercial desarrollado por Neurotechnology[2].
- **PCA-SVM system**. Este sistema de verificación usa PCA (Principal Component Analysis). El sistema usa imágenes normalizadas y recortadas, para entrenar un espacio de vectores PCA donde el 96% de la varianza se mantiene. Esto conduce a un sistema donde el espacio original de 5120 dimensiones se reduce a 249 dimensiones. Las comparaciones entre caras se calculan en este espacio de vectores PCA usando un clasificador SVM con núcleo lineal.
- **DCT-GMM system**. Este sistema de verificación usa imágenes de caras divididas en bloques, resultando en 285 bloques por cara segmentada. Se obtiene un vector de características de cada bloque aplicando la Transformada Discreta del Coseno (DCT); de la que sólo los 15 primeros coeficientes se mantienen. Los bloques se usan para derivar un modelo global GMM Ω_w y un modelo adaptado al usuario GMM Ω_c [10]. De experimentos previos se obtuvo que usando $(M = 1024)$ componentes de mezcla por GMM se obtenían los mejores resultados. El vector de características obtenido con la DCT de cada bloque se compara con ambos Ω_w y Ω_c para producir una puntuación de similitud logarítmica.

[2]http://www.neurotechnology.com/

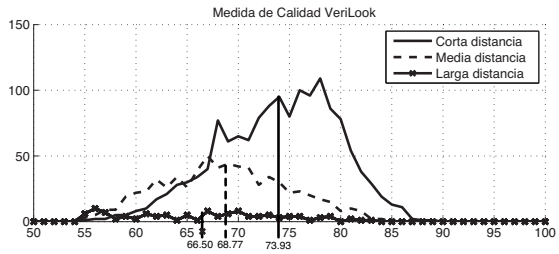

Fig. 2. Histograma de las medidas de calidad producidas por VeriLook SDK.

B. Protocolo Experimental

- *Close2close*. Este protocolo nos dará una idea sobre el rendimiento de los sistemas en condiciones ideales (ambas: registro y evaluación usando imágenes a corta distancia). Alrededor de la mitad de los datos (754 imágenes) se usa para el ajuste del sistema (entrenamiento del subespacio PCA, SVM, etc.), y el resto (714 imágenes) se usa para evaluar el rendimiento.
- *Close2medium*, y *close2far*. Estos dos protocolos usan como conjunto de datos de ajuste el conjunto completo de datos a corta distancia (1468 imágenes de la cara). Para evaluar el rendimiento de los sistemas, usamos los otros dos conjuntos de datos: 836 imágenes a media distancia para *close2medium*, y 680 imágenes a larga distancia para *close2far*.

C. Resultados

En la Fig. 3 se muestra el rendimiento de verificación para los tres escenarios considerados: *close2close*, *close2medium*, y *close2far*. Primero observamos que VeriLook es el mejor de los tres sistemas en *close2close* con una Equal Error Rate (EER) alrededor de 7%. Al mismo tiempo este sistema comercial es el que más se degrada en condiciones no controladas, con una EER cercana a 40% en *close2far*, mucho peor que los otros dos sistemas más sencillos. Este resultado corrobora la importancia de analizar y tratar adecuadamente los factores de variabilidad que surgen en la biometría a distancia.

Es evidente el empeoramiento que sufre el rendimiento de verificación de los sistemas al pasar del escenario de corta distancia al de media distancia y muy especialmente al pasar al escenario de larga distancia (ver Fig. 3). Una posible mejora del rendimiento en estos dos últimos escenarios (a media y larga distancia) es la fusión de rasgos biométricos adquiridos en el espectro visible (en este caso la cara) con rasgos adquiridos en el rango de MMW (como pueda ser la imagen del contorno del cuerpo, dada la transparencia de la vestimenta a esas frecuencias) [11].

También se observa en la Fig. 3 que el sistema basado en GMM funciona mejor a larga distancia que los otros sistemas,

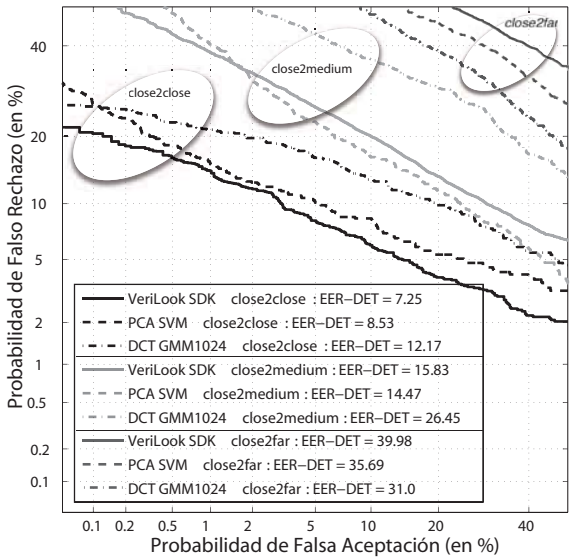

Fig. 3. Resultados del rendimiento de verificación para los tres escenarios y los tres sistemas considerados.

aunque es menos preciso en *close2close* y *close2medium*. Este resultado demuestra el mayor poder de generalización de esta aproximación al reconocimiento, y su robustez frente a condiciones de adquisición no controladas.

V. DISCUSIÓN Y TRABAJO FUTURO

Se ha estudiado el rendimiento de diferentes sistemas de reconocimiento facial que usan imágenes adquiridas en el espectro visible en tres escenarios distintos. Esto constituye la base sobre la que comparar el comportamiento de sistemas que aprovechen la información de imágenes adquiridas en el rango de los GHz. En concreto, en el escenario *close2far* la biometría clásica, en este caso el reconocimiento facial, no proporciona buenos rendimientos, que pueden ser mejorados mediante la fusión con imágenes en MMW. De la misma manera, este trabajo, conforma una aproximación experimental hacia el entendimiento de los factores de variabilidad en reconocimiento facial a distancia. En particular, se ha realizado un análisis de datos de tres escenarios realistas de adquisición a diferentes distancias (corta, media y larga, las dos últimas adecuadas para la adquisición con MMW), como primer paso hacia la creación de un método de reconocimiento adecuado capaz de trabajar en escenarios menos controlados. Este análisis se ha realizado para un subconjunto de datos del NIST MBGC v2.0 Face Stills.

Nuestro análisis se ha centrado en: 1) datos estadísticos (tamaños de las caras segmentadas y medidas de calidad), y 2) evaluación del rendimiento de verificación de los tres sistemas. Los resultados muestran que los sistemas considerados se degradan significativamente en el escenario a larga distancia, siendo la aproximación más simple, la más robusta a condiciones no controladas.

Vale la pena resaltar que los tres escenarios considerados en el presente artículo difieren no sólo en el factor distancia, sino también en la iluminación y la pose (siendo la variación en la iluminación mucho mayor a larga distancia que a corta distancia). Estos tres factores (distancia, iluminación y pose) son claves en las imágenes adquiridas en la banda de MMW, especialmente en la imágenes adquiridas en exteriores [2], [12]. Basándonos en los datos estadísticos obtenidos y los resultados de la evaluación del rendimiento, el estudio individual de los efectos de los factores mencionados se propone como trabajo futuro para el reconocimiento biométrico en el espectro visible a distancia. En el caso de reconocimiento biométrico mediante el uso de imágenes en MMW, se propone la adquisición de una base de datos de imágenes de usuarios de cuerpo entero, cuya silueta se pueda usar para la extracción de información que pueda ser utilizada en un sistema biométrico o en combinación con otro tipo de información proveniente de otros rasgos biométricos (*Soft Biometrics*) [13], [14], [11], como la facial considerada en este trabajo, de forma que se compensen sus limitaciones, que como hemos observado son muy severas para adquisiciones a cierta distancia.

AGRADECIMIENTOS

Este trabajo ha sido financiado parcialmente por los proyectos Bio-Challenge (TEC2009-11186), Contexts (S2009/TIC-1485), TeraSense (CSD2008-00068) y "Cátedra UAM-Telefónica". M. M.-M. y P. T. están financiados por un contrato CPI de la CAM y una beca FPU, respectivamente.

REFERENCES

[1] R. Appleby and R.N. Anderton, "Millimeter-wave and submillimeter-wave imaging for security and surveillance," *Proc. of the IEEE*, vol. 95, no. 8, pp. 1683–1690, 2007.

[2] L. Yujiri et al., "Passive millimeter wave imaging," *Microwave Magazine, IEEE*, vol. 4, no. 3, pp. 39–50, 2003.

[3] D.M. Sheen et al., "Active millimeter-wave standoff and portal imaging techniques for personnel screening," in *Technologies for Homeland Security, 2009. HST '09. IEEE Conference on*, 2009, pp. 440–447.

[4] J.N. Mait et al., "94 ghz imager with extended depth of field," *Antennas and Prop., IEEE Trans. on*, vol. 57, no. 6, pp. 1713–19, 2009.

[5] W. Zhao et al., "Face recognition: A literature survey," *ACM Comput. Surv.*, vol. 35, no. 4, pp. 399–458, 2003.

[6] J.R. Matey et al., "Iris on the move: Acquisition of images for iris recognition in less constrained environments," *Proc. of the IEEE*, vol. 94, no. 11, pp. 1936–1947, 2006.

[7] Z. Li Stan et al., *Handbook of Remote Biometrics for Surveillance and Security*, chapter Biometrics at a Distance: Issues, Challenges, and Prospects, pp. 3–21, Springer, 2009.

[8] Robust2008, "Robust biometrics: Understanding science & technology," http://biometrics.cylab.cmu.edu/ROBUST2008.

[9] MBGC, "Multiple biometric grand challenge," *NIST - National Institute of Standard and Technology*, http://face.nist.gov/mbgc/.

[10] J. Galbally et al., "On the vulnerability of face verification systems to hill-climbing attacks," *Pattern Recognition*, vol. 43, no. 3, pp. 1027–1038, 2010.

[11] J. Fierrez-Aguilar et al., "Discriminative multimodal biometric authentication based on quality measures," *Pattern Recognition*, vol. 38, no. 5, pp. 777–779, 2005.

[12] D. T. Petkie et al., "Active and passive imaging in the thz spectral region: Phenomenology, dynamic range, modes, and illumination," *J. Opt. Soc. Am. B*, vol. 25, no. 9, pp. 1523–1531, 2008.

[13] Bo Ye and Yumei Wen, "A new gait recognition method based on body contour," in *Control, Automation, Robotics and Vision*, 2006, pp. 1–6.

[14] Anil K. Jain et al., "Can soft biometric traits assist user recognition?," 2004, vol. 5404, pp. 561–572, SPIE.

BIOGIGA: BASE DE DATOS DE IMÁGENES SINTÉTICAS DE PERSONAS A 94 GHZ CON FINES BIOMÉTRICOS

M. Moreno-Moreno[1], J. Fierrez[1], P. Tome[1], R. Vera-Rodriguez[1], J. Parron[2], J. Ortega-Garcia[1]
{miriam.moreno, julian.fierrez, pedro.tome, ruben.vera}@uam.es, josep.parron@uab.es, javier.ortega@uam.es
[1]Dpto. Tecnología Electrónica y de las Comunicaciones. Universidad Autónoma de Madrid (UAM). 28049 Madrid, Spain.
[2]Dpto. Telecomunicació i d'Enginyeria de Sistemes. Universitat Autònoma de Barcelona (UAB). 08193 Barcelona, Spain.

***Resumen*—The baseline corpus of a new database, called BioGiga, acquired in the framework of the Terasense Consolider Project, is presented. The corpus consists of synthetic images at 94 GHz of the body of 50 individuals. The images are the result of simulations carried out on corporal models at two types of scenarios (outdoors, indoors) and with two kinds of imaging systems (passive and active). These corporal models were previously generated based on body measurements taken from the subjects. In this contribution, the methodology followed and the tools used to generate the database are outlined. Furthermore, the contents of the corpus (data and statistics) as well as its applications are described.**

I. INTRODUCCIÓN

Se denomina reconocimiento biométrico al proceso que permite asociar una identidad con un individuo de forma automática, haciendo uso de una o varias características físicas o de comportamiento, inherentes al individuo [1]. Son muchas las características que se han usado en reconocimiento biométrico: huella dactilar, firma manuscrita, iris, voz, cara, mano, etc. Algunos de estos rasgos biométricos tales como la oreja, la cara, la mano o la forma de andar, son adquiridos tradicionalmente con cámaras que trabajan en el espectro visible. Tales imágenes se ven afectadas por factores como las condiciones de iluminación y las oclusiones (provocadas por la ropa, el maquillaje, el pelo, etc.)

Con el fin de superar estas limitaciones, impuestas por el uso de imágenes adquiridas en el espectro visible, investigadores en biometría y seguridad [2] han propuesto el uso de imágenes adquiridas en otros rangos espectrales, a saber: rayos X [3], infrarrojo [4], ondas milimétricas (MMW) y submilimétricas (SMW) [5]. Además de solventar hasta cierto punto las limitaciones de las imágenes en el visible, las imágenes tomadas más allá del espectro visible presentan una ventaja extra: son más robustas frente ataques contra sistemas biométricos que otras imágenes.

La banda espectral propuesta en este trabajo para capturar imágenes de rasgos biométricos es la correspondiente a la de las ondas milimétricas (de frecuencia entre 30 y 300 GHz) [6]. La importancia de este tipo de radiación se halla en: 1) su capacidad para atravesar la ropa y otras oclusiones, 2) su inocuidad, y 3) el reciente desarrollo que están experimentando los sistemas de GHz-THz en aplicaciones de captura de imágenes (especialmente en el área de seguridad). Al contrario de lo que ocurre con la tecnología de captura de imágenes en el visible o infrarrojo, la tecnología de GHz-THz está en pleno desarrollo [7]. Este hecho, junto con los problemas de privacidad que presentan las imágenes corporales en esa banda, han hecho que, hasta la fecha, no existan bases de datos públicas con imágenes de personas adquiridas en ese rango de frecuencias. De hecho sólo existe un trabajo publicado hasta el momento sobre reconocimiento biométrico basado en imágenes de GHz [8].

Por todo lo anterior en este trabajo se describe la generación de una base de datos de imágenes simuladas de personas a 94 GHz, así como su contenido. El objetivo de esta base de datos es su futuro uso en el desarrollo de sistemas biométricos basados en dichas imágenes.

El artículo se estructura como sigue. La Sec. II introduce brevemente los diferentes sistemas de captación de imágenes en el rango de milimétricas existentes en el mercado actualmente. Además se describe el único sistema de reconocimiento biométrico basado en imágenes capturadas en la banda de las MMW. La Sec. III resume el proceso llevado a cabo para generar la base de datos: obtención del modelo corporal de cada persona a partir de medidas corporales y metodología usada para la simulación de imágenes a 94GHz a partir de tal modelo. A continuación, en la Sec. IV, se describe el contenido y características principales de la base de datos. Finalmente en la Sec. V se resume el trabajo realizado, las aplicaciones de esta base de datos y se esboza el trabajo futuro.

II. TRABAJOS Y SISTEMAS RELACIONADOS

Las MMW y SMW presentan diferentes propiedades que las hacen muy apropiadas para su uso en sistemas de adquisición de imágenes. La más importante de todas ellas es la penetración a través de la ropa y otros materiales dieléctricos no polares, incluso a distancia. Esta propiedad ha sido, en gran medida, la responsable del actual desarrollo de la tecnología de captura de imágenes en la banda de MMW y de SMW. De hecho, existe una serie de sistemas comerciales de captura de imágenes en este rango espectral.

A. Sistemas de captura de imágenes en la banda de MMW y SMW

Tanto en el rango espectral de las MMW/SMW como en los restantes, existen fundamentalmente dos tipos de sistemas de captura de imágenes: pasivos y activos. En los primeros las imágenes son generadas a partir de la radiación natural que ha sido emitida y reflejada por el escenario, obteniendo como imagen un mapa de temperatura. En cambio, en los

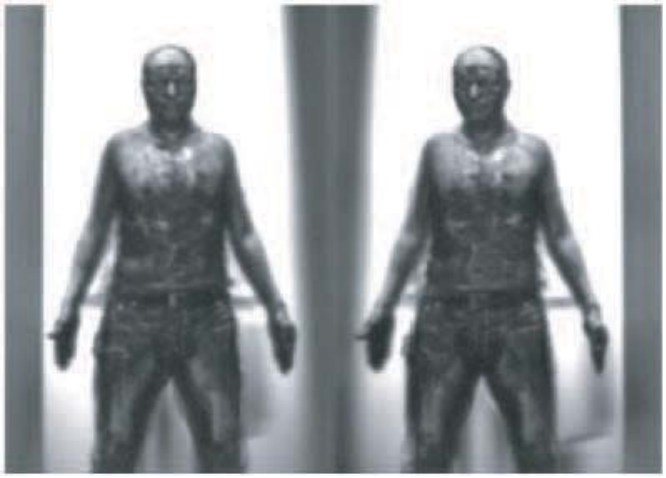

Fig. 1: Imágenes MMW extraídas de [8].

sistemas activos la radiación es transmitida al escenario y es recogida tras ser reflejada para formar la imagen, que en este caso corresponde a un mapa de reflectividad.

Dentro de los sistemas pasivos de captura de imágenes en MMW existen múltiples radiómetros en el mercado, como por ejemplo los fabricados por Quinetiq, Brijot, Alfa Imaging y Sago Systems. Mientras que entre los sistemas activos cabe citar los comercializados por Agilent y L-3 Communications. Finalmente, en la banda de las SMW las compañías Thruvision, Picometrix y Teraview producen sistemas de captación de imágenes pasivos (la primera) y activos (las dos últimas).

B. Trabajos de biometría

El uso de imágenes obtenidas en el rango de GHz en sistemas de reconocimiento biométrico ha sido propuesto con anterioridad [9]. Sin embargo, hasta la fecha sólo ha sido publicado un trabajo que use este tipo de imágenes con fines biométricos [8].

En dicho trabajo se adquiere una base de datos compuesta por imágenes de 50 personas obtenidas con un escáner radiométrico multivista a 94 GHz en exteriores (lo cual proporciona un mayor contraste en la imagen en comparación con las adquiridas en interiores por sistemas pasivos). De cada usuario se adquieren cuatro imágenes en poses diferentes (cuerpo de frente con la cara (i) frontal y (ii) girada a la izquierda) y con/sin oclusiones en la cara (barba, pasamontañas). Cada imagen (ver figura 1) incluye dos vistas, y tiene un tamaño de 696×499 píxeles (anchura×altura), siendo el tiempo de adquisición 15s. La temperatura equivalente de las imágenes varía entre 225K (regiones claras) y 300K (regiones oscuras).

Finalmente Alefs *et al.* explotan las características biométricas del cuerpo humano presentes en las imágenes descritas. En concreto se hace uso del tórax, de la cara y de medidas antropométricas, para llevar a cabo experimentos de reconocimiento biométrico. Éstos revelan que el reconocimiento mediante análisis multilineal con la parte del tórax es el que proporciona mejores resultados en comparación con la cara, medidas antropométricas e incluso fusión de cara y tórax.

III. Generación de la base de datos

La obtención de la base de datos se ha llevado a cabo conjuntamente en la Universidad Autónoma de Madrid (UAM) y en la Universidad Autónoma de Barcelona (UAB). El proceso para generar las imágenes que componen la base de datos, se puede dividir en las siguientes etapas: 1) Adquisición de medidas corporales de cada persona, 2) Generación del modelo corporal de cada usuario a partir de dichas medidas y 3) Simulación de las imágenes a 94 GHz a partir de cada modelo en los dos tipos de escenarios (interiores/exteriores) y los dos tipos de sistemas de captura (pasivos/activos).

Parámetros principales	Medidas corporales	
Género	Contorno del cuello	Contorno de la cintura
Edad	Altura del cuello	Distancia nuca-cintura
Tono Muscular	Contorno del brazo	Distancia cintura-cadera
Peso	Longitud del brazo	Distancia cuello-hombro
Altura	Longitud del antebrazo	Longitud del muslo
	Contorno de la muñeca	Longitud de la pierna
	Distancia frontal del pecho	Contorno del gemelo
	Contorno de pecho	Contorno del tobillo
	Contorno por debajo del pecho	Contorno del muslo
		Contorno de las caderas

Tabla I: Tabla de parámetros principales y medidas corporales tomados de cada sujeto.

A. Medidas corporales

Con el fin de disponer de modelos corporales realistas, se tomaron una serie de medidas corporales de cada persona. Estas medidas se especifican en la tabla I. Asimismo se tomaron de cada sujeto unas imágenes en el espectro visible con una cámara digital convencional.

B. Modelo corporal

El modelo corporal de cada sujeto se obtuvo mediante el software libre MakeHuman[1], que permite generar imágenes de cuerpos humanos en 3D. Para cada persona se introdujeron sus parámetros principales y medidas corporales a través de los menús disponibles para ello. Posteriormente se comparó el modelo 3D con la imagen adquirida en el visible para comprobar que el modelo obtenido se correspondiera con el cuerpo de la persona en cuestión.

Adicionalmente, MakeHuman, genera prendas de ropa adaptadas al cuerpo de cada modelo. Esto nos permitirá generar, en la siguiente etapa, imágenes a 94 GHz de personas con y sin ropa.

C. Simulación de imágenes

Los modelos generados en MakeHuman se importan con Blender[2], un software libre dedicado al modelado, animación y creación de gráficos 3D. Blender dispone un motor de trazado de rayos que trata la radiación a 94 GHz como si fuera luz que interacciona con la escena. Para obtener una buena simulación se deben definir las propiedades de los materiales (piel, ropa...) y fuentes de iluminación de acuerdo con sus características en el rango de 94 GHz [10].

Para acabar, las imágenes resultantes de Blender se post-procesan para añadirles ruido y las limitaciones de resolución que tenga el sistema de medida que se desee simular [10].

[1] http://www.makehuman.org/
[2] http://www.blender.org/

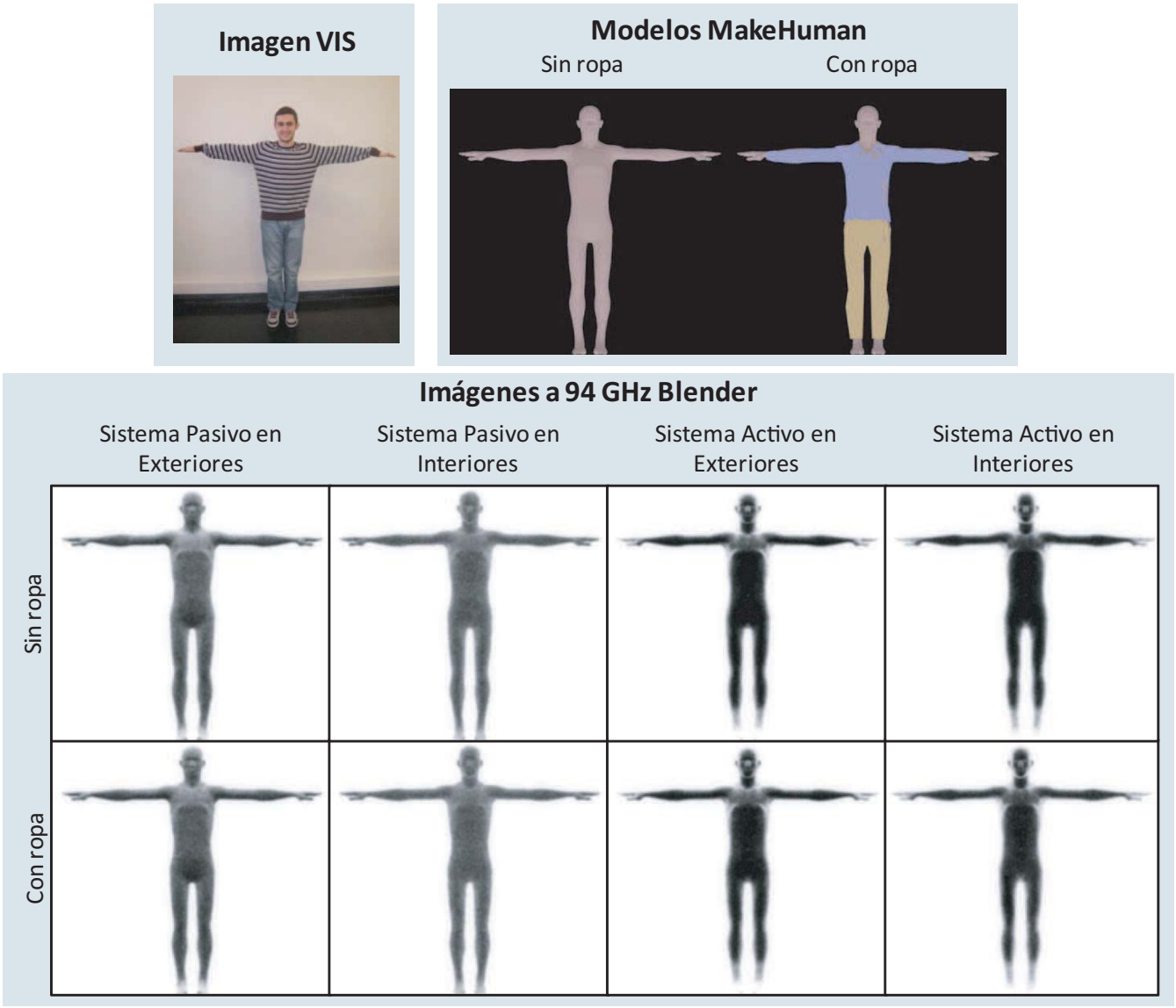

Fig. 2: Imágenes correspondientes a un usuario: imagen en el visible (arriba izquierda), modelos generados con MakeHuman (arriba derecha) e imágenes a 0º de orientación de la cámara en los cuatro sistemas considerados (abajo).

IV. Descripción de la base de datos

La base de datos está formada por imágenes simuladas, a 94 GHz, de 50 personas (25 hombres y 25 mujeres), con edades comprendidas entre los 15 y 55 años. Para cada sujeto se disponen de cuatro grupos de imágenes:

- Imágenes simuladas con un sistema pasivo en exteriores.
- Imágenes simuladas con un sistema pasivo en interiores.
- Imágenes simuladas con un sistema activo en exteriores.
- Imágenes simuladas con un sistema activo en interiores.

Dentro cada grupo anterior, se generaron, para cada usuario, las siguientes variantes de imágenes:

- Imágenes del modelo con ropa y ángulo formado por la cámara de -10º, 0º y +10º.
- Imágenes del modelo sin ropa y ángulo formado por la cámara de -10º, 0º y +10º.

Según lo anterior, para cada usuario, la base de datos cuenta con $4\times2\times3=24$ imágenes a 94 GHz. Por tanto, la base de datos está compuesta por $50\times24=1200$ imágenes.

La figura 2 muestra algunas de las imágenes correspondientes a un sujeto:

- Imagen en el visible.
- Modelos generados con MakeHuman sin ropa y con ropa.
- Imágenes simuladas a 94 GHz con Blender para cada tipo de sistema (pasivo/activo) y escenario(exteriores/interiores), todas con un ángulo de orientación de la cámara de 0º.

Se pueden resaltar algunas características de las imágenes a 94 GHz con respecto a (i) la influencia de la ropa y (ii) el contraste y nivel relativo de cada tipo de imagen. La vestimenta apenas se aprecia en las imágenes, de hecho, las imágenes simuladas a 94 GHz a partir del modelo con ropa y sin ropa son prácticamente iguales. Únicamente se observa ligeramente el efecto de la ropa en algunas regiones, correspondientes a lugares donde el tejido es más grueso o existen pliegues o varias capas de ropa. Esto ocurre en el cuello de la camiseta y la cintura, siendo más notorio en las imágenes de sistemas pasivos en exteriores.

Entre las imágenes simuladas con sistemas pasivos, las simuladas en exteriores presentan un mayor contraste que las simuladas en interiores, debido a la mayor diferencia de temperatura entre el cielo (100K) y el suelo (300K). Para exteriores, por tanto, las partes orientadas hacia el suelo presentan color oscuro (caliente) y las orientadas hacia el cielo color claro (frío). En cambio, en interiores el cuerpo presenta un color mucho más uniforme pues la temperatura del entorno no tiene grandes variaciones. Por otro lado, las imágenes simuladas con sistemas activos muestran un nivel de temperatura radiométrica mayor (son más oscuras) puesto que se radia a la persona con una fuente externa no natural, recogiendo esa radiación una vez ha sido reflejada por la persona. Por la misma razón no existen apenas diferencias entre las imágenes simuladas en exteriores e interiores.

Por último, en la figura 3 se recogen dos histogramas, uno correspondiente a la distribución de edades de los sujetos que forman la base de datos y el otro correspondiente a la distribución de alturas de los mismos.

V. Conclusiones

Uno de los principales problemas que se pueden encontrar a la hora de desarrollar y evaluar un sistema de reconocimiento biométrico es la carencia de bases de datos con un número alto de usuarios y de muestras por usuario. Esto ocurre especialmente con las imágenes de personas en el rango de las MMW y SMW.

En este trabajo se ha presentado una visión general de los diferentes sistemas de captura de imágenes en la banda espectral de las MMW y SMW, así como de los trabajos de reconocimiento biométrico que hacen uso de este tipo de imágenes. Asimismo se ha presentado la base de datos sintética BioGiga, formada por imágenes simuladas a 94 GHz de 50 usuarios en dos escenarios con dos sistemas de captura de imagen. Se ha descrito el proceso de generación de BioGiga así como sus principales características.

La principal aplicación de esta base de datos es la de su uso para el desarrollo de sistemas de reconocimiento biométrico basados en este tipo de imágenes. En concreto, a partir de estas imágenes se pueden extraer diferentes características representativas de cada individuo con las que realizar experimentos de reconocimiento. Asimismo, al disponer de diferentes tipos de imágenes para cada usuario, se puede realizar fusión a diferentes niveles para mejorar el rendimiento del sistema. Adicionalmente, el uso de este tipo de imágenes sintéticas permite la evaluación de vulnerabilidades de sistemas biométricos, basados en esas imágenes, frente a ataques externos.

Como trabajo futuro se prevé el uso a corto plazo de BioGiga para desarrollar un sistema de reconocimiento biométrico basado en tales imágenes. Cuanto mayor sea la población que forma la base de datos, más representativos serán los resultados obtenidos, por lo que la ampliación del número de usuarios sería muy deseable. Del mismo modo, disponer de otros rasgos biométricos de los mismos usuarios resultaría muy interesante para ser usados, conjuntamente con las imágenes a 94 GHz, en el mismo sistema y aumentar así su tasa de reconocimiento. Por esto resultaría muy interesante adquirir, de los mismos usuarios, otros rasgos como la cara, huella dactilar, etc.

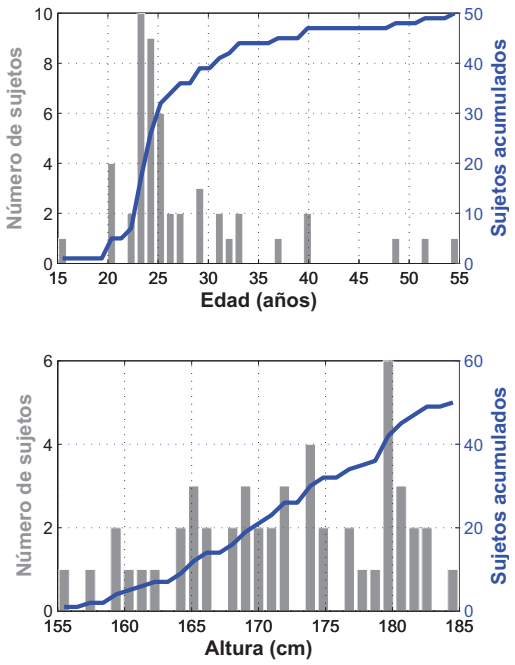

Fig. 3: Histograma de edades y de alturas de los 50 sujetos que forman la base de datos BioGiga.

Agradecimientos

Este trabajo ha sido financiado parcialmente por los proyectos Bio-Challenge (TEC2009-11186), Contexts (S2009/TIC-1485), TeraSense (CSD2008-00068) y "Cátedra UAM-Telefónica". M. M.-M., P.T. y R.V. son financiados por un contrato CPI de la CAM, una beca FPU y un contrato Juan de la Cierva, respectivamente.

Referencias

[1] A.K. Jain et al., "Biometrics: a tool for information security," *Information Forensics and Security, IEEE Transactions on*, vol. 1, no. 2, pp. 125–143, june 2006.

[2] Stan Z. Li et al., *Airline Passenger Security Screening: New Technologies and Implementation Issues*, chapter Biometrics at a Distance: Issues, Challenges, and Prospects, pp. 3–21, National Academy Press, 1996.

[3] Hong Chen and Anil K. Jain, "Dental biometrics: Alignment and matching of dental radiographs," *IEEE Transactions on Pattern Analysis and Machine Intelligence*, vol. 27, pp. 1319–1326, 2005.

[4] S.Z. Li et al., "Illumination invariant face recognition using near-infrared images," *Pattern Analysis and Machine Intelligence, IEEE Transactions on*, vol. 29, no. 4, pp. 627–639, 2007.

[5] R. Appleby and R.N. Anderton, "Millimeter-wave and submillimeter-wave imaging for security and surveillance," *Proceedings of the IEEE*, vol. 95, no. 8, pp. 1683–1690, aug. 2007.

[6] L. Yujiri et al., "Passive millimeter wave imaging," *Microwave Magazine, IEEE*, vol. 4, no. 3, pp. 39–50, sept. 2003.

[7] J.N. Mait et al., "94-ghz imager with extended depth of field," *Antennas and Propagation, IEEE Transactions on*, vol. 57, no. 6, pp. 1713–1719, june 2009.

[8] B.G. Alefs et al., "Thorax biometrics from millimetre-wave images," *Pattern Recognition Letters*, vol. 31, no. 15, pp. 2357–2363, 2010.

[9] Miriam Moreno-Moreno et al., "Biometrics beyond the visible spectrum: Imaging technologies and applications," in *Proceedings of BioID-Multicomm 2009*. September 2009, vol. 5707 of *LNCS*, pp. 154–161, Springer.

[10] J. Parron et al., "Millimeter-wave scene simulation using blender," in *Proceedings of XXV Simposium Nacional de Unión Científica Internacional de Radio*, September 2010.

Distance-based Feature Extraction for Biometric Recognition of Millimeter Wave Body Images

Miriam Moreno-Moreno, Julian Fierrez
and Ruben Vera-Rodriguez
ATVS - Biometric Recognition Group
Universidad Autonoma de Madrid, EPS
C/ Francisco Tomas y Valiente, 11. 28049 Madrid. Spain
{*miriam.moreno, julian.fierrez, ruben.vera*}*@uam.es*

Josep Parron
AMS - Antenna and Microwave Systems Group
Universitat Autonoma de Barcelona
Campus de la UAB, 08193 Bellaterra, Barcelona, Spain
josep.parron@uab.es

***Abstract*—In this work a complete process of feature extraction for biometric recognition of Millimeter Wave body images is described. The scope of this work is to find a small set of distance-based features that can be used in body geometry authentication obtaining good error rates. This approach constitutes a feature-based alternative to the holistic recognition methods already proposed on the mentioned kind of images. The system is tested on a database comprising 1200 synthetic images at 94 GHz of the body of 50 individuals. The results prove that the use of a small number distance-based features provide good class separation.**

***Keywords*-millimeter wave images; 94 GHz; synthetic database; image processing; body geometry; distance-based features; feature extraction; feature selection.**

I. Introduction

Many of the biometric characteristics used to identify individuals, such as ear, face, hand, and gait, are extracted from images acquired by cameras working at visible frequencies of the electromagnetic spectrum. Such images are affected by, among others factors, lighting conditions and the body occlusion (e.g. clothing, make up, hair, etc.) In order to circumvent these limitations, researchers have proposed the use of images acquired at others spectral ranges: X-ray, infrared, millimeter (MMW) and submillimeter (SMW) waves [1]. The images captured beyond the visible spectrum overcome, to some extent, some of the mentioned limitations; furthermore, they are more robust to spoofing than other biometric images/traits. Among the spectral bands out of the visible spectrum, the millimeter waves (with frequency in the band of 30-300 GHz) present interesting properties that can be exploited in biometrics [2]: ability to pass through cloth and other occlusions, its health safety, its low intrusiveness, and the recent deployment and rapid progress of GHz-THz systems in screening applications. In spite of the previous advantages, to date, there is only one published research work that performs biometric recognition using that kind of images, using a holistic recognition approach [3]. This shortage of biometric recognition research based on MMW images is due, in part, to the lack of databases of images of people acquired at GHz. This lack is a consequence of: (i) the privacy concern these images present, and (ii) most of the imaging systems working at the MMW/SMW band are either in prototype form or not easily accesible for research.

In this contribution we proposed and study new methods for processing and feature extraction for MMW body images. First, a database composed by synthetic images of the body of 50 individuals is generated. After processing the images, different distance-based features are extracted from some landmarks related to the silhouette of the body. Finally, some experimental validations are performed to determine the most discriminative features, and its discrimination power.

The paper is structured as follows. The baseline corpus and the main characteristics of the used database are briefly presented in Sect. II. Sect. III describes all the steps followed to obtain the feature vector: image segmentation, boundary extraction, landmark generation and feature vector construction. The evaluation of the selected features is performed in Sect. IV, where a cualitative and a quantitative analysis is carried out. Conclusions are finally drawn in Sect. V together with future work.

Main Parameters	**Corporal Measures**	
Gender	Neck circ.	Waist circ.
Age	Height	Nape to waist
Tone	Upper arm circ.	Waist to hip
Weight	Upper arm length	Shoulder to Neck
Height	Lowerarm length	Upperleg height
	Wrist circ.	Lowerleg height
	Front chest dist.	Calf circ.
	Burst circ.	Angle circ.
	Underburst circ.	Thigh circ.
		Hips circ.

Table I
MAIN PARAMETERS AND BODY MEASURES FOR EACH SUBJECT.

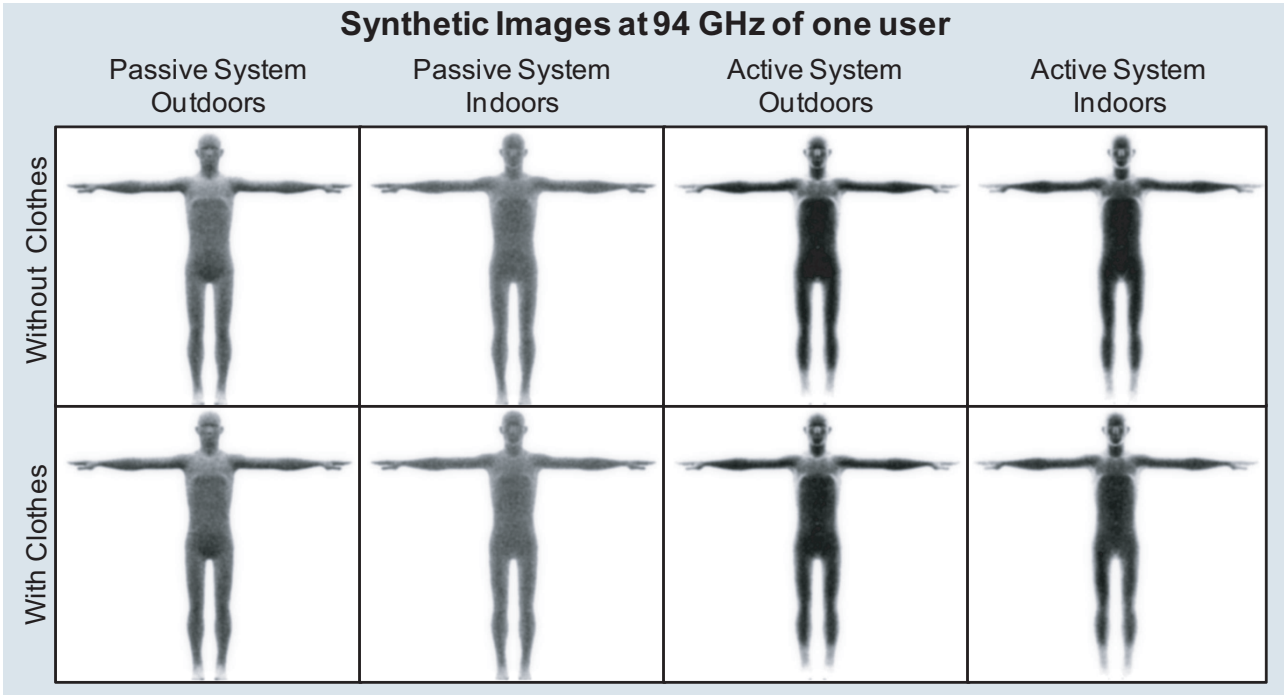

Figure 1. Synthetic images of one user simulated at 94 GHz with passive and active systems indoors and outdoors, and an orientation angle of the camera of 0 degrees.

II. BioGiga Database

The GHz-THz imaging technology is still in its infancy [4], therefore prices of the very few commercial imaging systems at that spectral band are still quite high. This fact together with the privacy problems the MMW images present, have caused the lack of public databases of MMW body images. That is the main reason why a synthetic database, called BioGiga, was generated in [5], with the objective of developing MMW-based biometric systems.

The baseline corpus of BioGiga consists of synthetic images at 94 GHz of the body of 50 individuals. The images are the result of simulations carried out on 3D-corporal models at two types of scenarios (outdoors, indoors) and with two kinds of imaging systems (passive and active). These corporal models were previously generated based on body measures taken from real subjects. The body measures considered are shown in Table I.

The database is gender balanced, consisting of 25 females and 25 males, with ages between 15 and 55 years old. For each user the database has four sets of images:

- Images simulated by a passive system outdoors.
- Images simulated by a passive system indoors.
- Images simulated by an active system outdoors.
- Images simulated by an active system indoors.

For each user and each of the previous sets the following data was generated:

- Images of the human 3D model with clothes and an angle formed by the camera of -10, 0 and +10 degrees.
- Images of the human 3D model without clothes and an angle formed by the camera of -10, 0 and +10 degrees.

According to what is stated above, for each user the database has $4\times2\times3=24$ images at 94 GHz. Hence, the total number of images in BioGiga is $50\times24=1200$.

Fig. 1 shows some of the images of one subject.

In this contribution, only images obtained from passive imaging systems are considered. Consequently, two types of images are treated: passive outdoor and passive indoor.

III. Image Processing and Feature Extraction

In order to obtain a distance-based feature vector for every image, we proposed the following steps. They are depicted in Fig. 2.

A. Image Segmentation

The first step is to binarize the image, separating the background from the body. A characteristic of the images simulated by passive systems is the different grey level they present in different parts of the body. For instance the abdomen is much darker than the feet. This fact difficults the segmentation process. This problem was overcome performing the segmentation in two steps:

- Border detection.
- Morphological operations.

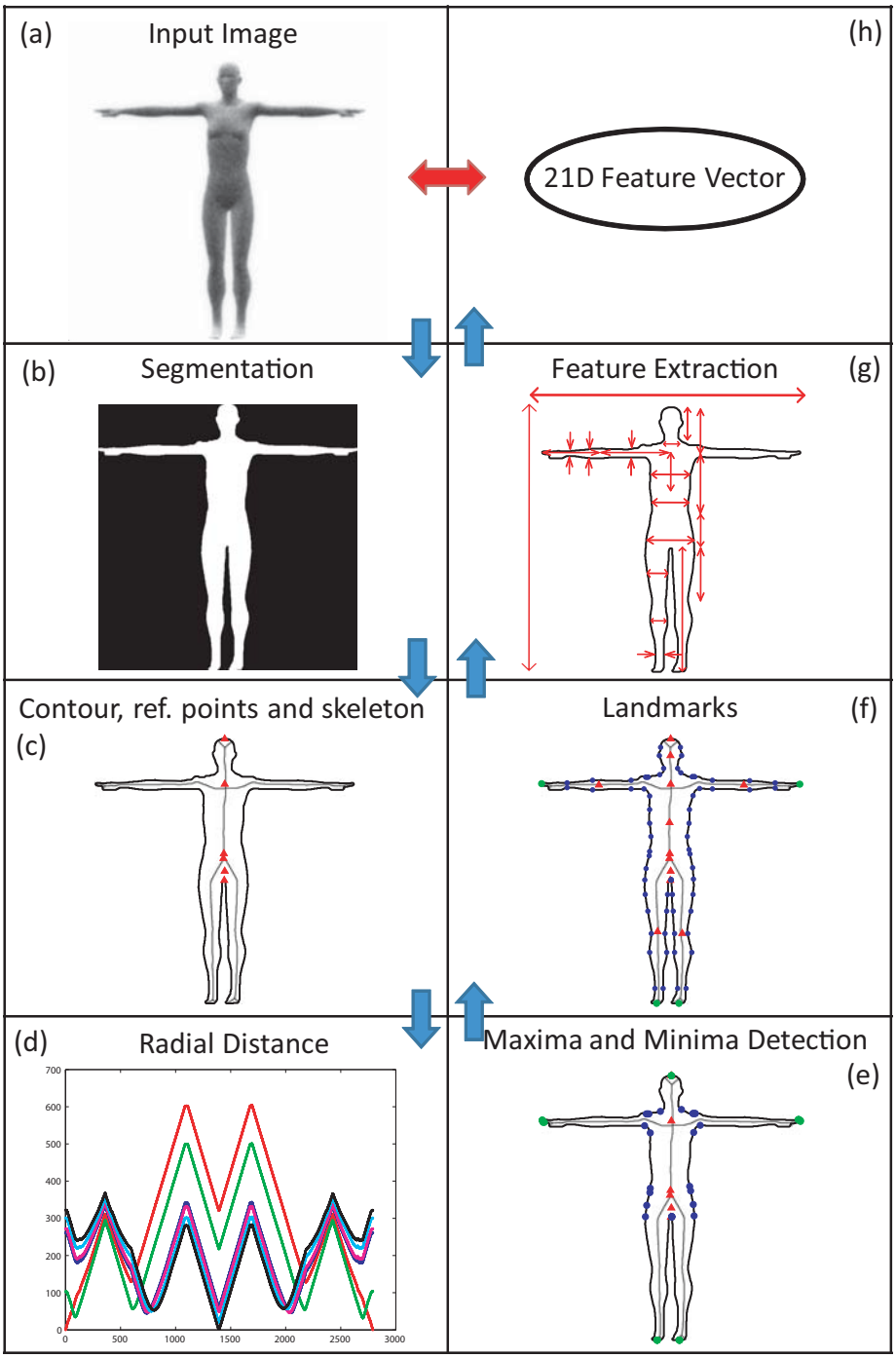

Figure 2. Main steps followed in our system to extract features. Original image (of a subject with clothing and a camera angle of -10 degrees) (a), segmented image (b), contour, reference points and skeleton (c), radial distance from each reference point to the contour (one curve per reference point) (d), addition of points with maximum and minimum distance from the reference points (e), all landmarks (f), distances used to form the feature vector (g) and the 21D feature vector (h).

A Canny border detector (whose parameters are previously tuned) is first applied to the image. After that, various morphological operations are conducted on the resulting border image. These morphological operations consists of closing operations with different structural elements in different areas of the image (head, arms, from arms to calf, and feet). Finally another set of morphological closing removes spurious irregularities.

An example image after this segmentation step is shown in Fig. 2(b)

B. Boundary Extraction

Once the input image is properly segmented, only the largest connected component is considered, assuming that it is the body. Then, the body boundary is extracted. After that, the middle point of the top of the head is detected. This point is fixed to be the first point of the extracted contour. The rest of the coordinates of the boundary are ordered in a clockwise direction. In addition to the boundary of the body, a basic skeleton of the body is obtained by means of morphological operations.

C. Landmark Generation

Six different reference points are first considered: (i) middle point of the top of the head, (ii) the crossing point of the arms line and the vertical line of the torso, (iii) the centroid of the body, (iv) the bifurcation of the skeleton in the abdomen area, (v) the central point of a bounding box including the whole body, and (vi) the pubis. An example image obtained after boundary extraction and the reference points detection is depicted in Fig. 2(c).

For each reference point, the Euclidean distance between the reference point and every point of the boundary is computed. Therefore, a one-dimensional function, showing the radial distance, is obtained for each reference point. An example of the six resulting radial distance functions is shown in Fig. 2(d). Every function is examined to find local maxima and minima. Maxima of the curve correspond to the head, hands, and feet outer points, while the minima correspond to points near the neck, shoulders, axilla, wrist and hips, depending on the considered reference point. Fig. 2(e) shows an example boundary together with the reference points and the maximum and minimum distance points.

In order to have enough geometric measures of the body, several extra points are detected inside the area of the body and in its boundary. To summarize, the following points are detected (see Fig. 2(f)):

- The centroid of some parts of the body: head, arms, torso and legs.
- Some points located at the boundary of the above mentioned body parts (for example in case of the torso, the points of the torso boundary located at three different heights are detected: at one quarter, at a half and at three quarters of the torso height.)

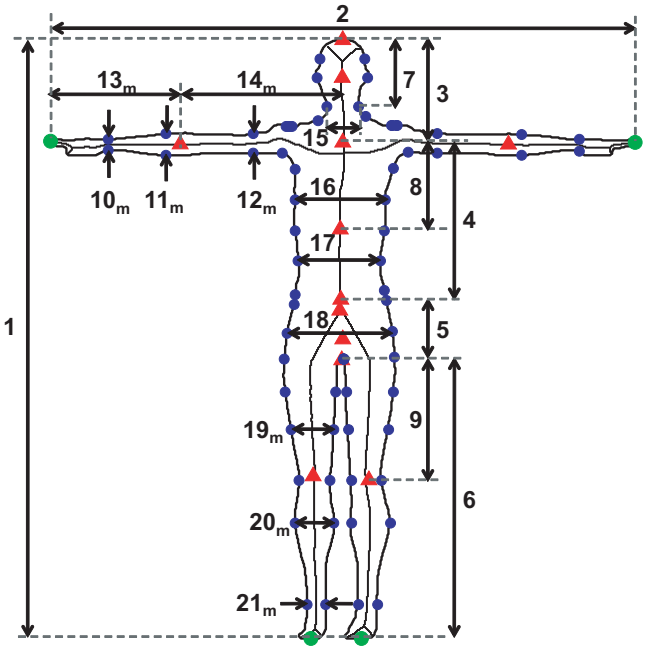

Figure 3. Body boundary, landmarks and distances extracted among them of the subjects and conditions of Fig. 2. These distances form the 21D feature vector. The number next to every distance is the component number in the feature vector. The ones whose number component appears with a subindex m are calculated as the average of that distance and the analog one of the right extremity. Red triangles represent the reference points and centroids of head, arms, legs and torso. Blue circles represent landmarks on the silhouette of the body (some of the them have minimum distance to the reference points). Green circles represent landmarks with maximum distance from the reference points.

D. Feature Generation

Once all the landmarks are obtained, the Euclidean distance between some of them is calculated. Specifically, 21 distances are obtained, which constitutes the feature vector. Fig. 2(g) and Fig. 3 show the considered distances. In Fig. 3, next to every distance there is a number that represents the component number in the feature vector (e.g. the height is the first component of the feature vector, it is feature number 1).

IV. Experimental Validation

In the following analysis only images simulated by a passive system indoors and outdoors are considered. The graphical results are shown exclusively for passive indoors images, for outdoors the results are quite similar. The same analysis for images simulated by active systems (indoors and outdoors) will be part of future work, in which a different image segmentation should be followed due to clearly visible differences between the images simulated by passive and active systems (e.g. the last ones present higher contrast).

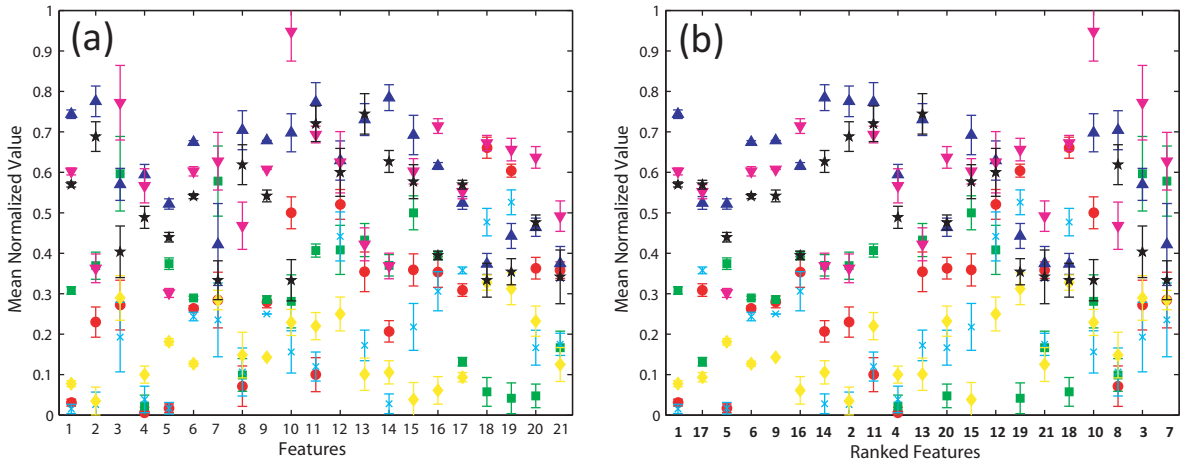

Figure 4. Mean normalized value of the feature vector of 7 randomly selected users. Each user vector has a different color and symbol.

A. *Evaluation of Features*

Fig. 4(a) represents the mean value and the standard deviation (as an error bar) of each normalized component (distance) of the feature vector, for seven subjects (a different color and symbol for each subject) randomly selected from the 50 available. As it can be seen, some component values are quite different from one subject to another, while others are more similar. On the other hand, the error bars overlap in some cases. To determine the most discriminative features, the components of the feature vector are ranked in descending order of degree of discrimination. For this purpose two magnitudes are calculated:

- **The average separation** between the mean values of each component from all subjects.
- **The overlap** between the error bars of the same component among all subjects.

The most discriminative feature will be the one with the largest average separation and the lowest overlap among different users. Hence, the features are ranked in descending order of the value of the quotient $average\_separation/overlap$. Fig. 4(b) shows the feature vector for the same seven subjects of Fig. 4(a) once its components have been ordered. Although the Fig. 4(b) shows the feature vector for 7 users, the ranking was conducted taking into account the vectors from all the 50 subjects. It can be seen the decreasing separation between mean values and the increasing overlap. The initial feature number (the same one as the one in Fig. 3) is written below the x axis with bold numbers. It is worth noting that the three most discriminative components (the three first ones in Fig. 4(b)) are: (i) the 1^{st} (height), (ii) the 17^{th} (waist width aprox.) and (iii) the 5^{th} (the distance between the centroid of the body and the pubis). The least discriminative one corresponds to feature 7^{th} (height of the head). Furthermore, these four features (three best ones and the worst one) obtained for images simulated by passive systems outdoors are the same ones when using images simulated indoors. It is not surprising that the height of the head is the least discriminating feature due to the process followed to obtain the 3D-body model from the body measures of real subjects. The head height was not considered, so all the models present approximately the same head height in their 3D body model used to simulate MMW images.

B. *Discrimination Power Analysis*

With the purpose of better assessing the discrimination power of the features, they are plotted in 2D graphs in Fig. 5:

- Fig. 5(a) plots the second PCA component vs the first PCA component of the 300 feature vectors (6 per user), having used all the 21D vectors to obtain the PCA transformation matrix.
- Fig. 5(b) plots the second most discriminative feaure (waist width aprox.) vs the most discriminative one (the height).

In both plots every user has its own color and symbol, so every user should be represented by a cluster of symbols with the same color and shape. In both cases, Fig. 5(a) and Fig. 5(b), it is patent that the clusters are clearly separated. Only in some regions of the 2D subspace some clusters overlap. This fact proves that the selected features are discriminative. Comparing both plots, it seems that the clusters in Fig. 5(b) are smaller and more separated among them than in Fig. 5(a). This reveals that even with only two features (height and waist width) it would be possible to distinguish different users. It must be noted that this analysis validates the proposed features but does not estimate their practical recognition capabilities. For doing so classification experiments should be performed, which will be conducted in future work.

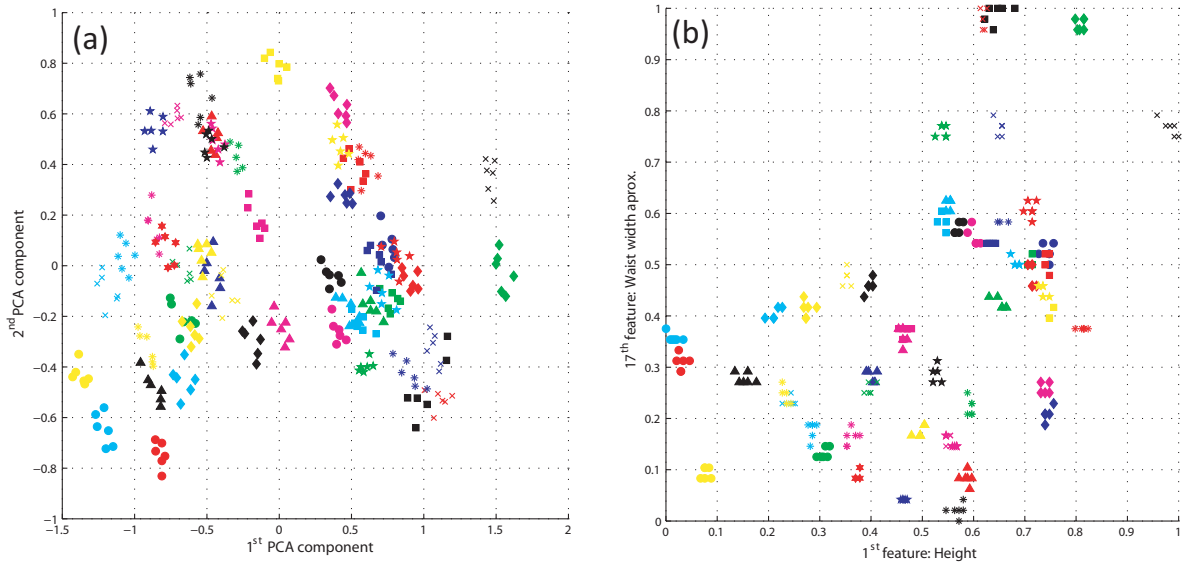

Figure 5. Bidimensional representation of the discrimination power of the extracted features. Second PCA component vs the first PCA component of the 300 feature vectors (6 per user) (a). Second most discriminative feature (waist width aprox.) vs the most discriminative one (the height) (b). In both plots every user has its own color and symbol.

V. Conclusions

A new feature extraction method for MMW images has been proposed. This method is based on the detection of relevant points of the body followed by the measure of 21 distances among them. These distances form the feature vector of every image. After an analysis of the selected features (using PCA and ordering them according to their individual discrimination degree), it has been proven that they have enough discrimination power to distinguish different users. Furthermore, even with only the two most discriminating distances, the users seem to be well classified.

The limitations of this work are related to the special characteristics of the database used. The BioGiga database is composed by images of only 50 users, besides, it consists of synthetic images. These two facts make the corpus limited when compared to the real data found in practice. However, the synthetic images are very similar to the ones really captured at 94 GHz (compare Fig. 1 with the images in [3].) Also, the synthetic images used are based on real measures from people. Therefore, the proposed features can be directly applied and are useful for practical MMW images.

Finally, the presented system should be completed with a classification stage. This will allow us to perform identification and/or verification experiments and to quantify the error rate using the 21D feature vectors or vectors with less components. A complete biometric system based on the proposed features for MMW images could be applied in the near future at airport security checkpoints and another screening scenarios.

Acknowledgment

This work has been partially supported by projects Bio-Challenge (TEC2009-11186), Contexts (S2009/TIC-1485), TeraSense (CSD2008-00068) and "Catedra UAM-Telefonica".

References

[1] M. Moreno-Moreno, J. Fierrez, and J. Ortega-Garcia, "Biometrics Beyond the Visible Spectrum: Imaging Technologies and Applications," in *Proceedings of BioID-Multicomm 2009*, ser. LNCS, vol. 5707. Springer, September 2009, pp. 154–161.

[2] ——, "Millimeter- and Submillimeter-Wave Imaging Technologies for Biometric Purposes," in *Proceedings of XXIV Simposium Nacional de Union Cientifica Internacional de Radio*, September 2009.

[3] B. Alefs, R. den Hollander, F. Nennie, E. van der Houwen, M. Bruijn, W. van der Mark, and J. Noordam, "Thorax biometrics from Millimetre-Wave images," *Pattern Recognition Letters*, vol. 31, no. 15, pp. 2357–2363, 2010.

[4] J. Mait *et al.*, "94-GHz Imager With Extended Depth of Field," *IEEE Transactions on Antennas and Propagation*, vol. 57, no. 6, pp. 1713–1719, June 2009.

[5] M. Moreno-Moreno, J. Fierrez, P. Tome, R. Vera-Rodriguez, J. Parron, and J. Ortega-Garcia, "BioGiga: Base de datos de imagenes sinteticas de personas a 94 GHz con fines biometricos," in *Proceedings of XXVI Simposium Nacional de Union Cientifica Internacional de Radio*, September 2011.

Simulation of Millimeter Wave Body Images and its Application to Biometric Recognition

Miriam Moreno-Moreno[a], Julian Fierrez[a], Ruben Vera-Rodriguez[a] and Josep Parron[b]

[a]Biometrics Research Lab.-ATVS, EPS, Universidad Autonoma de Madrid, Campus de Cantoblanco, C/ Francisco Tomas y Valiente 11, 28049 Madrid, Spain

[b]Antenna and Microwave Systems Group-AMS, Universitat Autonoma de Barcelona, Campus UAB, Bellaterra, 08193 Barcelona, Spain

ABSTRACT

One of the emerging applications of the millimeter-wave imaging technology is its use in biometric recognition. This is mainly due to some properties of the millimeter-waves such as their ability to penetrate through clothing and other occlusions, their low obtrusiveness when collecting the image and the fact that they are harmless to health. In this work we first describe the generation of a database comprising 1200 synthetic images at 94 GHz obtained from the body of 50 people. Then we extract a small set of distance-based features from each image and select the best feature subsets for person recognition using the SFFS feature selection algorithm. Finally these features are used in body geometry authentication obtaining promising results.

Keywords: Millimeter wave images, 94 GHz, image simulation, synthetic database, biometrics, image processing, body geometry, distance-based features, feature extraction, feature selection, SFFS algorithm, verification.

1. INTRODUCTION

Biometric Recognition is the process that allow to associate an identity with an individual automatically, using one or more physical or behavioral characteristics that are inherent in the individual.[1,2] Many of these biometric characteristics used to identify individuals, such as ear, face, hand, and gait, are extracted from images acquired by cameras working at visible frequencies of the electromagnetic spectrum. Such images are affected by, among others factors, lighting conditions and the body occlusion (e.g. clothing, make up, hair, etc.). In order to circumvent these limitations, researchers have proposed the use of images acquired at others spectral ranges: X-ray, infrared, millimeter (MMW) and submillimeter (SMW) waves.[3] The images captured beyond the visible spectrum overcome, to some extent, some of the mentioned limitations; furthermore, they are more robust to spoofing than other biometric images/traits. Among the spectral bands out of the visible spectrum, the millimeter waves (with frequency in the band of 30-300 GHz) present interesting properties that can be exploited in biometrics:[4] ability to pass through cloth and other occlusions, its health safety, its low intrusiveness, and the recent deployment and rapid progress of GHz-THz systems in screening applications. In spite of the previous advantages, to date, there is only one published research work that performs biometric recognition using that kind of images, using a holistic recognition approach.[5] This shortage of biometric recognition research based on MMW images is due, in part, to the lack of databases of images of people acquired at GHz. This lack is a consequence of: (i) the privacy concern these images present, and (ii) most of the imaging systems working at the MMW/SMW band are either in prototype form or not easily accessible for research.

For all above, in this contribution it is first described the generation and content of BIOGIGA, a new database composed of simulated images of people at 94 GHz. Then, we present a new biometric system based on that

Further author information: (Send correspondence to M.M.M.)
M.M.M.: E-mail: miriam.moreno@uam.es
J.F.: E-mail: julian.fierrez@uam.es
R.V.-R.: E-mail: ruben.vera@uam.es
J.P.: E-mail: josep.parron@uab.es

Main Parameters	Corporal Measures	
Gender	Neck circ.	Waist circ.
Age	Height	Nape to waist
Tone	Upper arm circ.	Waist to hip
Weight	Upper arm length	Shoulder to Neck
Height	Lowerarm length	Upperleg height
	Wrist circ.	Lowerleg height
	Front chest dist.	Calf circ.
	Burst circ.	Angle circ.
	Underburst circ.	Thigh circ.
		Hips circ.

Table 1. Main parameters and body measures for each subject.

kind of images totally different and complementary to the only one published so far. Our system is based on the geometry while the other one was based on a holistic approach over the grayscale after various dimensionality reduction techniques.[5] Finally, some verification experiments are performed to determine the performance and behavior of the developed system. An analysis of the features extracted and selected from the images is also carried out.

The paper is structured as follows. The generation, baseline corpus and the main characteristics of the used database are presented in Sect. 2. Sect. 3 presents the developed biometric system, describing all its modules: from the preprocessing of the input images to the identity decision. The evaluation of the biometric system is performed in Sect. 4, where the results of some verification and feature selection experiments are shown and analyzed. Conclusions are finally drawn in Sect. 5 together with future work.

2. BIOGIGA DATABASE

The corpus of the BIOGIGA database consists of synthetic images at 94 GHz of the body of 50 individuals. The images are the result of simulations carried out on corporal models at two types of scenarios (outdoors, indoors) and with two kinds of imaging systems (passive and active). These corporal models were previously generated based on body measurements taken from the subjects.

2.1 Generation of the Database

The generation of the database was carried out jointly at the Universidad Autnoma de Madrid (UAM) and Universidad Autnoma de Barcelona (UAB).[6] The process to generate the images that compose the database can be divided into the following stages: 1) Acquisition of body measures of each person, 2) Generation of the 3D body model of each user based on such measures, and 3) Simulation of the images at 94 GHz from each model in the two types of scenarios (indoor/outdoor) and two types of capture systems (passive/active).

2.1.1 Corporal Measures

In order to have realistic 3D body models, a set of body measures of each person was taken. These measures are specified in Table 1. Some pictures of each subject were also taken in the visible spectrum with a conventional digital camera).

2.1.2 Corporal Model

The body model of each subject was obtained using the free software MakeHuman*, which allows you to generate images of human bodies in 3D. For each person his or her main parameters and body measurements (see Table 1) were introduced through the menus available for it. Subsequently the 3D model was compared with the picture previously taken to verify that the obtained model corresponds to the body the concerned person.

Additionally, MakeHuman generates garments adapted to the body of each model. This allows us to generate, in the following stage, images of people with and without clothes at 94 GHz.

*http://www.makehuman.org/

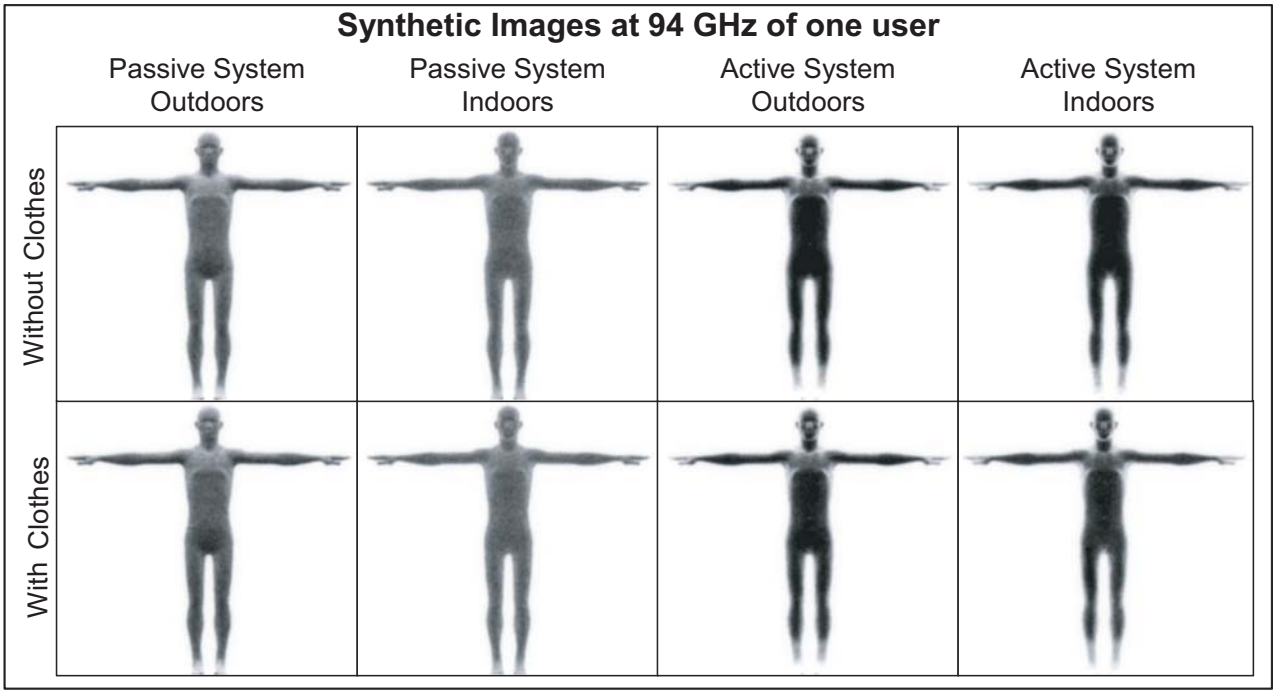

Figure 1. Synthetic images of one user simulated at 94 GHz with passive and active systems indoors and outdoors, and an orientation angle of the camera of 0 degrees.

2.1.3 Simulation of Images at 94 GHz

The models generated in MakeHuman are imported to Blender[†], which is a free software devoted to modeling, animation and 3D graphics creation. Blender provides a ray tracing engine that treats the radiation at 94 GHz as if it were light interacting with the scene. For a good simulation the properties of materials (skin, clothes ...) and light sources should be defined according to their characteristics in the range of 94 GHz.[7]

Lastly, the resulting images were postprocessed adding them the typical noise and resolution that the real system to be simulated has.[7]

2.2 Database Description

The database consists of images simulated at 94 GHz, of 50 people (25 females and 25 males), with ages between 15 and 55 years old. For each user the database has four sets of images, each of them simulated by:

- A passive system outdoors (PO).
- A passive system indoors (PI).
- An active system outdoors (AO).
- An active system indoors (AI).

For each user and each of the previous sets the following data was generated:

- Images of the human 3D model with clothes and an angle formed by the camera of -10, 0 and +10 degrees.
- Images of the human 3D model without clothes and an angle formed by the camera of -10, 0 and +10 degrees.

According to what is stated above, for each user the database has 4×2×3=24 images at 94 GHz. Hence, the total number of images in BIOGIGA is 50×24=1200. Fig. 1 shows some of the images of one subject. In this contribution, only images obtained from passive imaging systems outdoors are considered.

[†]http://www.blender.org/

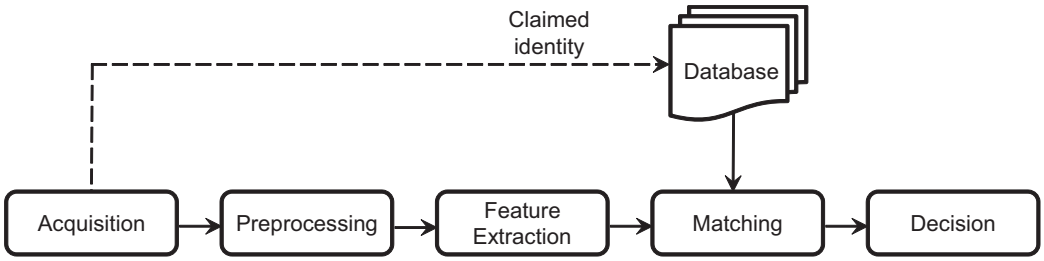

Figure 2. Architecture of a generic biometric system working either in verification or identification mode.

3. SYSTEM DESCRIPTION

3.1 Introduction to the Biometric Systems

A biometric system is the combination of devices, databases and processes that allow the recognition of an individual using one of his/her biometric features. The block diagram of a generic biometric system is shown in Fig. 2

Once the user has been enrolled, biometric systems can operate in two modes: 1) verification mode (the user claims an identity and presents his or her biometric trait, then the system determines if the real identity of the user corresponds to the identity claimed by him or her) and 2) identification mode (the user only present his or her biometric trait without claiming any identity, then the system tries to find his or her identity).

In the acquisition stage the biometric trait is captured. In our case, the biometric trait is the MMW image of the body. After that, the image is processed obtaining a more suitable image to perform the feature extraction, which is the following step. Next, the vector containing the features of the input image is compared with the feature vector of the claimed user (verification mode) or with all the feature vectors in the database (identification mode). Finally, a decision based on the result of that comparison is made.

The acquisition stage (which, in this work, corresponds to the simulation of the MMW images) was already explained in Sect. 2. The rest of the modules of the system are described in the next subsections: the image segmentation (Subsect. 3.2) belongs to the preprocessing while the boundary extraction (Subsect. 3.3), landmark generation (Subsect. 3.4), feature generation (Subsect. 3.5) and feature selection (Subsect. 3.6) are part of the feature extraction module. In the Subsect. 3.7 (matching) the similarity measure used to perform the comparison between feature vectors is introduced. The value of that similarity measure determines the final decision given by the system (Subsect. 3.8).

It is worth mentioning that the features extracted from the images are based on distances between points of the silhouette of the body. The process followed to obtain these features is depicted in Fig. 3.

3.2 Image Segmentation

The first step is to binarize the image, separating the background from the body. A characteristic of the images simulated by passive systems is the different grey level they present in different parts of the body. For instance the abdomen is much darker than the feet. This fact hinders the segmentation process. This problem was overcome performing the segmentation in two steps:

- Border detection.
- Morphological operations.

A Canny border detector (whose parameters are previously tuned) is first applied to the image. After that, various morphological operations are conducted on the resulting border image. These morphological operations consists of closing operations with different structural elements in different areas of the image (head, arms, from arms to calf, and feet). Finally another set of morphological closing removes spurious irregularities.

An example image after this segmentation step is shown in Fig. 3(b)

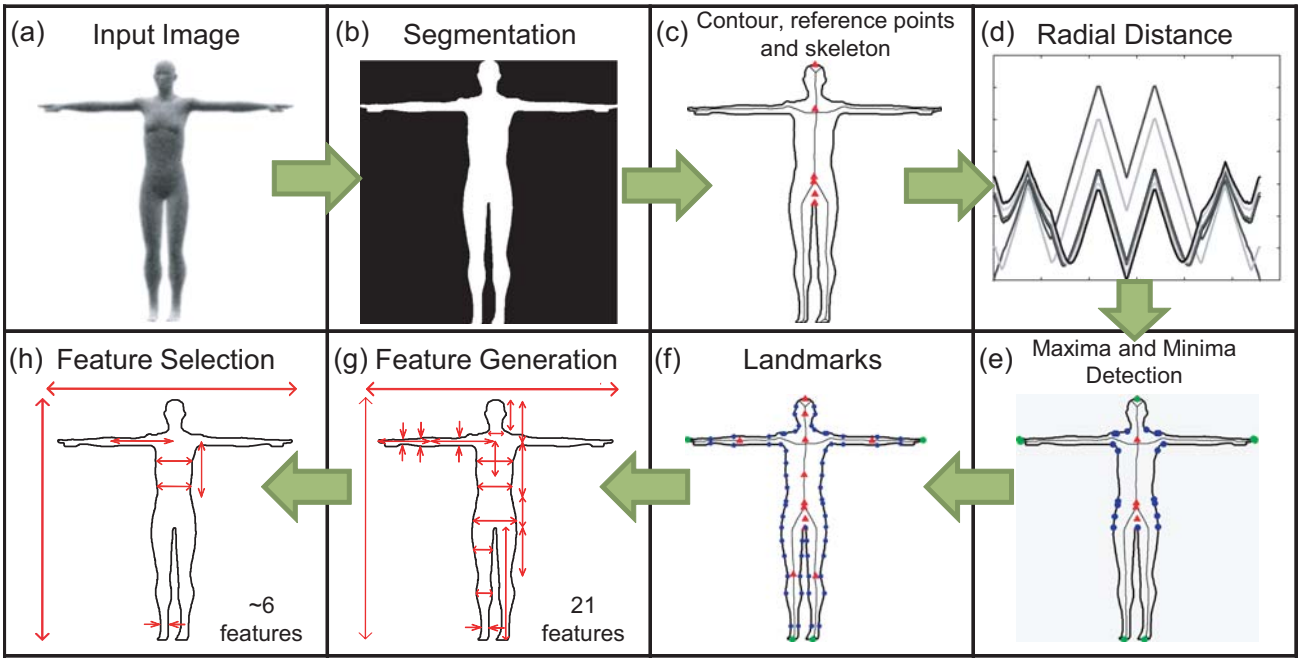

Figure 3. Main steps followed in our system to extract features. Original image (of a subject with clothing and a camera angle of -10 degrees) (a), segmented image (b), contour, reference points and skeleton (c), radial distance from each reference point to the contour (one curve per reference point) (d), addition of points with maximum and minimum distance from the reference points (e), all landmarks (f), distances used to form the feature vector (g) and the final selected features after applying the SFFS algorithm (h).

3.3 Boundary Extraction

Once the input image is properly segmented, only the largest connected component is considered, assuming that it is the body. Then, the body boundary is extracted. After that, the middle point of the top of the head is detected. This point is fixed to be the first point of the extracted contour. The rest of the coordinates of the boundary are ordered in a clockwise direction. In addition to the boundary of the body, a basic skeleton of the body is obtained by means of morphological operations.

3.4 Landmark Generation

Six different reference points are first considered: (i) middle point of the top of the head, (ii) the crossing point of the arms line and the vertical line of the torso, (iii) the centroid of the body, (iv) the bifurcation of the skeleton in the abdomen area, (v) the central point of a bounding box including the whole body, and (vi) the pubis. An example image obtained after boundary extraction and the reference points detection is depicted in Fig. 3(c).

For each reference point, the Euclidean distance between the reference point and every point of the boundary is computed. Therefore, a one-dimensional function, showing the radial distance, is obtained for each reference point. An example of the six resulting radial distance functions is shown in Fig. 3(d). Every function is examined to find local maxima and minima. Maxima of the curve correspond to the head, hands, and feet outer points, while the minima correspond to points near the neck, shoulders, axilla, wrist and hips, depending on the considered reference point. Fig. 3(e) shows an example boundary together with the reference points and the maximum and minimum distance points.

In order to have enough geometric measures of the body, several extra points are detected inside the area of the body and in its boundary. To summarize, the following points are detected (see Fig. 3(f)):

- The centroid of some parts of the body: head, arms, torso and legs.

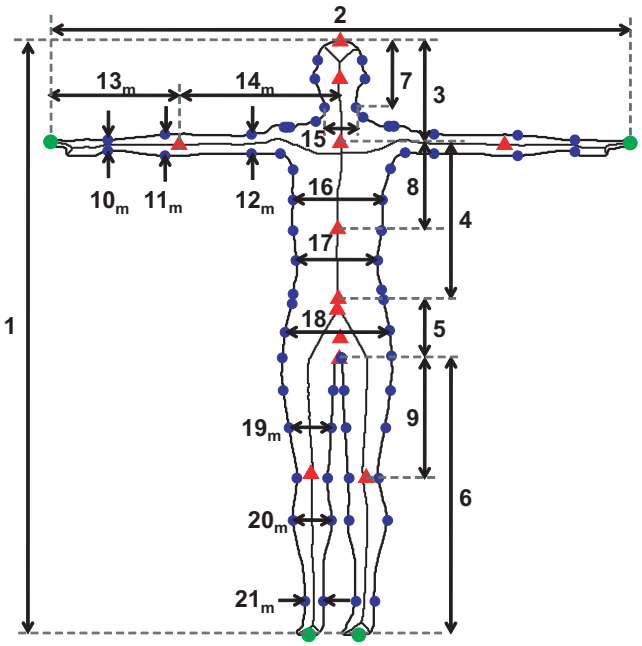

Figure 4. Body boundary, landmarks and distances extracted among them of the subjects and conditions of Fig. 3. These distances form the 21D feature vector. The number next to every distance is the component number in the feature vector. The ones whose number component appears with a subindex m are calculated as the average of that distance and the analog one of the right extremity. Red triangles represent the reference points and centroids of head, arms, legs and torso. Blue circles represent landmarks on the silhouette of the body (some of the them have minimum distance to the reference points). Green circles represent landmarks with maximum distance from the reference points.

- Some points located at the boundary of the above mentioned body parts (for example in case of the torso, the points of the torso boundary located at three different heights are detected: at one quarter, at a half and at three quarters of the torso height.)

3.5 Feature Generation

Once all the landmarks are obtained, the Euclidean distance between some of them is calculated. Specifically, 21 distances are obtained, which constitutes the feature vector. Fig. 3(g) and Fig. 4 show the considered distances. In Fig. 4, next to every distance there is a number that represents the component number in the feature vector (e.g. the height is the first component of the feature vector, it is feature number 1).

3.6 Feature Selection

In order to find the most discriminative set of distance-based features, and therefore increase the performance of the biometric system, a feature selection is performed. In addition, by reducing the number of features the computational cost decreases too.

Among the different feature selection algorithms,[8] the one employed in this work is the Sequential Floating Forward Selection (SFFS).[9] This suboptimal searching technique is an iterative process in which, in each iteration, a different set of features is used to compute a certain criterion. This is done until the criterion does not improve. For more details see[8] and.[9] In our case the criterion is related to the performance of the system.

3.7 Matching

Once the feature vector of an image is computed, either containing the 21 components or with only the components selected by SFFS, a similarity measure is computed. This similarity measure between two vectors is called score. In our biometric system the score is the opposite of the Euclidean distance between the two compared vectors. The reason for using the opposite is in order to have higher scores for more similar vectors.

3.8 Decision

The obtained scores are used to (i) decide wether the user is who he or she is claiming or not (verification) or to (ii) provide a list with the most likely identities (identification). In both cases, if the user's score is higher than a certain threshold, the user is accepted as a genuine user.

4. EXPERIMENTS

4.1 Performance Evaluation of a Biometric System

Once the system is implemented, an evaluation of its performance is desirable. This is done through quantitative measures, obtained from experiments, that reveal how well the system works and allow us to compare its performance with the performance of other biometric systems.

Although the developed system works in both kind of operational modes (verification and identification), the experiments and results shown below are obtained only when working in verification mode. In that case two main metrics are used to quantify the performance of the biometric system: 1) the False Acceptance Rate (FAR), which is the probability that an impostor is accepted by the system as a genuine one, and 2) the False Reject Rate (FRR), that reflects the probability that a genuine user is rejected by the system.

As the threshold value increases, the FRR increases too but the FAR decreases (the system becomes more secure by rejecting more genuine users and accepting less impostors). There is a value of the threshold for which the FAR and the FRR coincides. The value of both rates at that threshold is known as the Equal Error Rate (EER) and is the most widely used parameter to evaluate the performance of a biometric system working in verification mode. Plotting the FRR versus the FAR for all the different threshold values, gives the so-called DET curve (Detection Error Tradeoff curve).[10] This curve is an common way to graphically represent the behaviour of a biometric system, where the EER corresponds to the point where the DET curve and the bisector intersect each other (See Fig. 5(a)). The closer the curve is to the origin (and therefore the lower the EER is), the better the system is.

4.2 Experimental Protocol

Although the BIOGIGA database contains 6 PO, 6 PI, 6 AO and 6 AI images per user, in the following analysis only PO and PI images are considered. The graphical results will be shown exclusively for PO images, for PI images the results are quite similar. The same analysis for images simulated by active systems (AO and AI images) will be part of future work, in which a different image segmentation should be followed due to clearly visible differences between the images simulated by passive and active systems (e.g. the last ones present higher contrast).

We consider three different experimental protocols: 1) protocol 1:3, 2) protocol 2:3, and 3) protocol 3:3, where the first number refers to the number of training images considered per user, and the second number to the number of test images per user. The training images are the ones that the system previously have of each user and are used to enroll the user into the system, while the test images are the ones given by the user when he or she tries to be accepted by the system. In our experiments all the training images are images simulated with clothes, and the test images without clothes (in order to have the most challenging scenario with severe mismatch between enrollment and testing regarding clothing).

A mathematical model for each user is generated in the training and in the test set. Each model is simply the arithmetic mean feature vector of the considered images. Finally, the user test model is compared to the training model of each user in the database obtaining the corresponding score.

The experiments are carried out following the previous protocols in two ways: (i) considering all the components in the feature vector of the images, and (ii) after applying the SFFS algorithm, considering only the features selected by it. In short, there will be 6 different kind of experiments: each of then corresponds to a protocol working with all features or only with the selected ones.

	With all features	With features selected by SFFS		
Protocol	EER (%)	Number of selected features	Selected features	EER (%)
1:3	2.0000	6	1, 17, 16, 14, 4, 21	0.0816
2:3	2.0000	4	1, 17, 16, 2	0.0000
3:3	2.0000	3	1, 16, 2	0.0000

Table 2. Verification and SFFS feature selection results.

4.3 Results

The Table 2 includes the values of the EER for each experiment, together with the features selected by the SFFS algorithm, while Fig. 5(a) shows the verification performance, as DET curves, for the 6 experiments performed.

The EER is quite low (2%) when all the 21 features of the feature vector are considered. The SFFS algorithm selects different features in each experiment obtaining improved values of the EER (less than 0.1%). In fact, in protocols 2:3 and 3:3 the EER becomes zero, therefore, the corresponding DETs are only a dot in the origin in those cases.

Regarding the feature selection, first, it is worth mentioning that, according to the Table 2, as the number of training images increases, the number of selected features that optimizes the EER decreases. Bearing in mind *The Curse of Dimensionality*[11] this behavior is somehow surprising. According to this principle, a higher amount of training data allow to generate a more complex model (a higher dimension model, or a vector with more features), obtaining a better performance. However, our results show that, when there are more training data available, we obtain better results by considering less features. This could be due to the fact that, when there are more training data, the most discriminative features selected by the SFFS algorithm (mainly features #1, #16 and #2) become more relevant over the rest, while the rest of features are discarded in the feature selection process.

Secondly, the features selected most frequently in the three experiments are the height (feat.#1), the waist width (feat.#17), the wingspan (feat.#2) and the chest width (feat.#16) (they are represented with its number in Fig. 4 together with the rest of the features). The SFFS selects the most discriminative set of features for each experiment. That is, a group of uncorrelated features that optimizes the verification performance for an specific protocol. However, when considering independently each feature, we obtain that the most discriminative

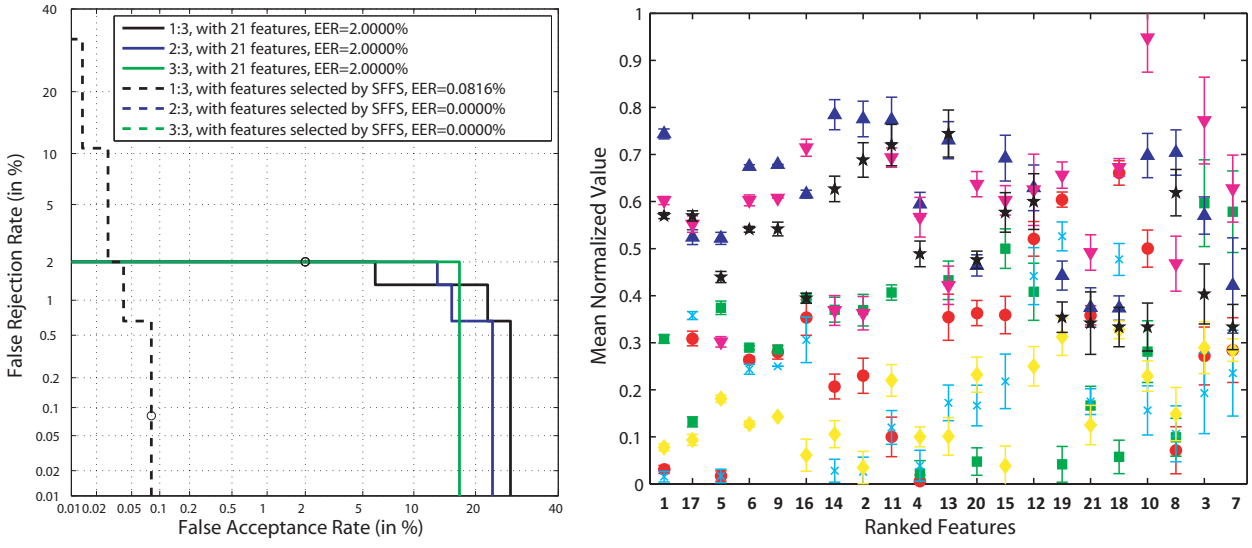

(a) (b)

Figure 5. (a) DET curves for the three protocols, using all the features or the ones selected by the SFFS algorithm. (b) Mean normalized value of each feature for 7 randomly selected users, the features have been ranked in descending order of their discrimination power.

ones are: the height (feat.#1), the waist width (feat.#17), the waist-pubis distance (feat.#5) and the leg length (feat.#6).

The computation of the most discriminative individual features was done ranking them in descending order of their discrimination power, which can be considered as the quotient *average_separation/overlap*. The numerator is the average separation among the mean values of the feature for all subjects, while the denominator is the overlap between the errors bars (standard deviation) of the same feature among all the subjects. This is graphically plotted in Fig. 5(b) where the mean value and standard deviation (as error bar) of every feature is plotted for 7 users, having the features ordered in descending order of *average_separation/overlap*. The feature number (the same one as the one in Fig. 4) is written below the x axis with bold numbers. It can be seen the decreasing separation between mean values and the increasing overlap.

The four most discriminative individual features are the first four ones in the Fig. 5(b), that is features 1, 17, 5 and 6, as we have previously stated. The height (feat.#1) and the waist width (feat.#17) are selected by SFFS algorithm in the three protocols, but the waist-pubis distance (feat.#5) and the leg length (feat.#6) are not. This is due to the fact that, although they are quite discriminative as isolated features, when forming a discriminative set of features, they are discarded because they provide info already given by other features that were first selected. For example, in protocol 2:3 the selected features are the height (feat.#1), the waist width (feat.#17), the chest width (feat.#16) and the wingspan (feat.#2). The height and the wingspan are highly uncorrelated, in fact only with those two features it would be possible to distinguish different users.[12] The chest and the waist width seem to be more correlated (both are widths of the torso), however, the images of the database reveal that they are not so correlated having people with the same chest width but different waist width (for instance women with a chest width similar to a man, tend to have less waist that men).

5. CONCLUSIONS

A new method to simulate images of people at 94 GHz has been proposed. This method first generates a 3D corporal model of the person from his or her body measures, afterwards the model is imported to Blender software, where the radiation at 94 GHz is treated as if it were light interacting with the scene, obtaining images of the person 3D model at that frequency. Images of 50 users were simulated at two types of scenarios (outdoors, indoors) and with two kinds of imaging systems (passive and active). These images comprise the BIOGIGA database, the first database of synthetic images of people at 94 GHz.

Next, a complete biometric system has been developed making use of the images of BIOGIGA. The use of MMW images instead of images acquired at other spectral bands present some advantages (mainly the transparency of clothing at that frequency range). In the development of the system we have proposed a feature extraction method based on the detection of relevant points of the body followed by the measure of 21 distances among them. These distances form the feature vector of every image. These vectors are compared in the matching stage obtaining a final a decision: the user is accepted by the system or not (in the verification operational mode).

Finally some verification experiments have been conducted using three different protocols (with one, two o three train images per user). Firstly, all the components in the feature vector of the images are considered in the experiments and, secondly, only the features selected by the SFFS algorithm are taken into account. Also a simple analysis of the selected features was carried out. The obtained verification performance is quite high (EER around 2% or lower) and the use SFFS algorithm considerably improves the performance of the system (EER around 0.1% or lower). In addition SFFS reveals the most discriminative set of features, that does not necessarily contain the most discriminative individual features.

The limitations of this work are related to the special characteristics of the database used. The BIOGIGA images are limited when compared to the real images acquired in practice. However, the synthetic images are very similar to the ones really captured at 94 GHz. Also, the synthetic images used are based on real measures from people. Therefore, the proposed features can be directly applied and are useful for practical MMW images.

Finally, a similar system should be developed when using images simulated with active systems. Furthermore, these systems (based on simulated images) should be improved and tuned to operate with real images acquired with MMW imaging systems. In that case the segmentation module should be adapted while the rest would

remain the same. These systems will allow us to perform identification and/or verification experiments with real images and could be applied in the near future at airport security checkpoints and another screening scenarios.

ACKNOWLEDGMENTS

This work has been partially supported by projects Bio-Challenge (TEC2009-11186), Contexts (S2009/TIC-1485), TeraSense (CSD2008-00068) and "Catedra UAM-Telefonica".

REFERENCES

1. Jain, A., Ross, A., and Prabhakar, S., "An introduction to biometric recognition," *Circuits and Systems for Video Technology, IEEE Transactions on* **14**, 4 – 20 (jan. 2004).
2. Jain, A. et al., "Biometrics: a tool for information security," *Information Forensics and Security, IEEE Transactions on* **1**, 125–143 (june 2006).
3. Moreno-Moreno, M., Fierrez, J., and Ortega-Garcia, J., "Biometrics Beyond the Visible Spectrum: Imaging Technologies and Applications," in [*Proceedings of BioID-Multicomm 2009*], *LNCS* **5707**, 154–161, Springer (September 2009).
4. Moreno-Moreno, M., Fierrez, J., and Ortega-Garcia, J., "Millimeter- and Submillimeter-Wave Imaging Technologies for Biometric Purposes," in [*Proceedings of XXIV Simposium Nacional de Union Cientifica Internacional de Radio, URSI 2009*], (September 2009).
5. Alefs, B., den Hollander, R., Nennie, F., van der Houwen, E., Bruijn, M., van der Mark, W., and Noordam, J., "Thorax biometrics from Millimetre-Wave images," *Pattern Recognition Letters* **31**(15), 2357–2363 (2010).
6. Moreno-Moreno, M., Fierrez, J., Tome, P., Vera-Rodriguez, R., Parron, J., and Ortega-Garcia, J., "BioGiga: Base de Datos de Imagenes Sinteticas de Personas a 94 GHz con Fines Biometricos," in [*Proceedings of XXVI Simposium Nacional de Union Cientifica Internacional de Radio, URSI 2011*], (September 2011).
7. Parron, J., Rossel, H., de Paco, P., Junkin, G., and Menendez, O., "Millimeter-Wave Scene Simulation using Blender," in [*Proceedings of XXV Simposium Nacional de Union Cientifica Internacional de Radio, URSI 2010*], (September 2010).
8. Molina, L. C., Belanche, L., and Nebot, A., "Feature selection algorithms: A survey and experimental evaluation," in [*Proceedings of the 2002 IEEE International Conference on Data Mining*], *ICDM '02*, 306–, IEEE Computer Society, Washington, DC, USA (2002).
9. Pudil, P., Novovicov, J., and Kittler, J., "Floating Search Methods in Feature Selection," *Pattern Recognition Letters* **15**(11), 1119 – 1125 (1994).
10. Martin, A., Doddington, G., Kamm, T., Ordowski, M., and Przybocki, M., "The DET curve in assessment of detection task performance," in [*Proceedings of the European Conference on Speech Communication and Technology*], **1**, 1895–1898 (1997).
11. Bishop, C. M., [*Pattern Recognition and Machine Learning (Information Science and Statistics)*], Springer, 1st ed. 2006. corr. 2nd printing ed. (Oct. 2007).
12. Moreno-Moreno, M., Fierrez, J., Vera-Rodriguez, R., and Parron, J., "Distance-based Feature Extraction for Biometric Recognition of Millimeter-Wave Body Images," in [*Proceedings of 45th IEEE International Carnahan Conference on Security Technology*], 326–331 (October 2011).